12-2010

FUor and EXor Variables: A NIR High-Resolution Spectroscopic Survey

Joseph Liskowsky
Clemson University, jliskow@clemson.edu

FUor and EXor Variables, a NIR High-Resolution Spectroscopic Survey

---

A Thesis
Presented to
the Graduate School of
Clemson University

In Partial Fulfillment
of the Requirements for the Degree
Master of Science
Physics and Astronomy

---

by
Joseph Paul Liskowsky
Dec 2010

Accepted by:
Dr. Sean Brittain, Committee Chair
Dr. Dieter Hartmann
Dr. Mark Leising
Dr. Bradley Meyer

Abstract

To better understand the labyrinth of heating and cooling processes in YSOs (young stellar objects), we study systems where there exists a large variability in the heating of this gas due to accretion. This research project focuses on several classes of early young eruptable T-Tauri stars, namely the FUors, the EXors and the so-called FU Ori-like, which all have the property of large amplitude oscillations in accretion rate. Each of these categories may well represent specific stages in early low-mass stellar evolution. While these objects have specific spectroscopic and circumstellar diagnostics (as means of identification) our research suggests that there are at least several objects that defy (typical) classification. The young objects ZCMa and L1551 IRS5 both show circumstellar diagnostics different from what is expected for an FUor (though ZCMa and L1551 are classified as such). In ZCMa we see an obvious accretion event, but the ro-vibrational overtone lines of CO are in emission. Typically, for an accreting FUor, these lines would be in absorption due to the physics of the disk. Very strangely, we see the fundamental lines in emission. Because of the relationship between the Einstein A coefficients for these transitions, we would expect to see either both the fundamental and overtone lines together in emission or absorption. This mystery may be solved by modeling and before we can make an intelligent claim about the heating mechanisms in YSOs, we need to understand these special cases first (it may turn out that these are not-so-special after-all and are indicative of a subclass of the FUor or EXor class).

Dedication

For Jessica Powell

Acknowledgments

I would like to acknowledge the generous support of the NASA Origins Grant and that of Clemson University. This work would not be possible for the patient support of my advisor. I would like to acknowledge our collaborators who have taken time to review my work - specifically I would like to acknowledge the work of Ted Simon, Terry Rettig, Sean Brittain, Erica Gibb in this regard. I would like to acknowledge Matt Troutman's assistance in understanding the data reduction process.

Table of Contents

List of Tables

List of Figures

Chapter 1

Introduction

1.1 The Luminosity Problem

The luminosity problem is outlined in Kenyon et al. (1990), in which they present an IRAS survey of the Taurus-Auriga molecular cloud, and provide data to quantify some stellar evolution parameters. In this survey, which they claim to be complete, there are detections of approximately 11 heavily extincted young stars and approximately 100 visible (in the optical) pre-main-sequence TTSs (T-Tauri stars). They estimated the ages of these stars to be approximately 10^6 years, which gives a star formation rate of approximately 10^{-4} stars per year. If we assume that the ratio of obscured to unobscured stars is proportional to the timescale of a star remaining obscured by the total timescale (lifetime-so-far) of the stars, then we find that the obscured (embedded) phase lasts 10^5 years. This number is very important because it tells us that a 1 solar mass star must have an average accretion rate of 10^{-5} solar masses per year in order to form in the timescale allowed by statistically measured populations. That is, the measured accretion rates are not sufficient to account for the population of non-extincted and extincted sources. This places a strong constraint on any model of early stellar evolution. This model also assumes that the accretion phase is truncated at the end of the embedded phase.

The theory for this model was initially developed (in part) by Lynden-Bell & Pringle (1974), who show that simple models of circumstellar disks (at least for low mass stars) reproduce the spectra and lightcurves obtained from measured T-Tauri stars; the models are capable of reproducing the infrared excess observed and, with the addition of a boundary layer where material is transferred

onto the central star, reproducing visible and ultraviolet emission found in T-Tauri stars. Lynden-Bell and Pringle study the evolution of disks over timescales of 10^8 years, showing that the angular momentum problem can be solved if a large portion of the nascent circumstellar disk moves towards the gravitational center during which time its angular momentum decreases while a small portion of this disk mass is pushed to large radii but given a comparatively large angular momentum. Hence, the angular momentum of the systems under consideration shed their angular momentum by transferring it to distant portions of the disk, where the gas is much less dense and not as detectable. Shu (1977) shows that this model is consistent with an isothermal collapse model of a massive gas cloud: a cloud collapsing under its own gravity forms a disk structure and a central core. Hence, the basic principles of solar system formation were in place by the late 70s. However, the full details of solar system formation are yet to be uncovered; to wit: the mass accretion timescale appeared to be quite off. Hartmann and Kenyon posited that if they could find a star that had an event where the accretion rate increased dramatically then the contemporaneous prevailing theory of star formation could be salvaged, given that survey data matched the required frequency of eruptions. They concluded that the FU Orionis objects - a group of young, erupting sources, might be the answer for which they were looking.

The luminosity function peaks at approximately .3 $L_\odot$. If we use the well-known accretion luminosity equation

$$L = GM\dot{M}/R \tag{1.1}$$

and assume that the vast majority of the luminosity is generated by accretion, we find that the accretion rate is $\dot{M} = 10^{-7} M_\odot yr^{-1}$. This value calculated assumes a radius of 1 $R_\odot$, a mass of M = .1 $M_\odot$, where the assumption that the lowest mass stars (or cores) are the most frequent, and where the radius is determined by Stahler (1988) for the given mass and for weak accretion (quoted accretion rates are approximately $10^{-6} M_\odot yr^{-1}$) as well as a vanishing deuterium supply. Stahler (1988) shows that the deuterium abundance dramatically affects the stellar radius but also the luminosity of the source. The value of the accretion rate is dependent upon the luminosity which we have assumed comes entirely from mass accretion onto the young star. This assumption is not entirely valid because these sources are undergoing gravitational contraction and are therefore radiating. Therefore, this value for the mass accretion represents an upper-limit. However, this mass

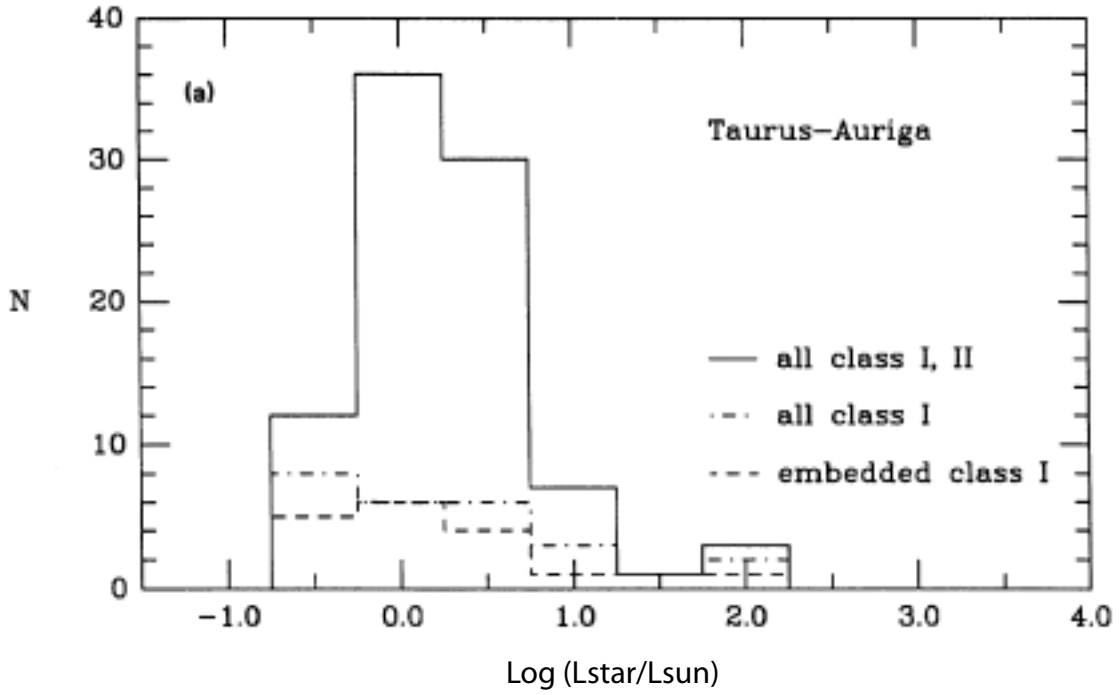

Figure 1.1: The Luminosity function for the Taurus Auriga molecular cloud. Taken from Kenyon et al. (1990)

accretion rate is two orders of magnitude lower than the required $10^{-5} M_{\odot} yr^{-1}$ average. Clearly, if we are to explain early stellar evolution, we need to find from where the final mass of the star accretes.

One possible way to solve this factor of one hundred riddle is by allowing all young stellar objects to undergo a period of extremely rapid accretion. In such an event it would be somewhat statistically unlikely to find one object undergoing an outburst in a small sample, but such that enough material is able to be accreted onto the central star during the 10^5 year embedded time scale to account for the final mass at the beginning of the visible (non-embedded) epoch.

Such a period of rapid accretion could plausibly be explained by the phenomenon associated with FU Orionis. If the luminosity increases by a factor of several hundred during these events, and we attribute the increase in luminosity to accretion, then it would be possible to explain ostensible luminosity problem by requiring all young stellar objects to undergo multiple FU Orionis eruptions.

1.2 History

The FU Orionis system's flare-up was first discovered by Wachmann in 1939 (Hoffleit, 1939). During the 1940's the star was observed at approximately 16th magnitude. Then, suddenly, in the late 1930's, FU Orionis abruptly rose in brightness to 9.5 magnitudes. This is a change of approximately 5-6 magnitudes, corresponding an increase in luminosity of a factor of several hundred. Clearly, this represents an highly energetic event, though its cause remained unclear.

Figure 1.2 is the data collected by Herbig (1977). Clearly, there was a strong rise in brightness near 1936. The decay timescale is long, if extant. Perhaps a timescale of 100 years can be intuited from this graph, however the variation within the data is sufficient to make that assumption dubious.

FU Orionis remained an intriguing yet lone curiosity until another example of this enigmatic source appeared: in 1969 V1057 Cygnus showed a remarkable increase in brightness over the course of approximately 390 days (Simon, 1975; Herbig, 1977): rising from 16th magnitude to 10th magnitude during this time. V1057 Cyg also shows a much more rapid decline in brightness than FU Orionis; the source decreases by approximately two magnitudes in approximately 6 years. Without comment on the cause of this increase (and subsequent decrease) in brightness, it appeared to be another example of the outburst FU Orionis showed thirty years previous. Additionally, a second source

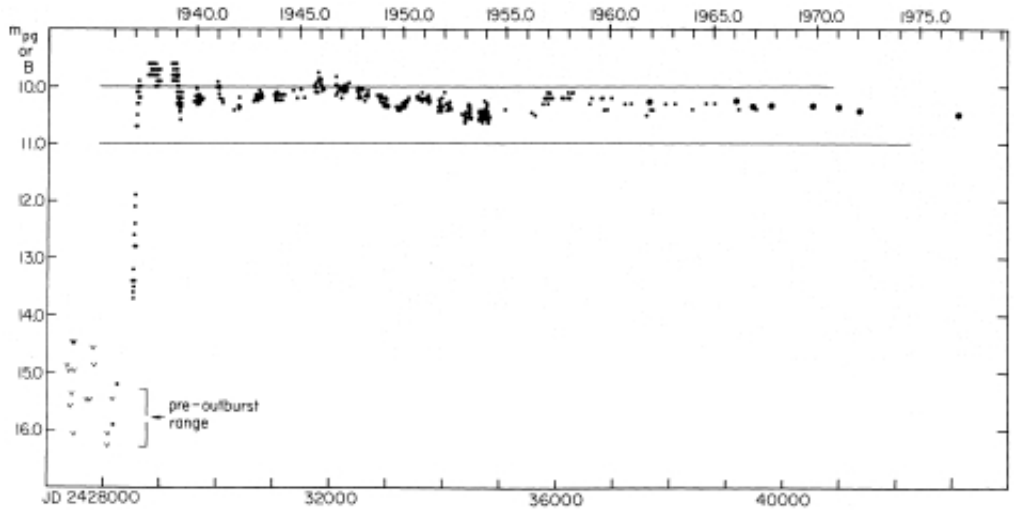

Figure 1.2: FU Orionis' light curve compiled by Herbig (1977)

showed a similar lightcurve to V1515 Cygnus and FU Orionis: V1515 Cygnus showed a remarkably slow but nonetheless dramatic increase in brightness from the 1920s to the 1970s, rising from 17th magnitude in the 1920s to the 13th in the 1970s. The evidence that these three objects were related was not based on the considerations of lightcurves alone; multi-wavelength spectra show numerous similarities among the group.

Because the possible FU Orionis solution to the luminosity problem is an attractive solution, it becomes important to perform large scale surveys trying to detect such objects and to find their relative frequency in star forming regions, to find their accretion rates, and ascertain the validity of the FU Orionis hypothesis.

In order to perform large scale surveys, it is necessary to find diagnostics which clearly identify FU Orionis objects. It is not feasible to conduct surveys of thousands of young stellar objects over the time periods in which FUors identify themselves via lightcurve analysis, so it becomes important to understand the physics of these disks in order to find a spectroscopic diagnostic which unambiguously identifies an FUor.

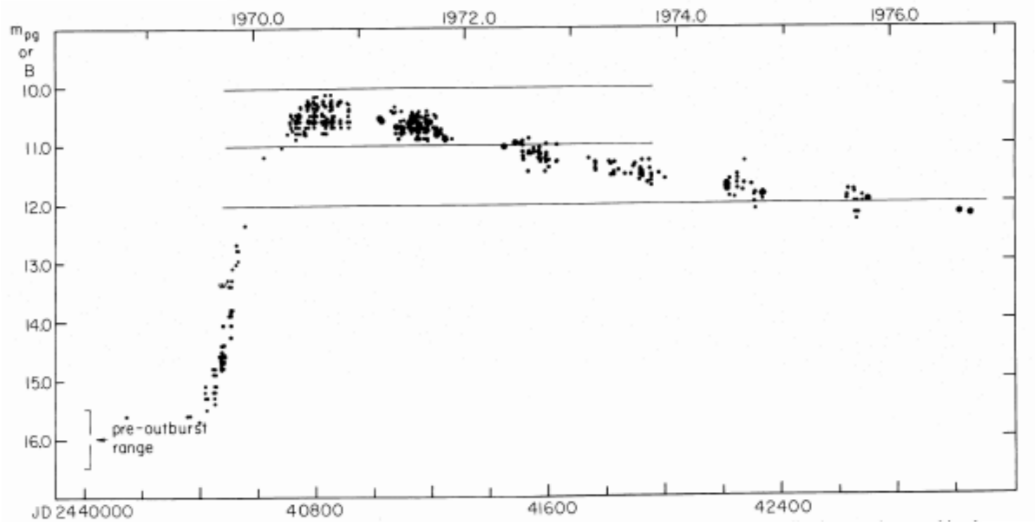

Figure 1.3: V1057 Cygnus' light curve compiled by Herbig (1977)

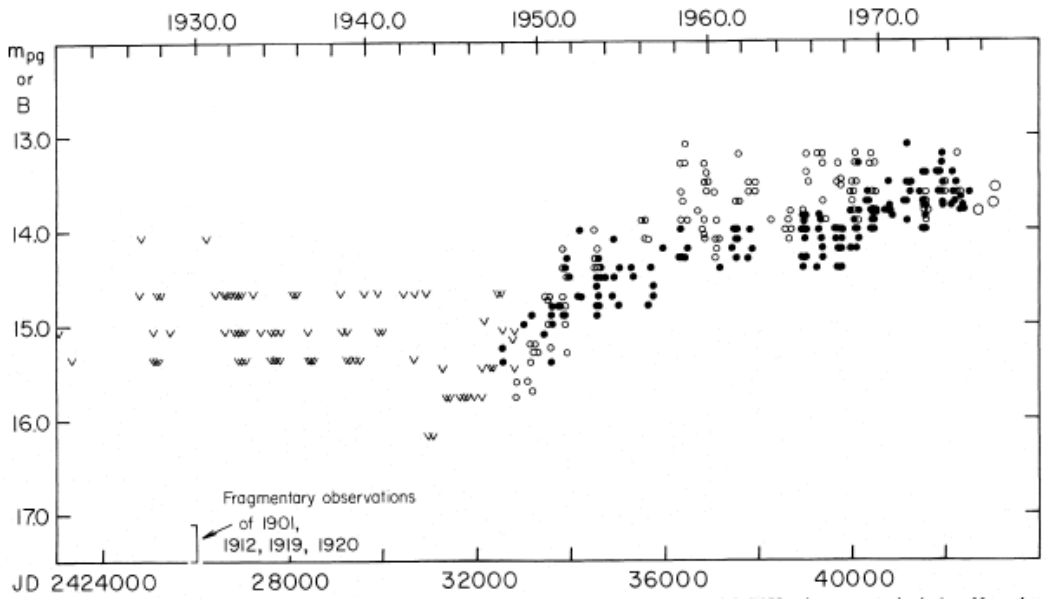

Figure 1.4: V1515 Cygnus' light curve compiled by Herbig (1977)

1.3 Spectroscopic Characteristics of Disks

In all objects (post outburst) observations of Hα show a P-Cygni like line structure, velocity shifts in Hα show multiple shell components, many displaced by several hundred kilometers per second. Additionally, the spectra looked much like F or G supergiants with deep absorption lines, which appear strongly broadened. Li I absorption was observed at 6707 $\mathring{A}$ which is in the visible range (Herbig, 1977). However, at other wavelengths (NIR) the sources look more like M supergiants (Mould et al., 1978). Also, these sources each show a strong infrared excess. The models which fit these parameters would come with Hartmann and Kenyon's work on these sources by interpreting these spectroscopic characteristics as being generated by circumstellar material in an accreting disk (Hartmann & Kenyon, 1985).

The FUor variables in their high accretion state can be classified as having active disks (Greene et al., 2008). An active disk is self luminous (Bertout & Bouvier, 1989) and accretes a relatively massive amount of material onto the central star in a short period of time. Typical accretion rates for an FUor are approximately $10^{-4} M_{\odot} yr^{-1}$. The midplane of the disk reaches several thousand Kelvin and emits as a blackbody. Because the temperature of the disk decreases further from the midplane, the more tenuous gas in the disk atmosphere absorbs. Hence, the resultant spectra look like those of a circumstellar disk with absorption features. Specifically, we expect to see CO in absorption assuming that CO is extant in the disk among other factors. Glassgold et al. (2004) shows that temperature and column density strongly determine which heating and cooling processes dominate in the disk. This work was inspired mainly because many models assume that all disk material is shielded from stellar photons, which is clearly false because observations of CO emission due to recombination are ubiquitous. Another assumption of models is that the dust and gas in the disk are in LTE (local thermodynamic equilibrium); the dust absorbs stellar photons as a blackbody and collisionally deposits energy to the gas, which radiates it away. However, there must exist some critical density such that this LTE process is no longer efficient (where the dust heats the gas). This occurs at a specific low density. The heating and cooling processes in the disk directly affect the type of spectra we observe. It is imperative to have models which can explain observables. We show later that models for purely active disks or purely passive disks do not account for all spectroscopic characteristics which are presented in this work.

Because of the violent radially inward rush of mass during the accretion event, for an FUor

we expect to see an active disk's spectra. Hence, for CO in the disk atmosphere, we anticipate seeing the ro-vibrational lines in absorption. Because the CO bandheads are much easier to detect at low resolution, this diagnostic has been used as a classification of active disks in the past. Indeed, each of the FUors in our sample that are labeled "FUor-like" have been identified on (partly) this basis; this categorization is based (generally) on spectroscopy, and when no outburst has been detected.

If we see the overtone ro-vibrational bandheads in absorption, we would also expect to see the fundamental lines in absorption (due to values of their corresponding Einstein As), and for most of these sources, that is the case. However, several of our sources do not follow the expectations of their classification as either EXors or FUors, which are found within the literature. These curious sources are to be discussed in the results section.

Indeed, Mould et al. (1978) shows that a small sample of FUors (FUor and V1057 Cygnus) show strong CO overtone absorption and strong water absorption. This phenomenological observation was applied to L1551 IRS 5 in Carr et al. (1987), giving L1551 IRS 5 the status of an FUor based on the CO overtone absorption and a weak water absorption feature. However, simply observing these simple spectroscopic diagnostics is not sufficient to determine the active or passive nature of the disk, let alone determine its status as an FUor, as shown in data presented in this work. Any survey that is searching for FUors may not rely solely on the interpretation of overtone spectra to classify YSOs as FUors. Spectra from both Mould et al. (1978) and Carr et al. (1987) are shown Figures 1.5 and 1.6, respectively.

Additionally, if our resolution is sufficient, we expect to find line doubling; the absorption features, if they are from the disk, are expected to be doubled. This is a result of the differential rotation of the disk. This effect is discussed more in Appendix N. Hartmann & Kenyon (1985) found this affect in V1057 Cygnus in their 1985 paper. The figure which shows this is included in this work to exhibit the affect using an actual spectra. We did not see this in any of our spectra.

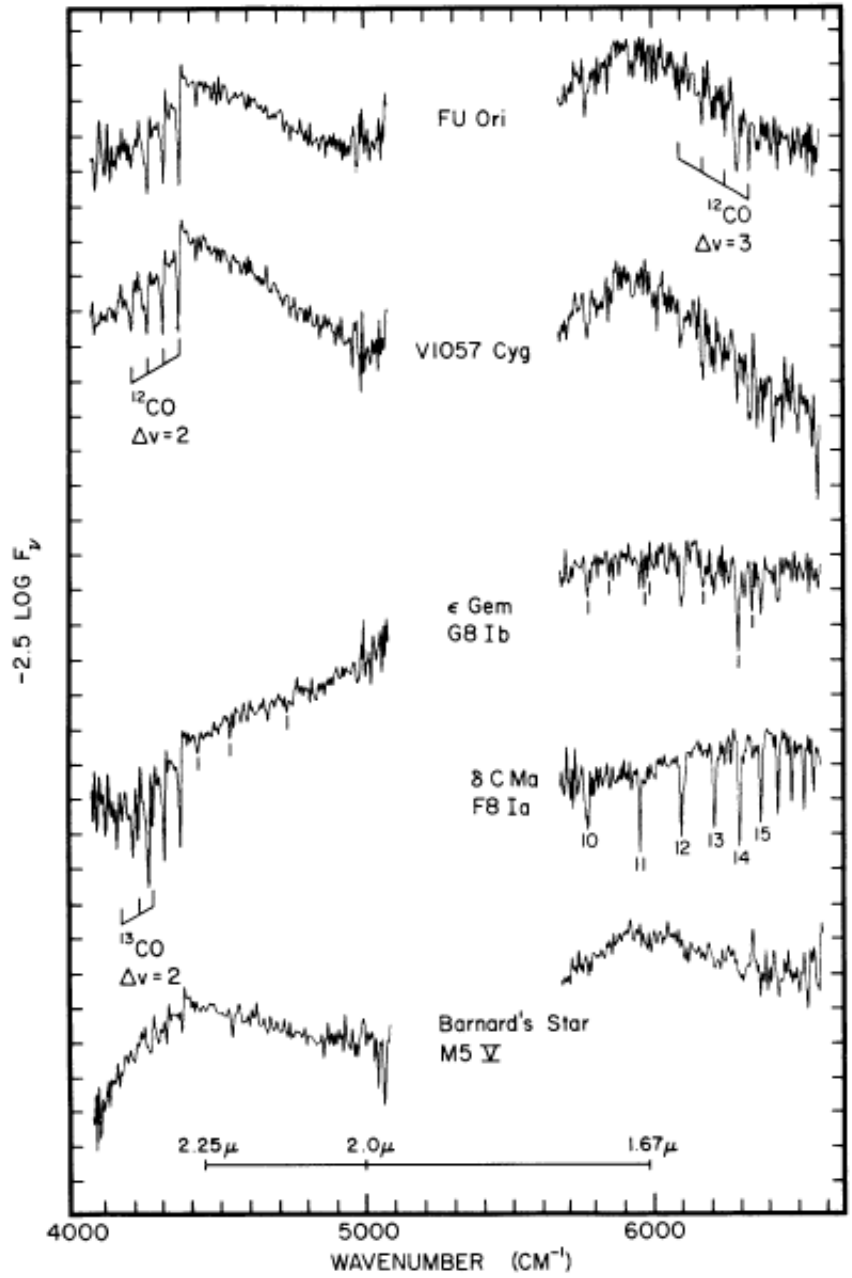

Figure 1.5: Spectrum of FU Ori and V1057 Cyg. Mould shows two spectra of the classic FUor FU Ori and V1057 Cyg in comparison with F and G supergiants and Bernard's Star (type M). Note the CO overtone and water vapor absorption in the FUors and how these features are both not present in either the F or G supergiants or the late-type M star.

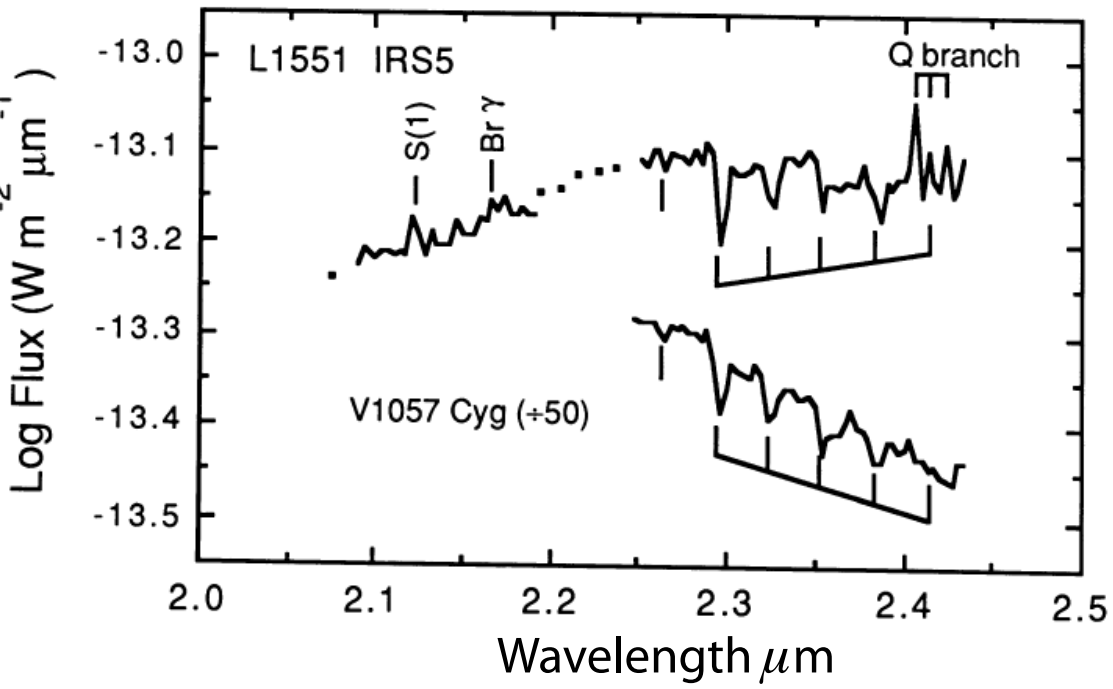

Figure 1.6: The spectrum of L1551 in 1987, taken from Carr et al. (1987). The spectra we show are similar in the absorption features shown in the overtone CO lines.

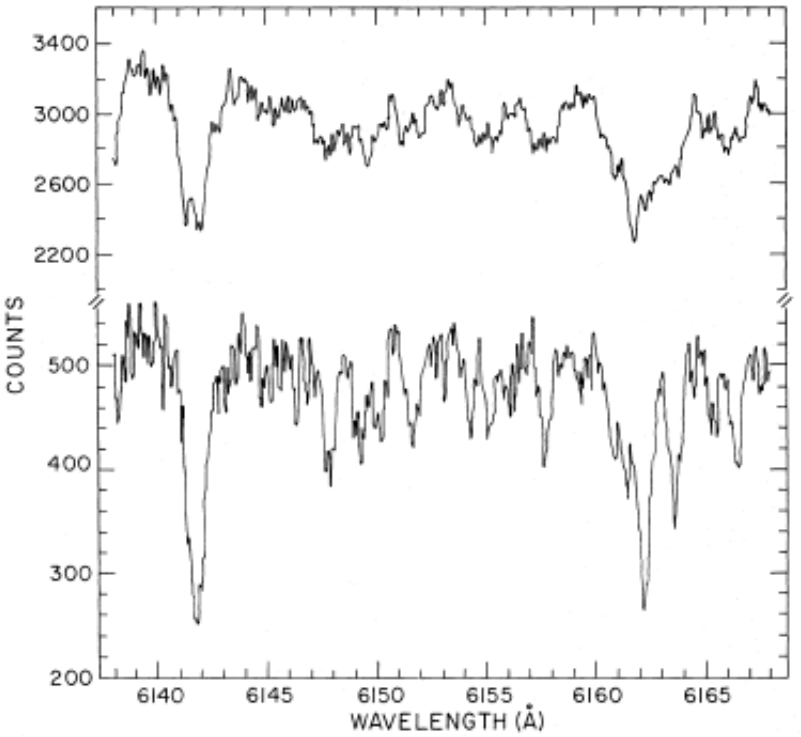

Figure 1.7: Spectra of V1057 Cyg (top) and V1515 Cyg (bottom), taken from Hartmann & Kenyon (1985).

1.4 Potential Causes of FUor Accretion Events

While it is clear that accretion through the disk and onto the surface of the central star may be responsible for the increase in luminosity, the initial cause of the accretion event still remains unclear. Many theories have been proposed to account for the supposed drastic increase in accretion rate in a short period of time. An attractive and intuitive suggestion may be that molecular viscosity causes drag forces to dissipate the kinetic energy of the matter in the disk. However, because the molecular viscosity of the disk is insufficient to cause appreciable drag, and therefore cannot cause material to flow appreciably towards the central star, any theory promulgated as a solution to the initiation of the accretion event necessarily cannot be based on molecular viscosity; another mechanism is needed to explain accretion. A theory which overcomes this limitation is the thermal accretion model. This theory posits that an effective viscosity is generated by turbulent mixing across adjacent radii, which effectively causes radial mass transport between adjacent annuli. In the model, the disk is divided into annuli and allows mass to flow between them (Shakura & Sunyaev, 1973). The turbulence itself may be caused by a magnetic instability, where a magnetic field threads the disk (due to moving plasma), and since these annuli rotate at different velocities, a radial velocity gradient exists within the disk. This exerts a torque on each annulus, causing a breaking effect on the inner annuli, and a speeding up effect on the outer annuli. This has the effect of transporting angular momentum out of the system (to larger and larger radii). Other mechanisms for inducing accretion have also been proposed, such the self gravitation of a sufficiently massive disk or a magnetorotational instability (Armitage et al., 2001).

Another proposed model makes note that many of these systems are binaries. If the binaries are close, a gravitational perturbation may induce turbulence in the disk (Bonnell & Bastien, 1992). A similar perturbative effect may be caused by an orbiting planet forming within the disk. Alternatively, a large gas giant forming in the disk may actually artificially curtail accretion on the central star by removing the accreting material from the disk and gravitationally binding it within the gas giant (Clarke & Syer, 1996).

The small sample size of these systems, as well as the their evident complexity and variation amongst themselves makes it difficult to narrow down the possibilities for incipient disk accretion. Indeed, the proposed solutions to this accretion issue are nearly as numerous as the sources.

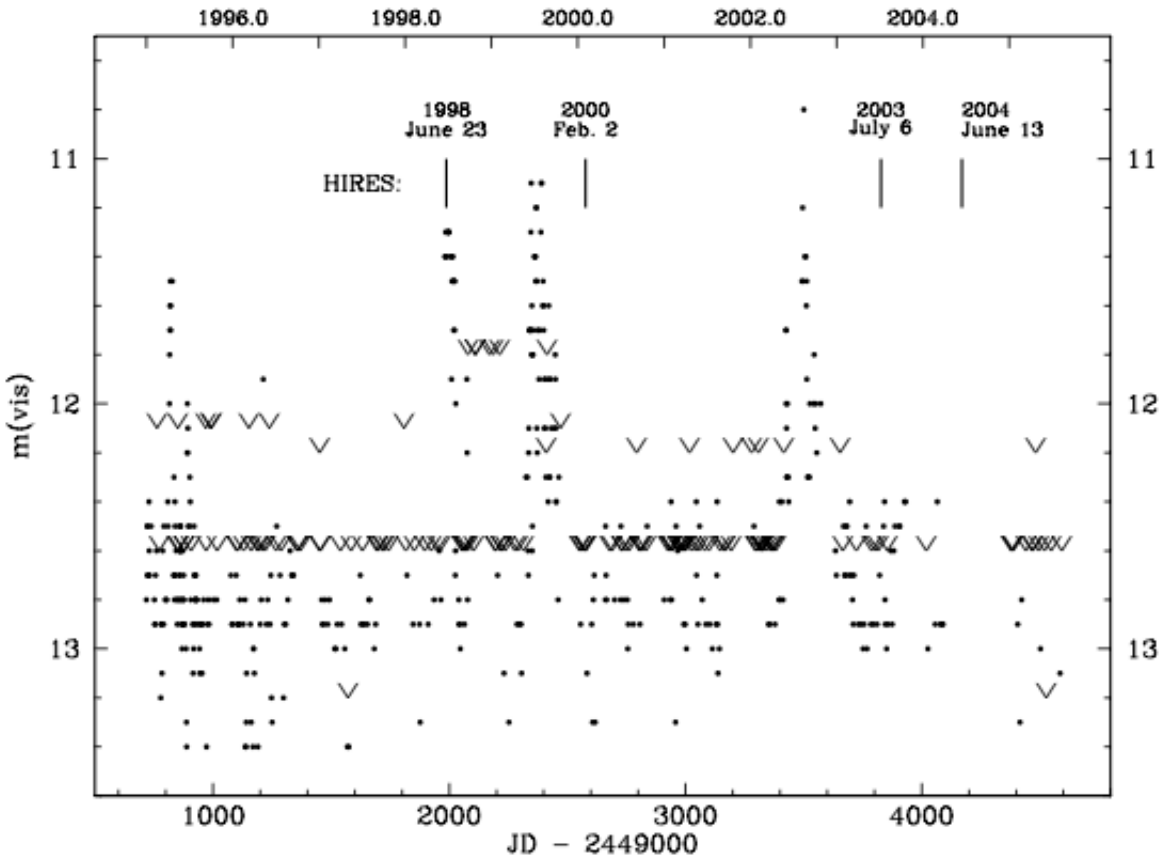

Figure 1.8: EX Lupi's light curve compiled by Herbig (2007). Carets show the maximum value for that date. Dates shown in the plot area are dates when HIRES data were taken.

1.5 Brief Summary of EXors

The prototypical case of an EXor is a star called EX Lupi. The figure shows a lightcurve over a short period of time which shows the stars' very frequent episodic outbursts. Because accretion from EXors flows to the central star from funnel flows, we see hydrogen emission, specifically, Brackett γ. The disk is assumed to be passive, reprocessing starlight, showing an emission spectrum (at least in the atmosphere of the disk, but this can be a very complex interaction). The eruptions from the EXor variable are less intense than those of the FUor, but they occur on a much faster timescale, while the distinction between the two may simply imply that these (observations of) processes are part of a spectrum of accretion processes in early, low-mass stellar evolution.

Chapter 2

Data Reduction and Acquisition

All data were acquired on KECK II using the NIRSPEC (Near Infrared Spectrometer) (McLean et al., 1998) NIRSPEC is a cross-dispersed echelle spectrograph with an instrument profile intrinsic width of approximately 12 km s^{-1}, yielding a spectral resolution of approximately 25,000. The slit width is .5". The data were taken over the course of several nights in 2007 and 2009. A data log is given below.

The data reduction for all sources was completed following Brittain (2004). A brief description of the data reduction process follows: The source was aligned in the slit and a ABBA nod pattern was used to cancel the sky background to first order (see appendix M). Each nod position is stored in a .fits file. After the observing run, we add the fits files together in the A - B - B + A pattern. The result is divided by two to ensure that the final nodded two dimensional image has the correct number of counts. Each beam (combined A and B) is then manually selected. Because the blaze angle of the spectrograph is not exactly aligned (in some cases, quite a bit off) with the CCD chip (a 1024x1024 IR array), a 'detilting' routine is sometimes run to align the beams. This allows easier (possibly more accurate) wavelength calibration later, but is not entirely necessary. The resultant two dimensional image has hot pixels removed using a boxcar routine, and what remains is the source spectra with telluric features. We then generate a spectra by summing over the rows of each beam (the beams may be several pixels 'wide') and, if the spectra are properly calibrated such that the A beam and B beam are aligned to within one pixel, the two beams are added together and the result is divided by 2.0 (again, to obtain the correct number of counts.) We manually (by eye) define a continuum from the spectra which we will use later to normalize each to

Source	*Date*	*Filter/Band*	*Grating Setup*	*Integration Time (s)*
AR6A	Feb 1 2009	K	61.83/35.53	240
AR6A	Feb 1 2009	MW	60.58/37.05	240
HR3888	Jan 31 2009	MW	62.12/37.05	60
HR3888	Jan 31 2009	K	61.93/35.49	20
HR3888	Feb 1 2009	K	63.16/35.66	60
HR3888	Feb 1 2009	K	61.83/35.53	60
HR3888	Feb 1 2009	MW	60.58/37.05	60
HR8515	Jul 24 2007	MW	61.12/37.05	60
HR8515	Jul 24 2007	K	62.53/35.55	60
L1551	Jan 31 2009	MW	62.12/37.05	240
L1551	Jan 31 2009	K	61.93/35.49	180
PVCep	Jan 31 2009	MW	61.12/37.05	120
PVCep	Jan 31 2009	K	62.53/35.55	60
RNO15	Feb 1 2009	MW	60.58/37.00	120
RNO15	Feb 1 2009	K	61.83/35.53	180
V1057	Jul 24 2007	K	62.53/35.55	60
V1057	Jul 24 2007	MW	61.12/37.05	120
V1118	Jan 31 2009	MW	62.12/37.05	120
V1118	Jan 31 2009	K	61.93/35.49	120
V1118	Feb 1 2009	MW	60.58/37.00	240
V1331	Jul 24 2007	MW	61.12/37.05	120
V1331	Jul 24 2007	K	62.53/35.55	60
V1515	Jul 24 2007	MW	61.12/37.05	60
V1515	Jul 24 2007	K	62.53/35.55	60
V1735	Jul 24 2007	MW	61.12/37.05	60
V1735	Jul 24 2007	K	62.53/35.55	60
XZ Tau	Jan 31 2009	MW	62.12/37.05	60
XZ Tau	Jan 31 2009	K	61.93/35.49	60
Z CMa	Jan 31 2009	MW	62.12/37.05	60
Z CMa	Feb 1 2009	MW	60.58/37.05	60
Z CMa	Feb 1 2009	K	61.83/35.53	60

Table 2.1: Log of Spectroscopic Data Obtained

its median value along the artificially defined continuum. We then apply a desloping routine (this is optional). The spectra may have an inherent slope due to ice (CO or H_2O), a large spectral feature (such as those found in hydrogen), or due to the blackbody continuum. The spectra now must be wavelength calibrated. Each spectrum is compared to either a model or a standard star which has a proper wavelength solution already. The standard star was reduced using the model. The source spectra and the model or standard are matched as closely as possible. A residual is calculated after each iteration to guide in the minimization process. Each wavelength calibrated spectrum is then divided by the standard star and the ratio is taken as the finished spectrum, with a correction for the airmasses of the two observations taken into account. Any region of any spectrum where the transmittance of the atmosphere was under 50% has been automatically cut from the spectrum. Noise varies greatly in these regions and our science data is washed out by noise. Each spectrum is then stored in an IDL save file and plotted.

Chapter 3

Sources

3.1 Overview of Sources

Presented is a list of approximately 10 sources, some of which have been defined as FUor, EXor, or FUor-like (a source having similar visible and NIR spectra as a classic FUor, but one which has not undergone an outburst).

HR8518, or Gamma Aquarii, was used as the standard star for the 2007 observations. It is an A0V star (Chalonge & Divan, 1952).

V1057 Cygnus This star is one of the few bona-fide FU Orionis objects (if we define the class as having the properties of an active disk, with a light curve which has been observed to increase more than several magnitudes in a remarkably short period of time). Herbig (1977) first remarked on the the light curve and several spectroscopic properties similar to FU Orionis. The star took approximately 390 days to rise to its peak light, and has since declined in brightness. Herbig quotes a decline rate of 1.7 magnitudes over the first 6 years after peak light. This fading from an FUor is expected: FU Orionis' lightcurve also shows decay, albeit at a much slower rate (see light curves in the Introduction).

V1331 Cygnus V1331 Cygnus shows .5 $M_{\odot}$ circumstellar disk (Weintraub et al., 1991) which is embowered by a gas envelope approximately 6000 AU in size in its largest dimension. A bi-polar outflow and a gaseous ring (approxinately 10^4 AU, minimum mass of .07 $M_{\odot}$), which is expanding at approximately 22 km s^{-1}, have been detected (McMuldroch et al., 1993). This star was included in our sample because of its spectroscopic similarity to another source, V1057 Cygnus

Souce	*FUor*	*FUor-Like*	*EXOr*	*Reference*
RNO15...			X	Carr (1989)
V1118...			X	see Audard et al. (2010)
				see Lorenzetti et al. (2009)
XZ Tau...			X	see Lorenzetti et al. (2009)
PV Cep...			X	see Cohen et al. (1981)
Z CMa...		X	X?	Hartmann et al. (1989), Liskowsky et al. 2010 (in prep)
L1551 IRS5...	X		X?	Mundt et al. (1985); Carr et al. (1987)
				? Brittain et al. (2010)
AR6A...		X		Aspin & Reipurth (2003)
V1057 Cyg...	X			Herbig (1977)
V1331 Cyg...	*			McMuldroch et al. (1992)
V1515 Cyg...	X			Herbig (1977)
V1735 Cyg...	X			Elias (1978)

Table 3.1: A summary of our spectroscopic data. *V1331 is conjectured to be in a pre-FUor outburst state. A ? indicates a partial classification of a source based on data presented in this work and is not meant to be a definitive reclassification.

before it 'erupted'. Spectra of V1057Cyg taken pre-outburst (Herbig, 1958) show a striking similarity to V1331 Cygnus (Welin, 1976). The Ca II line at approximately 3393 $\mathring{A}$ is observed strongly in emission in both cases, and neutral hydrogen feature at 3968 $\mathring{A}$ is not observed in either.

V1515 Cygnus This source is also one of the few bona-fide FU Orionis objects in our sample. This star was first considered an FUor by Herbig (1977). While the time to maximum light on this star was much longer than in V1057 Cyg (it has a rise time on the order of a decade), it nonetheless brightened by 5.5 magnitudes. Several high velocity components of ejecta were observed spectroscopically. Its spectra currently suggest an active disk of an accreting star.

V1735 Cygnus This source was shown to brighten from below 20th magnitude to 15th magnitude in the R band from 1952 to 1975 (Elias, 1978). In the optical, the source appears to resemble an F or G supergiant. H α has a P-Cygni profile, while water and CO are in absorption. These photometric and spectroscopic categorizations identify this source as an FUor.

HR3888 We used HR3888, or Upsilon Ursae Majoris, as our standard star. HR3888 is a delta scuti star (Eggen, 1956) of type F2IV (Breger, 1969). This standard exhibits a broad Br γ absorption feature, hence for spectroscopic data reductions done in the K band order 35 (the order which contains Br γ) we have used a spectral synthesis program to ratio our spectra.

RNO 15 RNO 15 shows CO absorption (Carr, 1989).

V1118 Orionis This source is a resolved binary (Reipurth et al., 2007) which shows frequent

variability in its luminosity (Audard et al., 2010), having outburst as recently as 2007. Herbig (2008) notes a strange variability in Li I line at 6707 $\mathring{A}$; during the 2007 outburst the line was in emission, and after the outburst (while in quiescence) the feature was seen in absorption. Additionally, H α was shown to have a P-Cygni profile during the outburst, which, after the outburst, was not seen. Clearly, there is something specific about the accretion event that causes an observational change.

AR6A This source is a member of NGC 2264, a star forming region in Monoceros. Aspin & Reipurth (2003) reported photometric and spectroscopic data on this object, as well as several near-by objects (labeled AR6B and AR6C). Spectroscopically, AR6A showed overtone CO absorption and Br γ absorption. Neutral sodium and calcium lines were also reported in absorption, albeit weakly. Curiously, our spectra do not match those taken by Aspin and Reipurth. Our spectra do not show strong CO bandhead absorption, but rather weak bandhead absorption, as well as weak Br γ absorption. The 2 μm data (overtone region) also show numerous additional emission and absorption features not part of the band structure. Additionally, we see the high J fundamental lines strongly in absorption. Aspin & Reipurth (2003) reports an absorption bandhead feature at about 5 percent below the continuum, while our bandhead absorption feature is at about the 10 percent level, but there is no obvious bandhead structure. The time between observations is approximately 6 years, which is not an inconceivable timescale of variability for these systems. Possible explanations of this effect are a change in magnitude of AR6A or a change in the veiling of the CO overtone lines.

The identification as an FUor candidate was based on spectroscopic evidence (bandheads in absorption, Br γ absorption) and photometric evidence (NIR excess), as well as being associated with reflection nebulosity and having spectroscopic features presumably generated by a low surface gravity environment (indicative of a disk atmosphere).

XZ Tau The double (possibly triple) star system XZ Tau (Cohen & Kuhi, 1979; Carrasco-González et al., 2009) has been quite well-studied. Krist et al. (1999) shows the ejection of material from this system in the form of a bubble with knots, presumably a nascent Herbig Haro object, with the first discovery of outflowing material by Mundt et al. (1988). Kenyon et al 1998 identified this as a Class II source, having strong Br γ emission. The binary is separated by 0".3 at a distance of 140 pc (Haas et al., 1990; Elias, 1978B).

L1551 IRS 5 This is also a well-studied object. It was first identified as a FUor (or more appropriately, FUor-like) by Mundt et al. (1985) using the P-Cygni structure of the Hα line while Carr et al. (1987) showed using low resolution near infrared spectroscopy that the CO rovibrational

overtone bandheads as well as water vapor features were in absorption, implying an active disk. The estimated accretion rate is $2 \times 10^{-6} M_{\odot} yr^{-1}$ (Osorio et al., 2003), which is low for an FUor (Hartmann & Kenyon, 1985). More recently, this object has shown remarkable spectroscopic characteristics (Brittain et al., 2010). Our data indicate that the overtone CO spectra have an overall redshift of approximately 1 kayser, where 1 kayser is defined to be $1 cm^{-1}$. At this energy this corresponds to an overall redshift of 70 km s^{-1}, while the fundamental CO lines show strong emission and are shifted by an overall amount of approximately 0.5 kaysers, corresponding to a overall redshift of approximately 70 km s^{-1}, hence these two CO features are coming from the same place in velocity space. Whether this shift implies a real correspondence to a locality is uncertain. Interestingly, the CO in the overtone energy range is broadened by (say, has a FWHM) 1 kayser. The fundamental lines on the other hand have a FWHM of approximately 0.25 kaysers. If these lines both emanate from the inner disk, then they are effectively broadened by the same turbulent value. If these lines are rotationally broadened, then it becomes obvious that the overtone lines are originating much closer to the star than the fundamental lines. It is possible that the emission lines are a result of a passive disk in the outer regions of the disk, while the inner portion of the disk is active, showing absorption. The existence of the transition region is unclear at the present, however a more extensive study of L1551 may show an unambiguous detection of this supposed superposition of disk prototypes.

PV Cep This source has shown remarkable variability over the short period of time it has been observed. An outburst which brightened the source from 16th to 11th magnitude between 1977 and 1978 (Cohen et al., 1981). This classified as an EXor and not an FUor at this point because of the lack of the disappearance of specific emission lines - a phenomenon indicative of the small sample of FUors at the time. Lorenzetti et al. (2009) show a remarkable variability in the brightness of this source as well as in several typical molecular lines (CO, H) over many years of observation.

Chapter 4

Results

4.1 Data Reduction Results - Ratios of Spectra

These are the combined results of the data reduction process. The table below attempts to succinctly summarize the spectroscopic data obtained from 2007 to 2009. These exists a strange discrepancy in Z CMa and PVCep. For the case of Z CMa, there is fundamental absorption in the CO ro-vibrational band, however, it clearly shows emission in the ro-vibrational 2-0 bandheads. For an active disk interpretation, this needs to be explained. A detection of the bandheads for this source would lead to a false conclusion regarding its status as an FUor.

The source AR6A fits the mold for an FUor and an active disk; all energy ranges have CO in absorption. The source XZ Tau is confusing as well. For an EXor we would expect to see Brackett γ in emission,which it is, however we clearly see evidence for an active disk in the CO measurements. Observations of the bandheads would classify this object as an FUor, where these data suggest it is a combination of an active and passive disk.

The data from V1118 Ori are very noisy, and the spectra are inconclusive. It appears that the Brackett γ emission fits with its classification as an EXor, as well as the (tentative) emission seen in the fundamental band.

As in Z CMa, PV Cep shows a strange dual spectrum; the fundamental bands are in absorption and the overtone bands are in emission. Brackett γ is also in emission, further complicating its spectroscopic interpretation. The fact that these two objects are classified as an FUor and EXor, respectively, indicate a need to reconsider their initial classification.

Source	*CO Fund*	*CO Fund*	*CO Overtone*	*CO Over*	$Br\gamma$	*Status in literature*
AR6A...	A	A	A	A	A	FUor-Like
RNO15...	-	A	A	A	A	EXor
V1118...	E?	E?	-	-	E	EXor
XZ Tau...	A	A	A	A	E	EXor
Z CMa...	A	A	E	E	E	FUor-like
PV Cep...	A	A	E	E	E	EXor
V1057 Cyg...	A	A	A	A	A	FUor
V1331 Cyg...	E	E	A/E	E	E	FUor*
V1515 Cyg...	A	A	A/E	A	-	FUor
V1735 Cyg...	A	A	A/E	A	A?	FUor
L1551 IRS5...	?	E	A/E	A	-	FUor-like

Table 4.1: Summary of spectroscopic data. "A" stands for absorption, "E" for emission. Several spectra show absorption and emission features and are labeled accordingly. The first CO fundamental is approximately at 1990 to 2020 wavenumbers, while the second CO fundamental column spans approximately 2120 to 2150 wavenumbers. The first CO overtone column spans 4215 to 4270 wavenumbers, while the second CO overtone column spans 4345 to 4400 wavenumbers. The $Br\gamma$ feature is centered at approximately 4619 wavenumbers. *V1331 Cyg is conjectured to be in a pre-FUor outburst state. Question marks (?) indicate an uncertain emission or absorption classification.

V1331 Cyg shows emission in all measured bands. This source looks very much like an EXor, while V1515 Cyg, V1057 Cyg and V1735 Cyg all look like their FUor classification.

The main conclusion that should be drawn is that simple measurements of bandheads in absorption in low-resolution studies are not sufficient to classify these objects are active or passive disks (or as FUor and EXors). Before large scale surveys are to take place, it is very much necessary to understand these specific young systems and any spectroscopic properties they have before any large scale surveys take place which seek to understand the role of accretion in early stellar evolution.

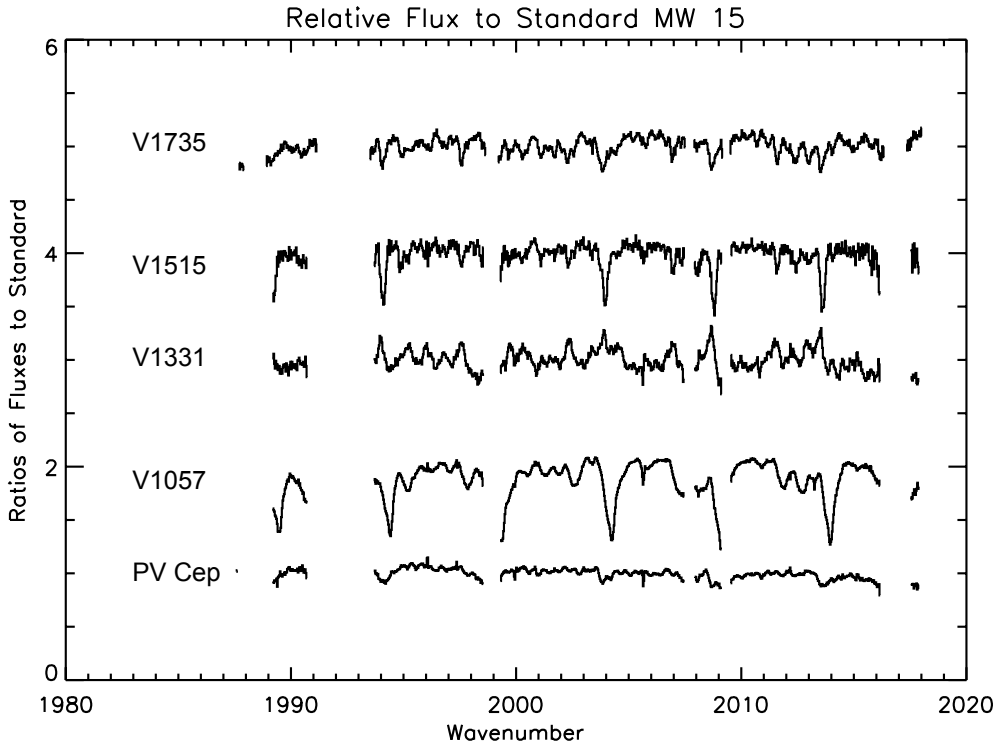

Figure 4.1: Spectra for MW order 15, data from 2007.

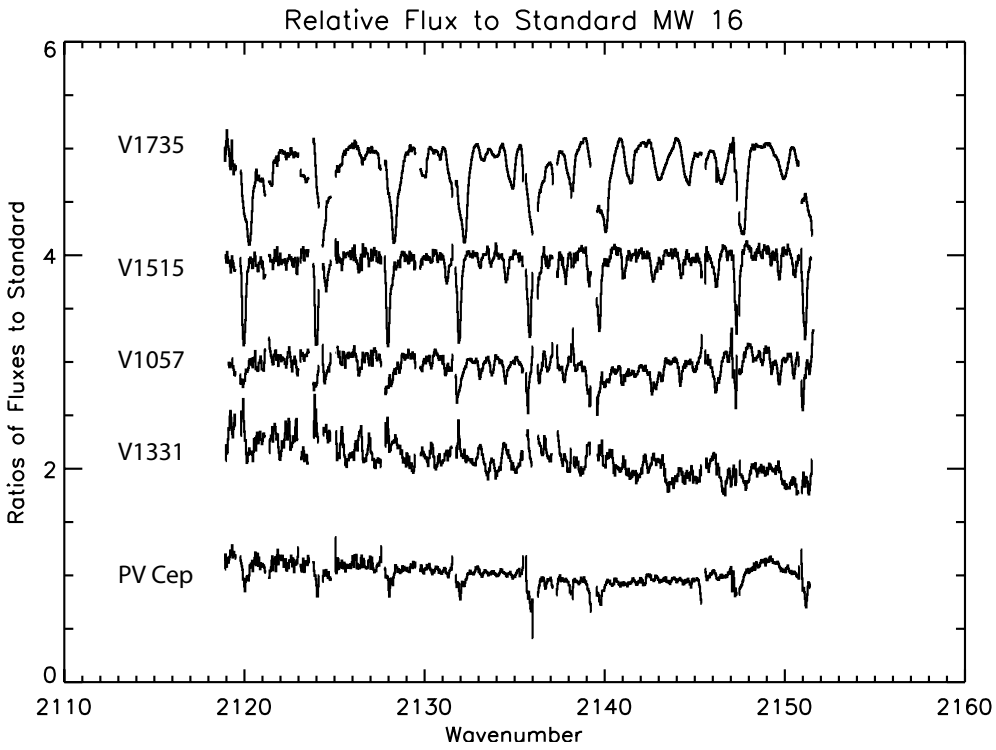

Figure 4.2: Spectra for MW order 16, data from 2007.

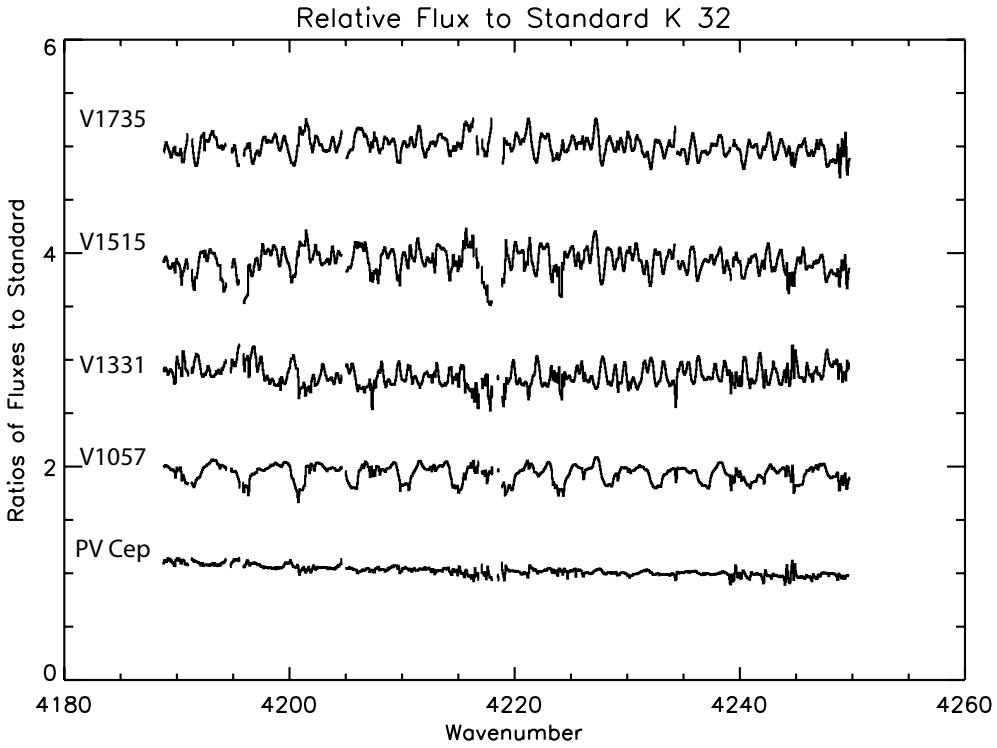

Figure 4.3: Spectra for K order 32, data from 2007.

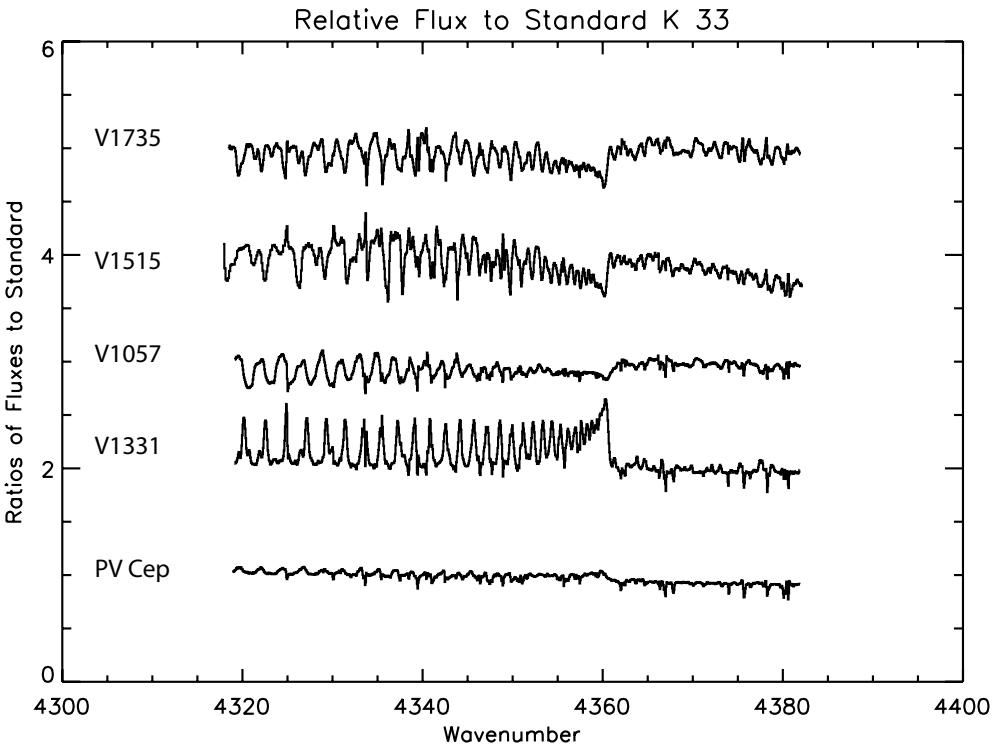

Figure 4.4: Spectra for K order 33, data from 2007.

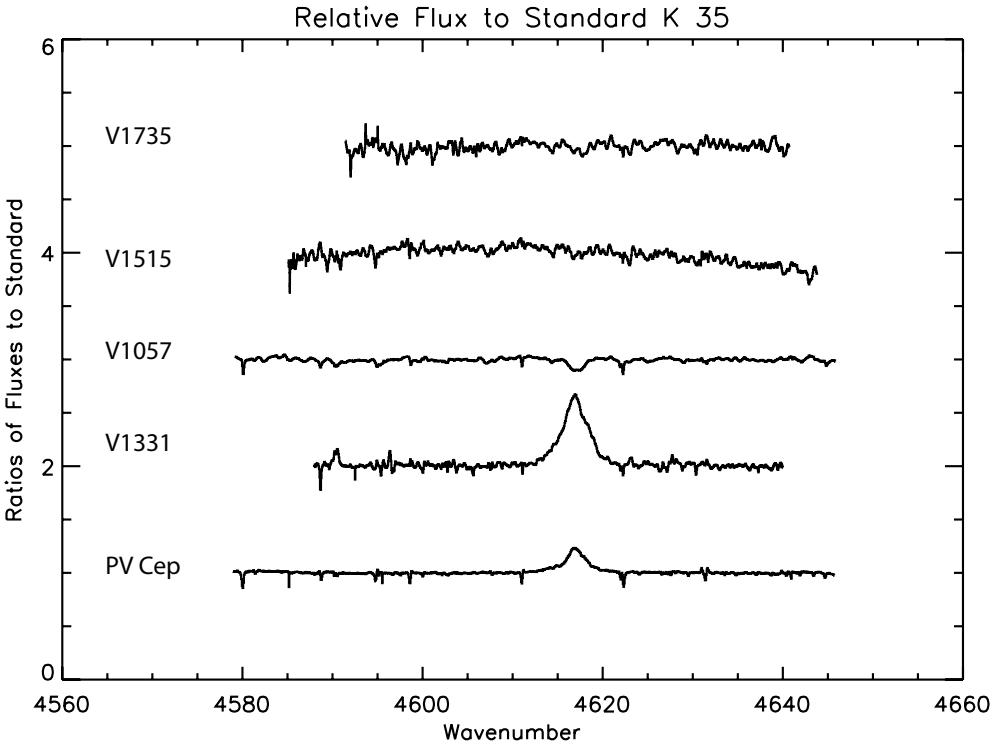

Figure 4.5: Spectra for K order 35, data from 2007.

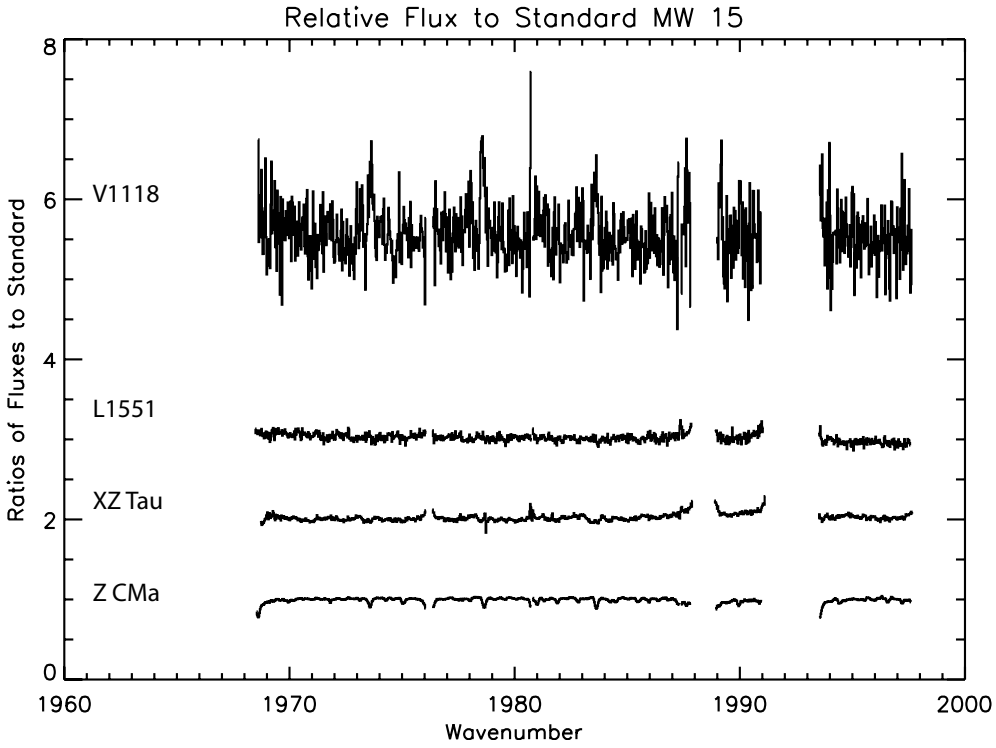

Figure 4.6: Spectra for MW order 15, data from 2009.

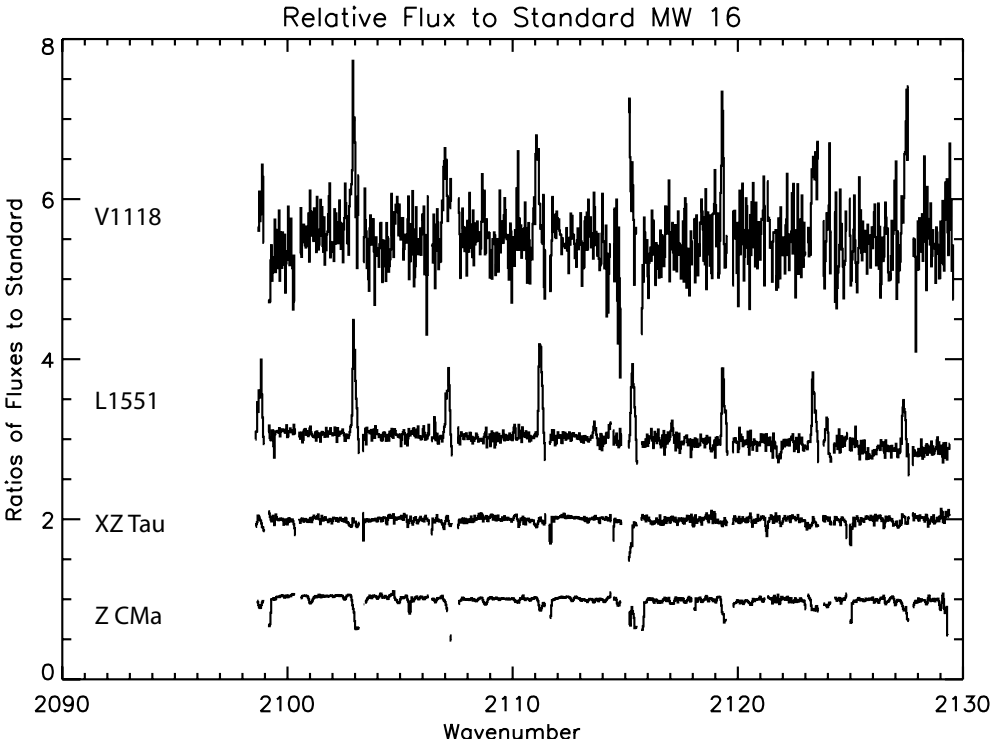

Figure 4.7: Spectra for MW order 16, data from 2009.

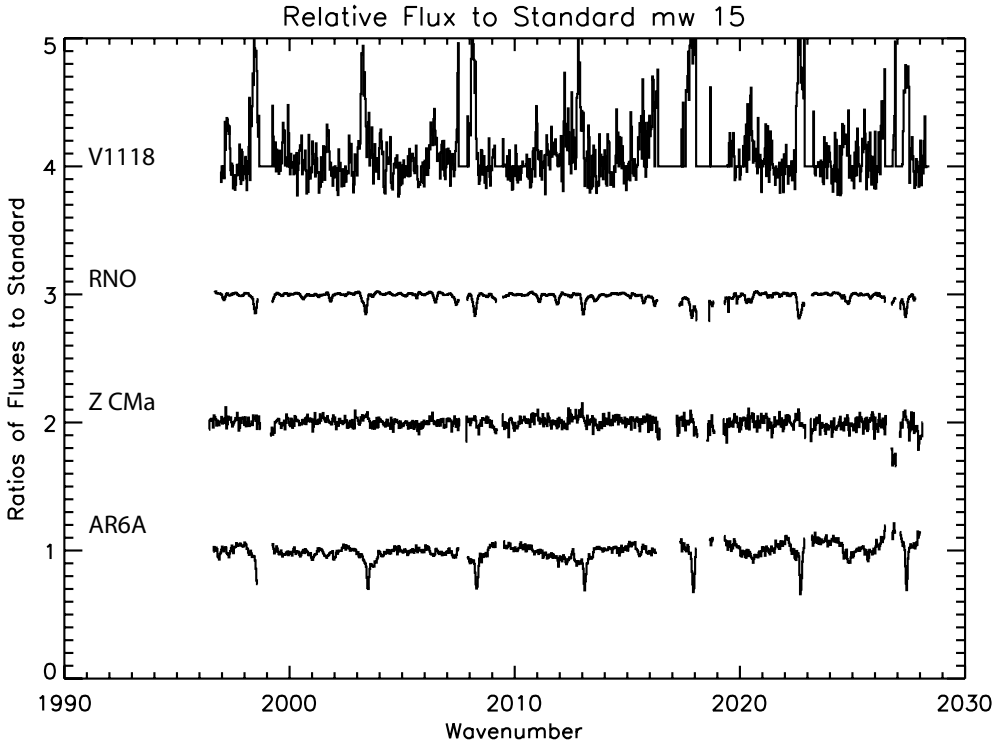

Figure 4.8: Spectra for MW(2) order 15, data from 2009.

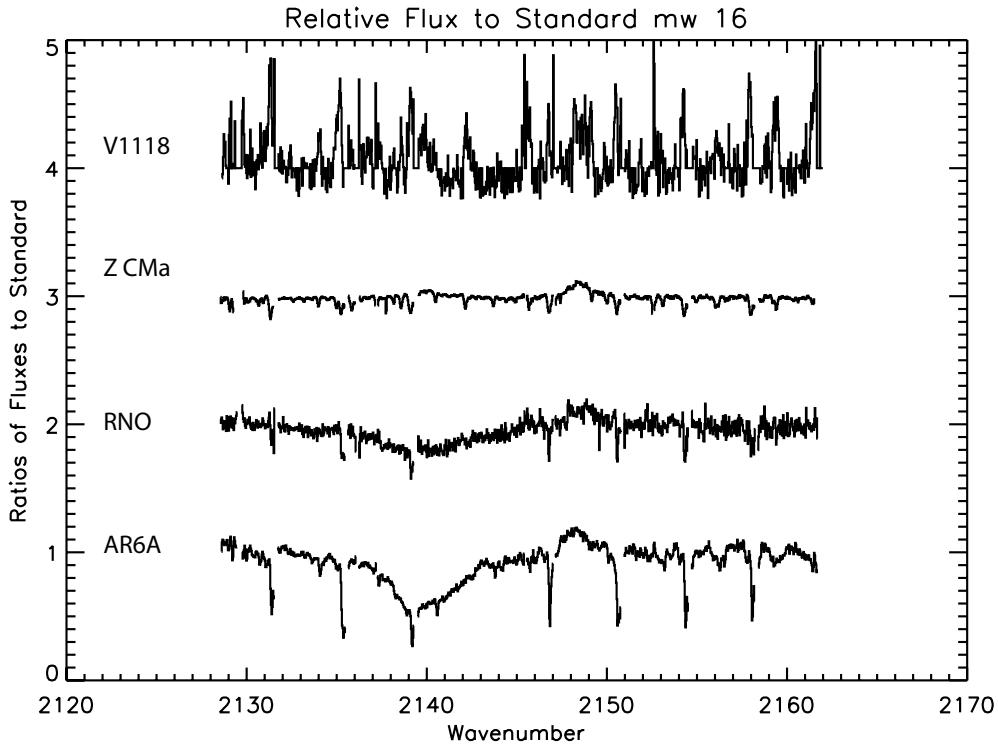

Figure 4.9: Spectra for MW(2) order 16, data from 2009.

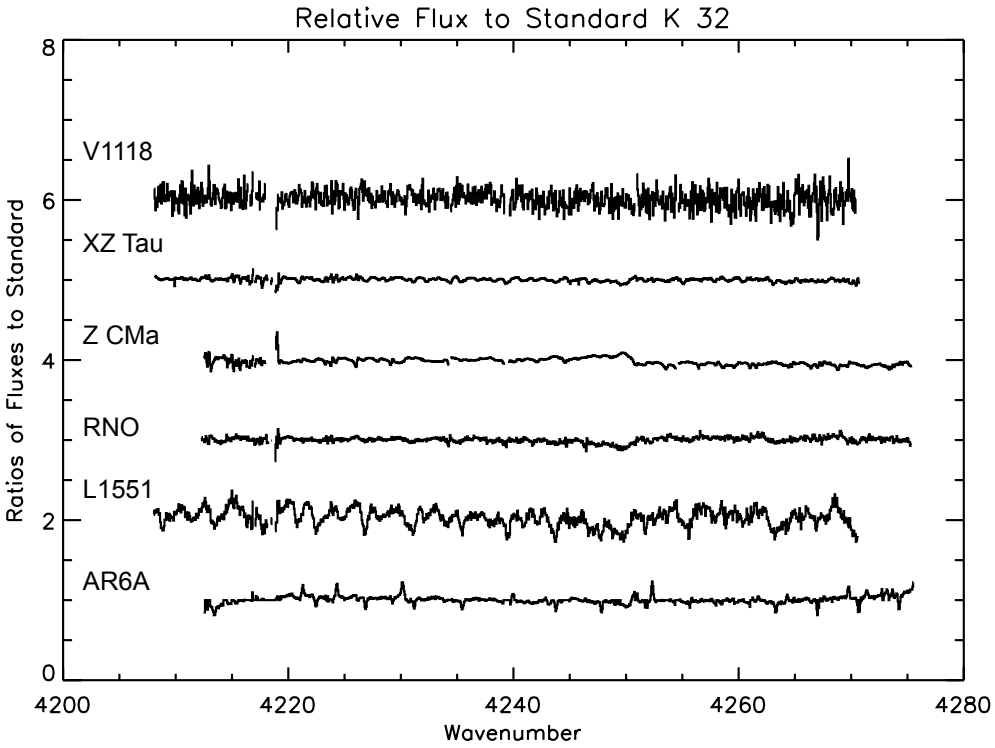

Figure 4.10: Spectra for K order 32, data from 2009.

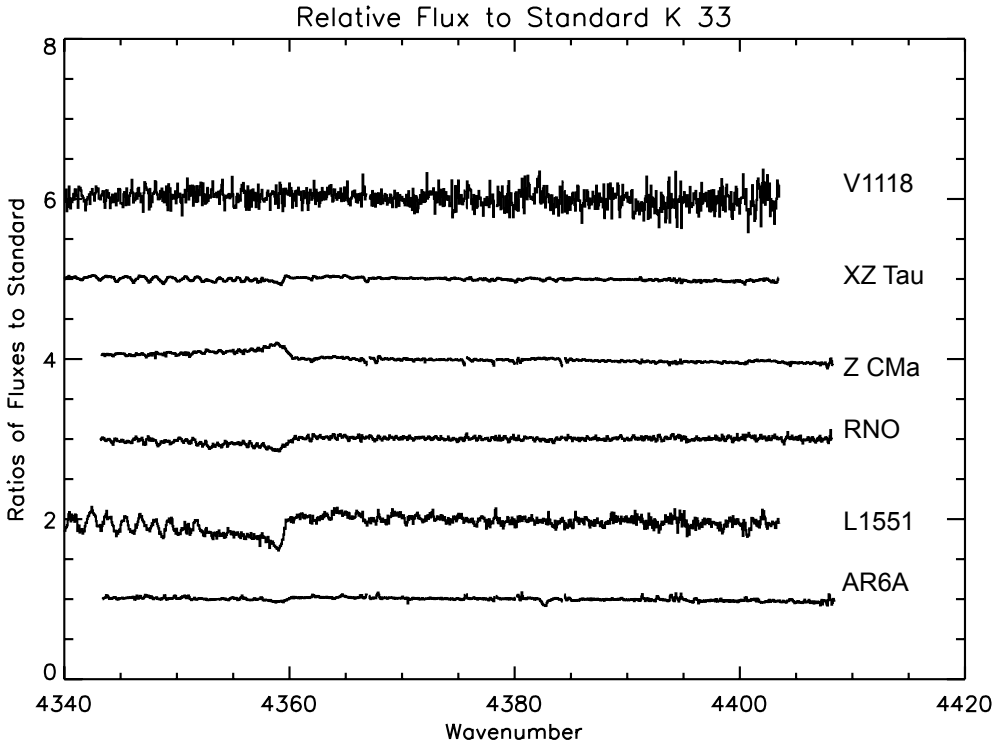

Figure 4.11: Spectra for K order 33, data from 2009.

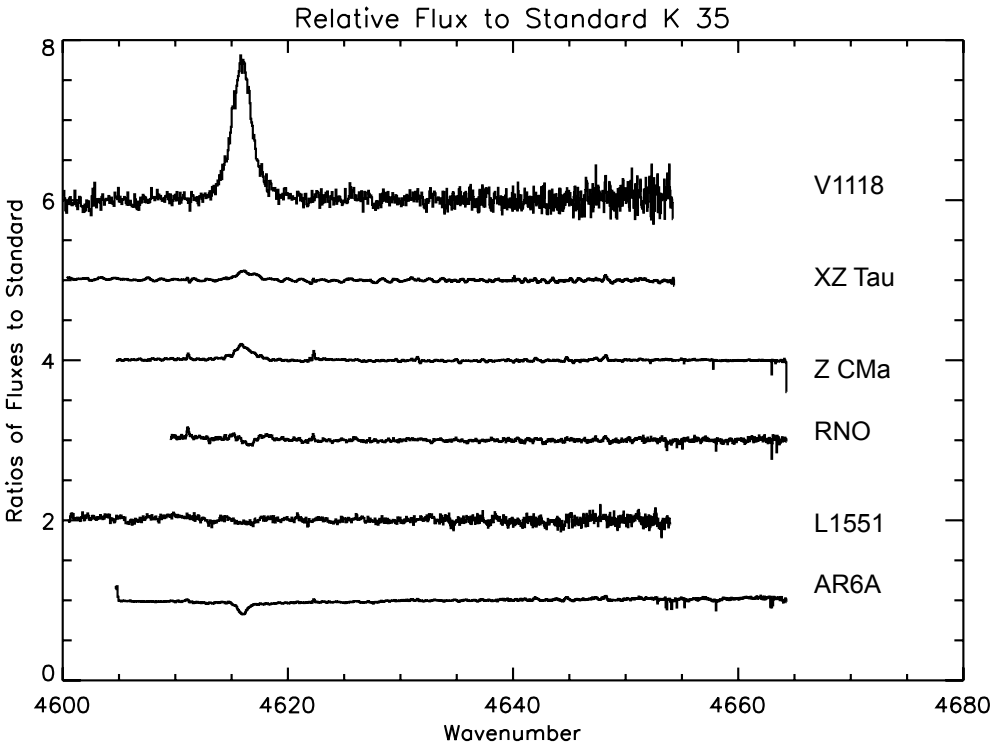

Figure 4.12: Spectra for K order 35, data from 2009.

4.2 Cross Correlation Results

We calculate the cross correlations of each source in each order. Not all correlations were calculated because the 2007 data and 2009 data did not have a significant overlap. Hence, the correlations were only calculated within each year. The R values are presented here.

Each cross correlation is given by the equation

$$r(l) = \frac{\sum_{i=0}^{n}(sa(i-l)-ma) \times (sb(i-l)-mb)}{\sqrt{\sum_{i=0}^{n}(sa(i-l)-ma)^2}\sqrt{\sum_{i=0}^{n}(sb(i-l)-mb)^2}}. \tag{4.1}$$

Currently, the R values are being calculated by finding the height of the cross correlation peak within the interval -100 km s^{-1} to 100 km s^{-1}, which is then divided by the standard deviation of the rest of the cross correlation (the region outside the previously mentioned interval) and $\sqrt{2}$. This closely models the prescription given in Tonry & Davis (1979), where the authors carried out spectroscopic observations of galaxies, but the principle is transferable. The calculation of a cross-correlation function indicates the similarity between two spectra (or discrete sequences). A positive correlation value indicates that the spectra tend to vary together. The R values quantify the similarity between two spectra as well as make comparisons as simple as reading a table of numbers, instead of having to compare many spectra.

In the 2007 data, the M band order 15 R values presented for indicate that PVCep looks much more like the sample of included (classic) FUors. The source V1331 Cygnus has a similarity to PVCep, but a strong dissimilarity to the FUors. And, the order 16 wavelength range essentially says the same thing as the wavelength coverage of order 15: PVCep looks like the FUors and V1331 Cyg looks like none of the others. We remember that PVCep was classified as an EXor, and in the fundamental CO band it looks more like an FUor, that is, it looks like it has an active disk. This is fascinating considering the K band data which show that PVCep doesn't really look like any of the other sources, while maintaining the clear distinction between the classic FUor sample and the EXor V1331 Cygnus. Looking at the spectra this makes sense because we see the CO bandheads in (weak) emission in PV Cep and in strong emission in V1331 Cyg. The FUor sample exhibits typical active disk features with the CO bandheads in absorption. The Brackett γ line shows weak emission from PVCep, and strong emission from V1331. It would appear that the higher the energy of the transition, the more PV Cep looks like V1331 Cyg.

Source	***PVCep***	***V1057***	***V1331***	***V1515***	***V1735***
PVCep...	15.73	5.866	3.381	10.22	2.106
V1057...	X	12.49	-3.028	7.725	5.383
V1331...	X	X	15.18	-5.601	-9.381
V1515...	X	X	X	12.94	8.165
V1735...	X	X	X	X	14.46

Table 4.2: Summary of R Values for MW 15 2007

Source	***PVCep***	***V1057***	***V1331***	***V1515***	***V1735***
PVCep...	11.16	4.541	1.960	5.941	8.264
V1057...	X	20.36	-1.918	11.31	9.884
V1331...	X	X	17.35	-4.590	-1.857
V1515...	X	X	X	15.76	10.28
V1735...	X	X	X	X	16.52

Table 4.3: Summary of R Values for MW 16 2007

Source	***PVCep***	***V1057***	***V1331***	***V1515***	***V1735***
PVCep...	12.06	1.579	2.377	0.8342	1.174
V1057...	X	2.957*	-2.130	2.701	2.786
V1331...	X	X	19.22	-10.37	-10.70
V1515...	X	X	X	12.57	9.280
V1735...	X	X	X	X	16.40

Table 4.4: Summary of R Values for K 32 2007. * Multiple correlation peaks within the cross correlation function reduce the R value. This cross correlation is actually quite strong: something not indicated by the R value.

Source	***PVCep***	***V1057***	***V1331***	***V1515***	***V1735***
PVCep...	10.41	-6.846	7.172	4.256	-6.264
V1057...	X	3.637*	-3.855	-1.641	3.053
V1331...	X	X	9.597	1.740	-7.382
V1515...	X	X	X	8.055	2.322
V1735...	X	X	X	X	9.316

Table 4.5: Summary of R Values for K 33 2007. * Multiple correlation peaks within the cross correlation function reduce the R value. This cross correlation is actually quite strong: something not indicated by the R value.

Source	***PVCep***	***V1057***	***V1331***	***V1515***	***V1735***
PVCep...	4.615	-2.920	4.756	2.669	3.793
V1057...	X	10.93	-3.396	-1.782	0.8250
V1331...	X	X	6.592	1.419	1.144
V1515...	X	X	X	9.504	1.786
V1735...	X	X	X	X	123.8

Table 4.6: Summary of R Values for K 35 2007

In the 2009 data, L1551 looks very much like V1118 in the fundamental CO lines, while Z CMa looks very much like XZ Tau. Because of the noise of the V1118 Ori spectra, the R values for this observing run may not as clearly correspond to a comparison of the spectra as the 2007 R values to their spectra. V1118 Ori, AR6A, Z CMa and RNO 15 all show emission in Pfund β, yet AR6A and RNO 16 show Brackett γ in absorption (as well as L1551, however we do not have Pfund β coverage for this source). The other sources show emission in Brackett γ. Also, there exist some CO ice features near 2140 kaysers in several stars. Because the ice cannot exist in the disk, their existence and variability between sources is probably best explained by interstellar CO ice. Regardless, these data are quite peculiar. In this set, we observed four sources classified as EXors: V1118 Ori, XZ Tau, RNO 15 and PV Cep. Three objects do not have the spectroscopic characteristics of an EXor. RNO 15, XZ Tau, and PV Cep all have fundamental CO absorption. If we have a high enough resolution spectrograph and measure these lines to be in absorption, we would expect to see the bandheads in absorption as well. Of these three sources, we only find that this is true for RNO 15 and XZ Tau. Regardless of the fact that these observations may indicate the presence of a active disk, we are stuck with the unfortunate puzzle of trying to explain the source PV Cep. It shows absorption in the fundamental CO lines and emission in the overtone lines (2-0, 4-2 bandheads). The source Z CMa also shows the same strange spectroscopic features. As if this weren't enough, both sources (PV Cep and Z CMa) show a Brackett γ line in emission. If either of these were purely active disks, we would expect to see the Brackett γ line in weak absorption.

Additionally, the source L1551 is strange, but explainable if strong emission is coming from an outer part of the disk which is passively reradiating stellar photons (which are not strong enough to excite the overtone transitions sufficiently to show overall emission), while the inner part of the disk is causing absorbing in the fundamental transitions as well the overtone transitions. This theory should be tested by the modeling of a disk with a transition region between active and passive.

We now have at least two examples of YSOs that, if a low resolution survey were to take place which measured the overtone lines looking for active disks in an attempt to measure accretion rates, would be missing extra sources which may be active disks. It becomes very clear that the work of the theorist is not done regarding the interpretation of L1551, Z CMa, and PV Cep, and possibly, the identification of FU Orionis objects by the overtone lines showing up in absorption is not a sufficient NIR criterion. If we expect to solve the luminosity problem by invoking FU Orionis events as a major contributor to the final mass of these T-Tauri stars, it becomes imperative to

create a list of spectroscopic diagnostics which unambiguously identify these sources as the high mass accretors we need them to be to solve the problem.

Source	***L1551***	***V1118***	***XZTau***	***ZCMa***
L1551...	17.26	0.9383	3.138	-1.239
V1118...	X	21.29	-3.323	-5.255
XZTau...	X	X	32.77	-5.178
ZCMa...	X	X	X	10.01

Table 4.7: Summary of R Values for MW 15 2009

Source	***L1551***	***V1118***	***XZTau***	***ZCMa***
L1551...	22.53	8.021	-6.023	-10.87
V1118...	X	17.93	-4.405	-5.759
XZTau...	X	X	27.75	8.470
ZCMa...	X	X	X	29.03

Table 4.8: Summary of R Values for MW 16 2009

Source	***AR6***	***RNO***	***V1118***	***ZCMa***
L1551...	22.57	-9.454	-7.272	5.646
V1118...	X	21.32	-2.248	3.188
XZTau...	X	X	15.23	-7.637
ZCMa...	X	X	X	11.51

Table 4.9: Summary of R Values for MW2 15 2009

Source	*AR6*	*RNO*	*V1118*	*ZCMa*
L1551...	15.68	11.780	-2.246	6.437
V1118...	X	13.99	2.009	2.229
XZTau...	X	X	10.61	-2.406
ZCMa...	X	X	X	8.119

Table 4.10: Summary of R Values for MW2 16 2009

Source	*AR6*	*L1551*	*RNO*	*V1118*	*XZTau*	*ZCMa*
AR6-N	15.90	-1.592	4.942	3.307	4.269	-1.527
L1551-K...	X	10.79	9.314	2.922	7.705	-3.344
RNO-N	X	X	17.14	1.419	2.710	-4.515
V1118-K	X	X	X	20.85	2.5770	1.799
XZTau-K	X	X	X	X	11.44	-1.368
ZCMa-N	X	X	X	X	X	7.961

Table 4.11: Summary of R Values for K 32 2009

Source	*AR6*	*L1551*	*RNO*	*V1118*	*XZTau*	*ZCMa*
AR6-N	8.467	4.044	4.959	2.130	4.367	-4.906
L1551-K...	X	8.47	5.790	-6.306	6.653	-5.692
RNO-N	X	X	7.206	-4.626	4.441	-6.721
V1118-K	X	X	X	13.89	2.220	7.027
XZTau-K	X	X	X	X	9.832	-3.102
ZCMa-N	X	X	X	X	X	7.891

Table 4.12: Summary of R Values for K 33 2009

Source	*AR6*	*L1551*	*RNO*	*V1118*	*XZTau*	*ZCMa*
AR6-N	10.77	-2.376	1.254	-5.846	-6.360	-4.859
L1551-K...	X	18.03	0.4037	-0.8404	1.116	0.9990
RNO-N	X	X	30.93	3.234	1.487	1.803
V1118-K	X	X	X	6.425	5.515	5.719
XZTau-K	X	X	X	X	6.371	6.308
ZCMa-N	X	X	X	X	X	7.290

Table 4.13: Summary of R Values for K 35 2009

Appendices

Appendix A Appendix A

I used the following code to calculate the cross correlations of two idl save files. These save files contained all the relevant reduced data for an object.

```
;this will cross correlate two spectra

;first, find the mean of each ra and rb
if counta gt 0 then begin
meana = double(0.)
meanb = double(0.)
meancounta = double(0.)
meancountb = double(0.)
disp = double(0.)
dispcount = double(0.)


for i = 0,counta-1 do begin
if (finite(ra(i)) eq 1) then begin
meana = meana + ra(i)
meancounta = meancounta + 1.
endif
if (finite(rb(i)) eq 1) then begin
meanb = meanb + rb(i)
meancountb = meancountb + 1.
endif
;what is the dispersion per pixel? find the average
if (i gt 0) then begin
if ((finite(fa(i)) eq 1) and (finite(fa(i-1)))) then begin
disp = disp + (fa(i) - fa(i-1))
dispcount = dispcount + 1.
endif
endif
endfor
meana = meana/meancounta
meanb = meanb/meancountb
if (dispcount gt 0.) then begin
disp = disp/dispcount
endif
```

```
endif


rbhere = 0


for lag = 0, counta - 1 do begin
topa = double(0.)
bota = double(0.)
botb = double(0.)
; r is the cross correlation here (this lag)
;compare both arrays of data
for j = 0,counta-1 do begin ;for this lag, for each element of each spectra, find the cross
correlation r
if (j - lag) ge 0 then begin
rbhere = j-lag
endif else begin
rbhere = counta - 1 + (j-lag)
;rbhere = j - lag
endelse
if ((finite(ra(j)) eq 1) AND (finite(rb(rbhere)) eq 1)) then begin
topa = topa + (ra(j)-meana)*(rb(rbhere)-meanb)
bota = bota + (ra(j)-meana)^2.
botb = botb + (rb(rbhere)-meanb)^2.
endif
endfor
bota = bota·5
botb = botb·5


if (bota gt 0.) and (botb gt 0.) then begin
r(lag) = topa/(bota*botb)
endif
endfor


;now, we have to take r and plot it over a useful range.
;let's do + or - 500 km/s
maxcor = double(500.)
```

```
;what is the average wavenumber?
avewavenumber = double(0.)
avenum = double(0.)
for i = 0,counta-1 do begin
if (finite(fa(i)) eq 1) then begin
avewavenumber = avewavenumber + fa(i)
avenum = avenum + 1.
endif
endfor
if (avenum gt 0.) then begin
avewavenumber = avewavenumber/avenum
endif
numofpixtomax = fix((maxcor/2.99792d5)*avewavenumber/abs(disp))

;so now we translate this to mean something for our r plot.
tophalf = dblarr(numofpixtomax)
lowerhalf = dblarr(numofpixtomax)

tophalf = r(0:numofpixtomax-1)
lowerhalf = r(counta-1-numofpixtomax:counta-1)

cor = dblarr(numofpixtomax+numofpixtomax)
cor(0:numofpixtomax-1) = lowerhalf(0:numofpixtomax-1)
cor(numofpixtomax:numofpixtomax + numofpixtomax -1) = tophalf(0:numofpixtomax-1)

;now we have to create a velocity shift array
vf = dblarr(numofpixtomax+numofpixtomax)
vf = dindgen(numofpixtomax+numofpixtomax)
vf = vf - double(numofpixtomax)
vf = vf*abs(disp)
vf = vf*2.99792d5/avewavenumber

indexpeak = where(vf ge -100.0 and vf le 100.0);take-100 to 100, out of -400 to 400
indexdev = where((vf lt -100.0 and vf gt -300.00) or (vf gt 100.0 and vf lt 300.00))

sss = stddev(cor(indexdev)*(2.^5))
```

```
h = max(abs(cor(indexpeak)))/sss
hwhere = where(h eq abs(cor)/sss)
if (cor(hwhere) lt 0.) then h = -h
```

Appendix B Reduced Spectra for AR6A

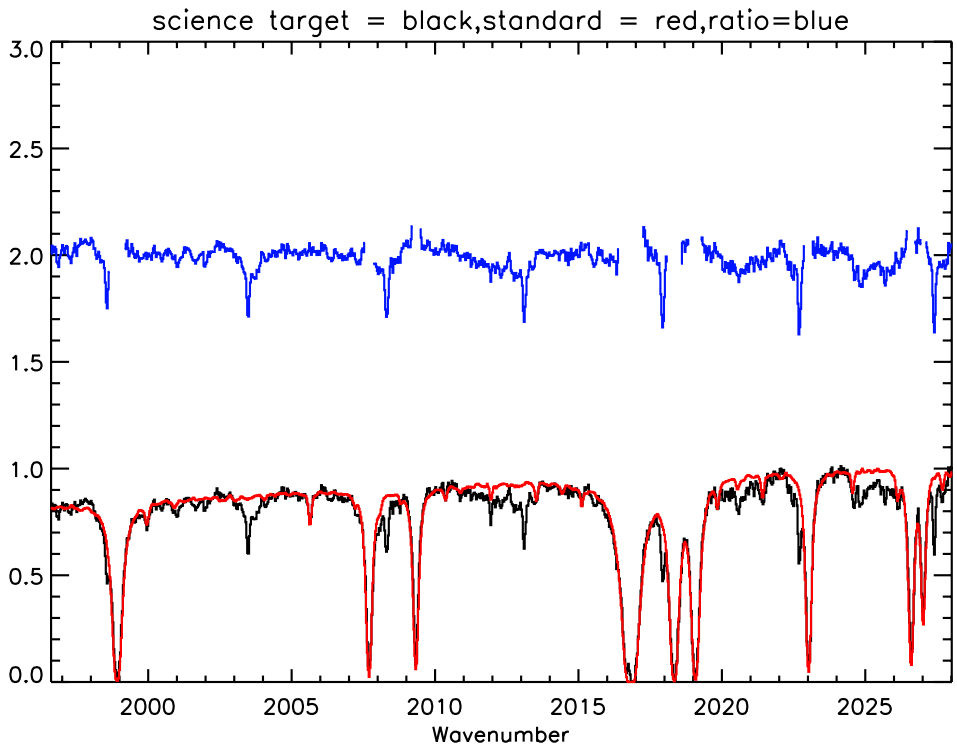

Figure 13: Spectra for AR6A order MW(2) 15, data from 2009.

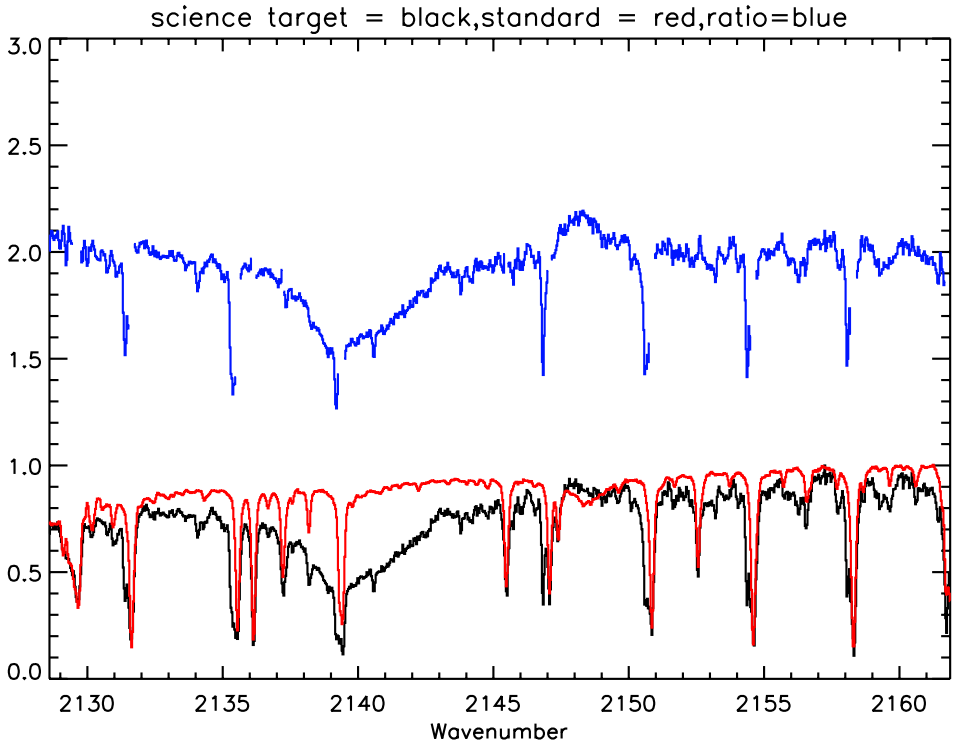

Figure 14: Spectra for AR6A order MW(2) 16, data from 2009.

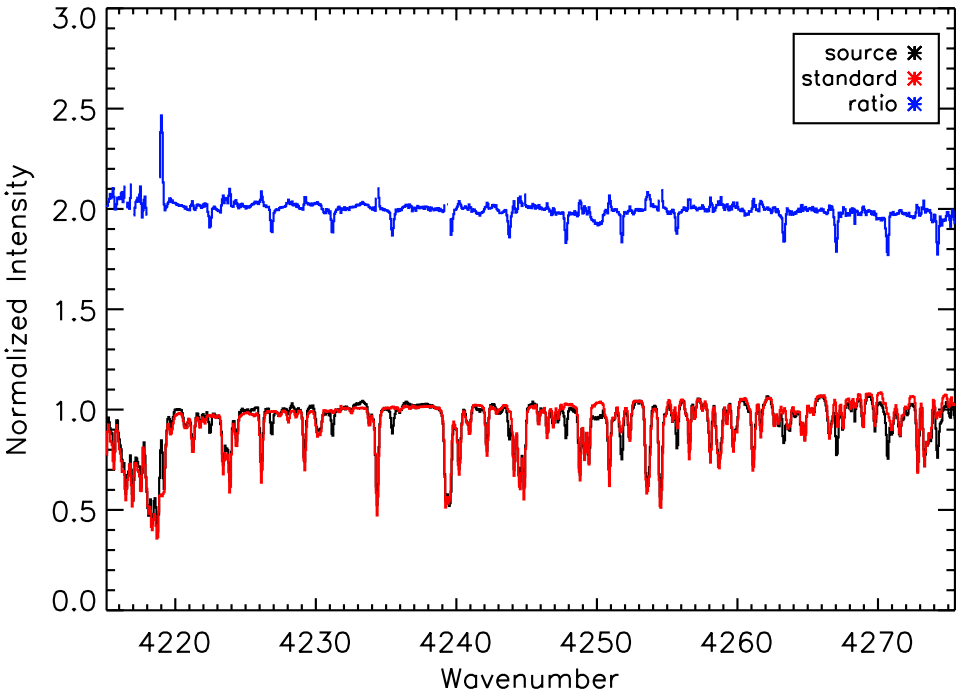

Figure 15: Spectra for AR6A order K 32, data from 2009.

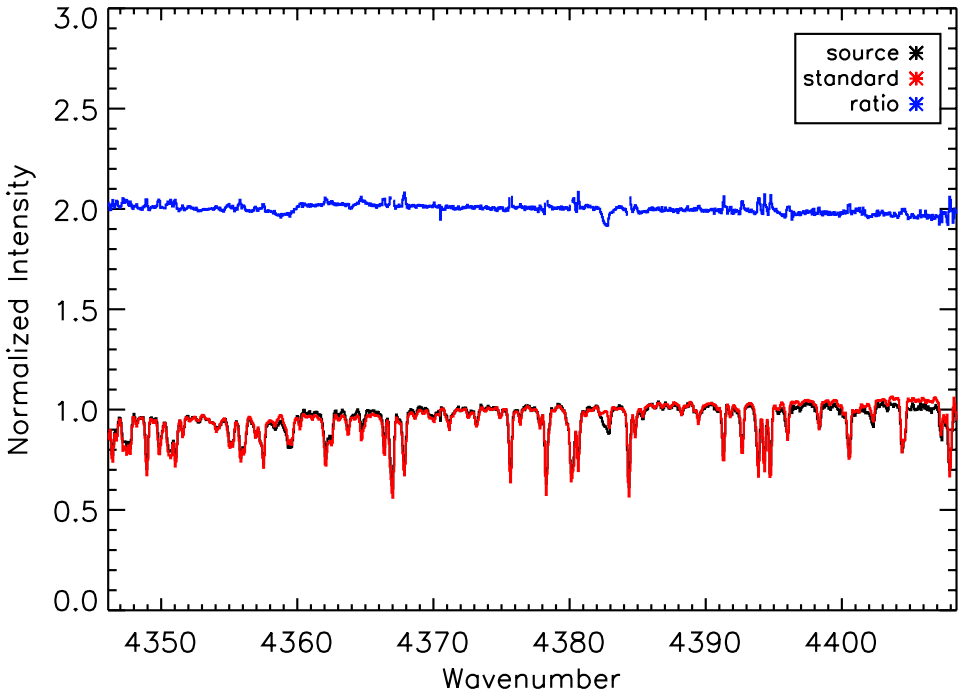

Figure 16: Spectra for AR6A order K 33, data from 2009.

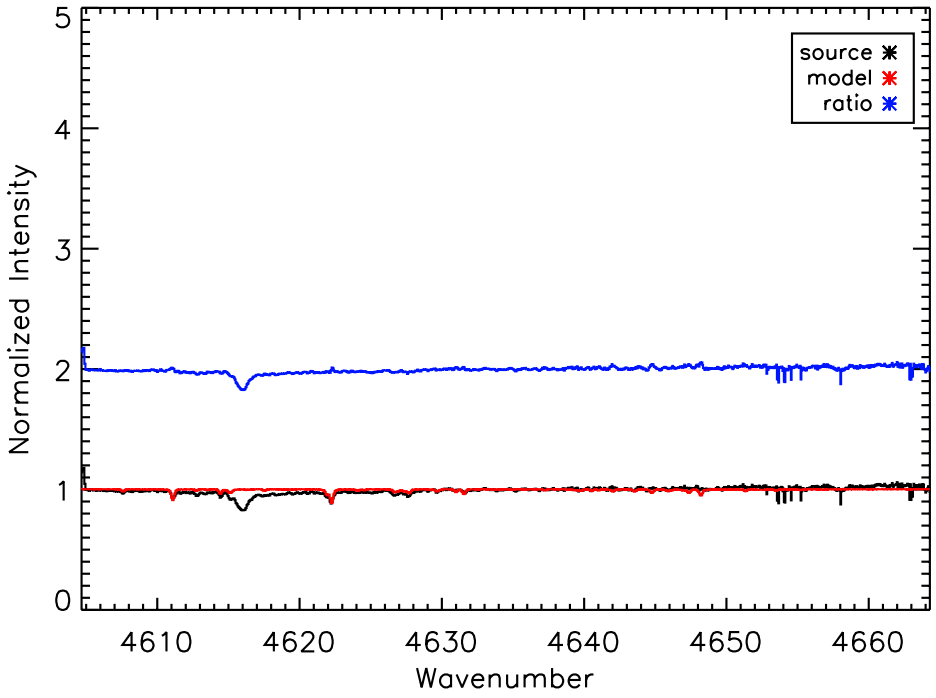

Figure 17: Spectra for AR6A order K 35, data from 2009.

Appendix C Reduced Spectra for L1551 IRS5

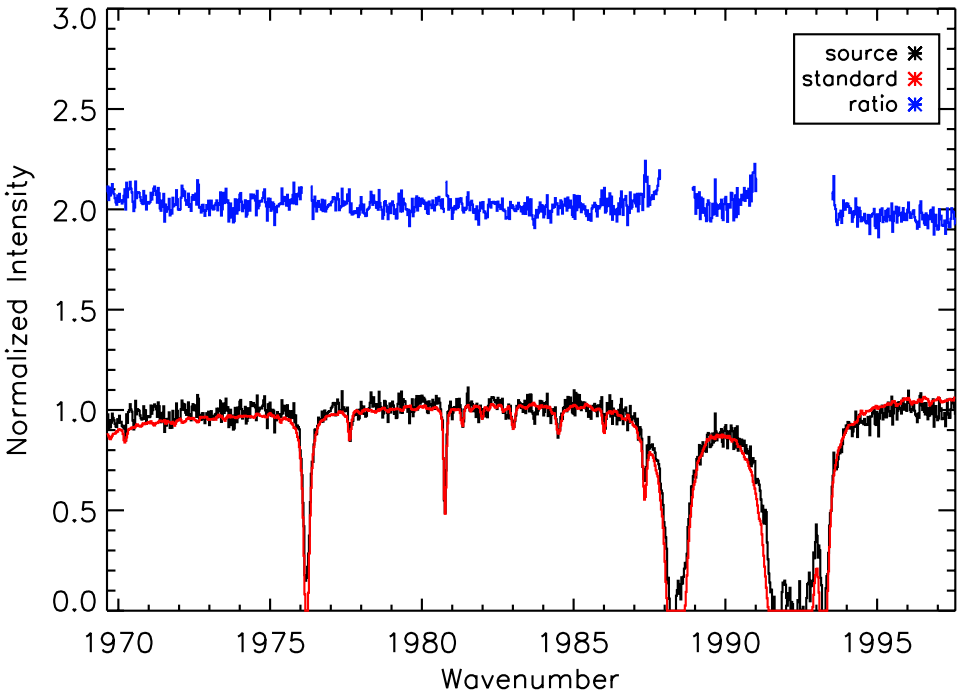

Figure 18: Spectra for L1551 order MW 15, data from 2009.

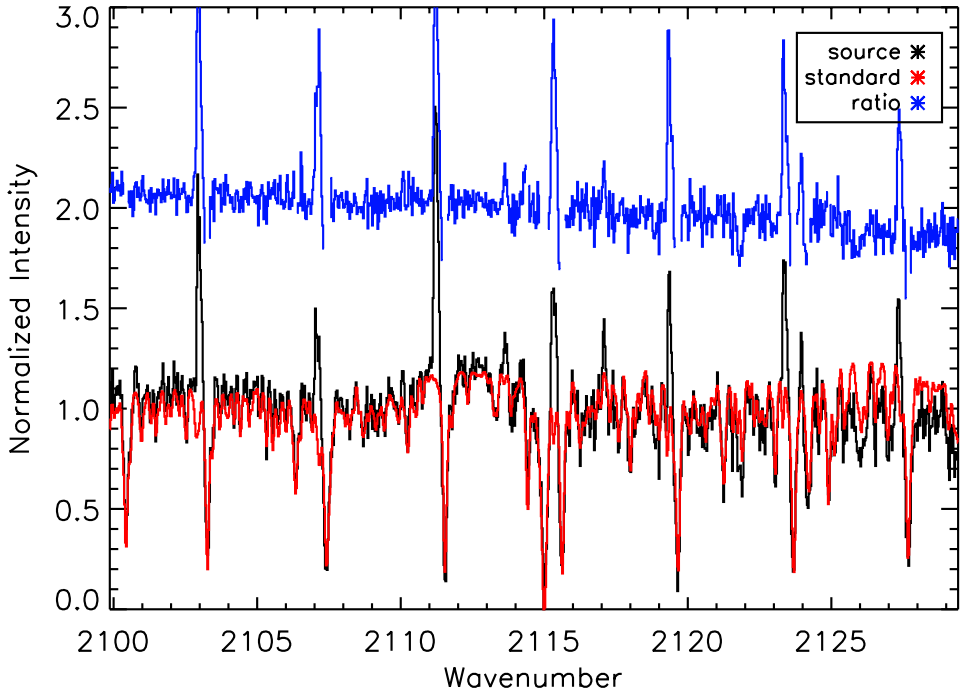

Figure 19: Spectra for L1551 order MW 16, data from 2009.

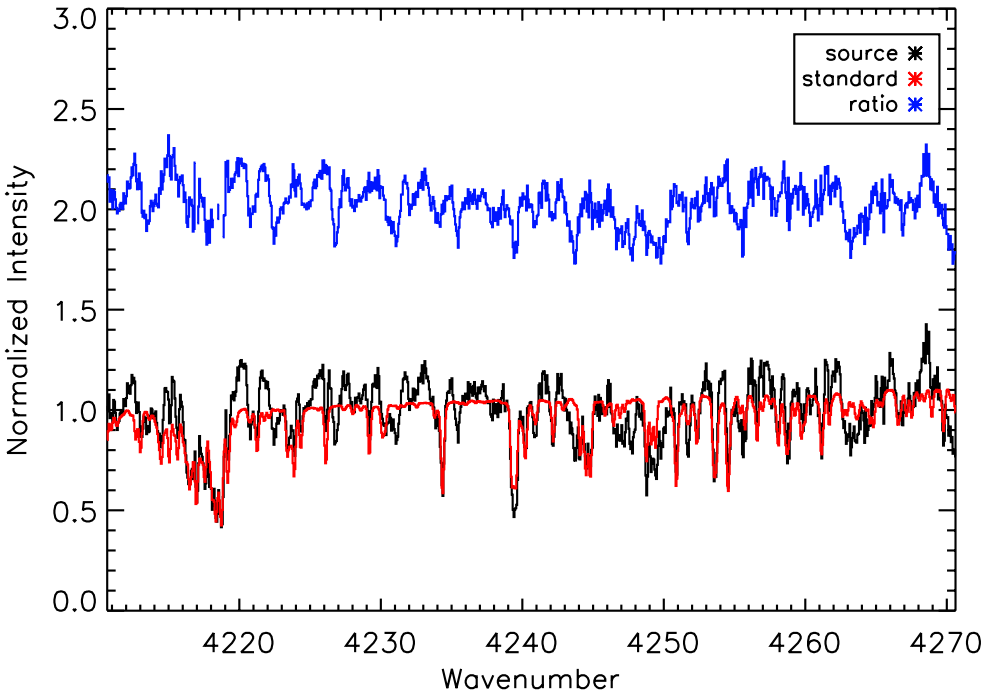

Figure 20: Spectra for L1551 order K 32, data from 2009.

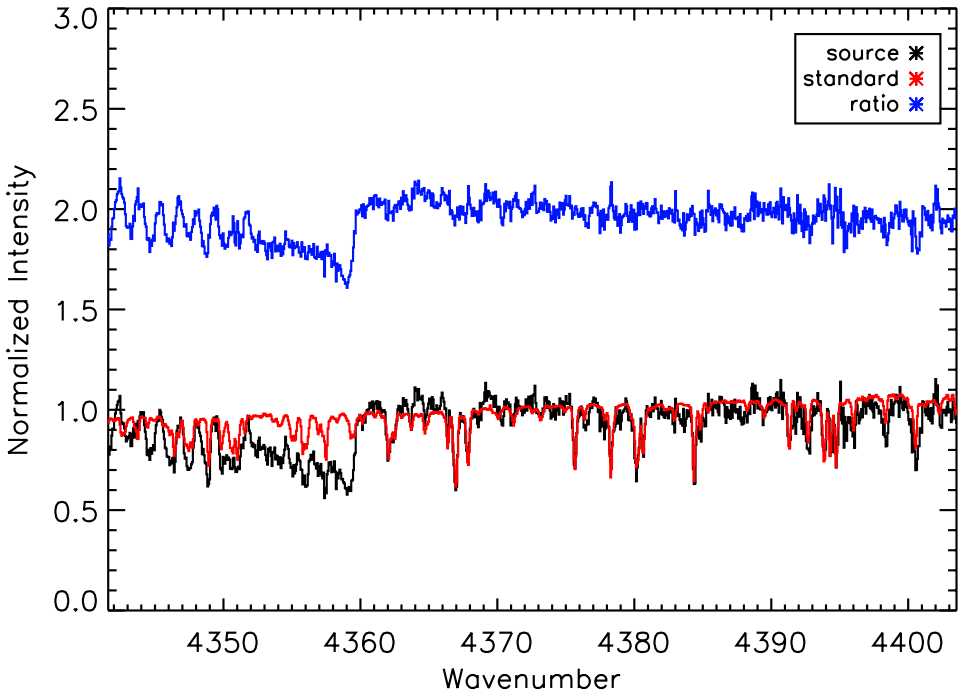

Figure 21: Spectra for L1551 order K 33, data from 2009.

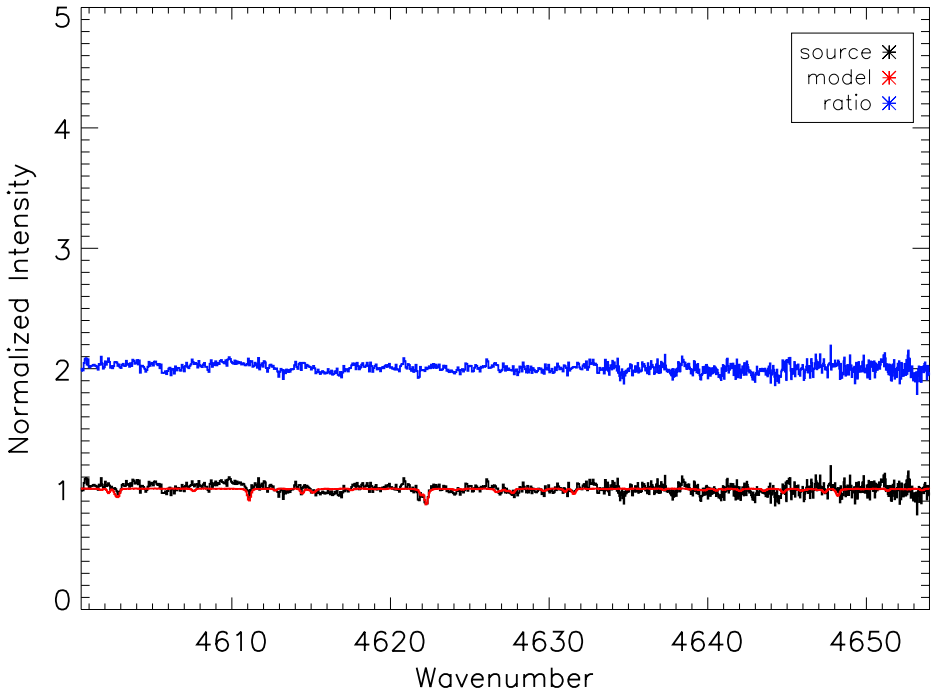

Figure 22: Spectra for L1551 order K 35, data from 2009.

Appendix D Reduced Spectra for PVCep

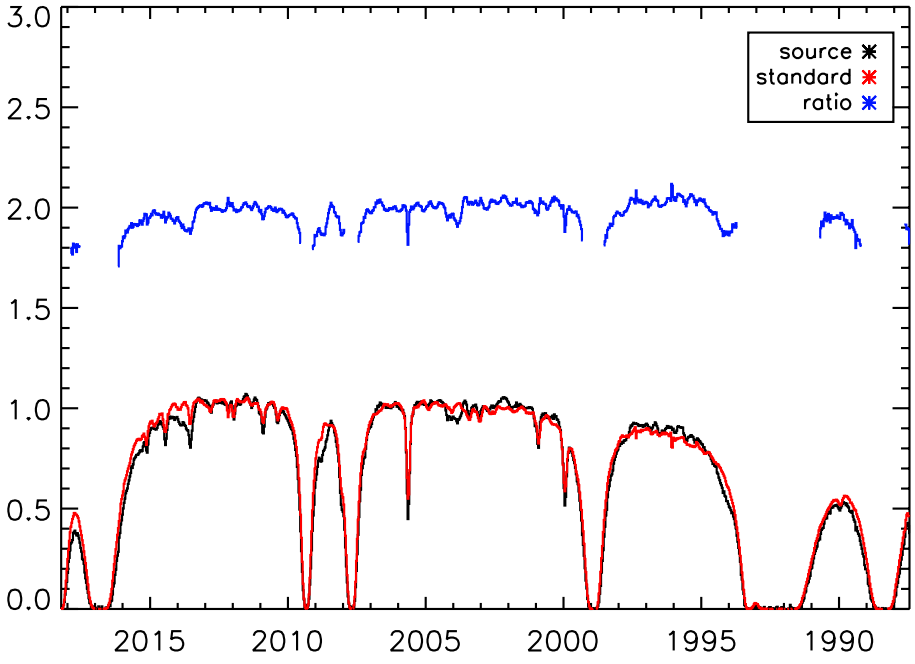

Figure 23: Spectra for PVCep order MW 15, data from 2007.

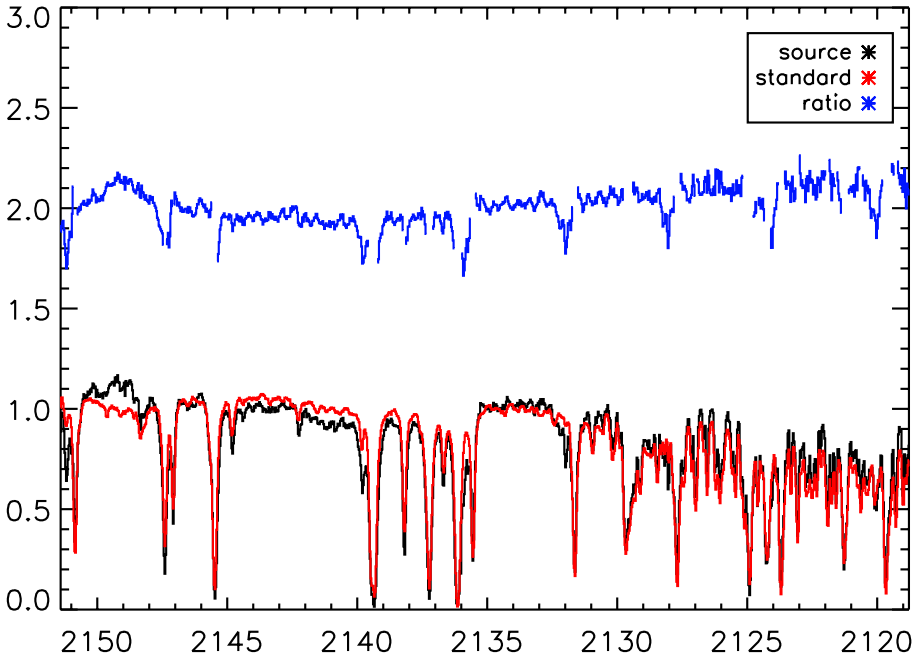

Figure 24: Spectra for PVCep order MW 16, data from 2007.

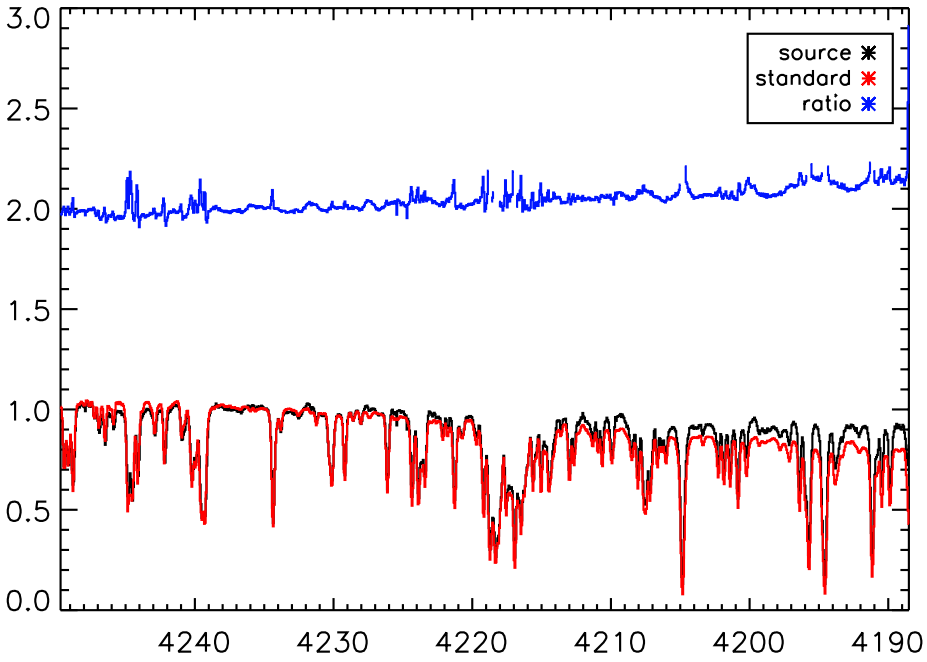

Figure 25: Spectra for PVCep order K 32, data from 2007.

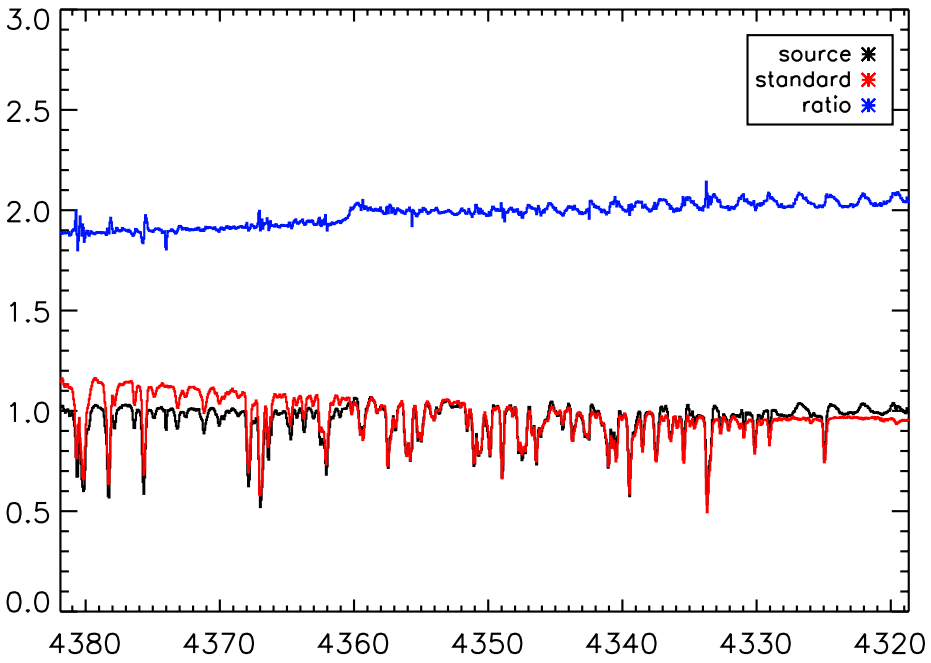

Figure 26: Spectra for PVCep order K 33, data from 2007.

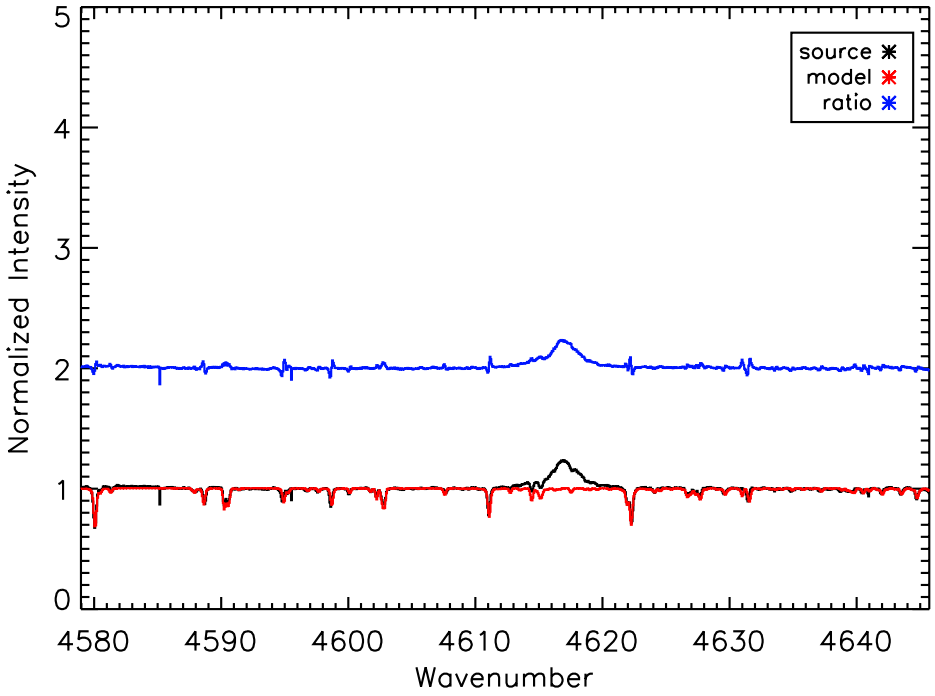

Figure 27: Spectra for PVCep order K 35, data from 2007.

Appendix E Reduced Spectra for RNO15

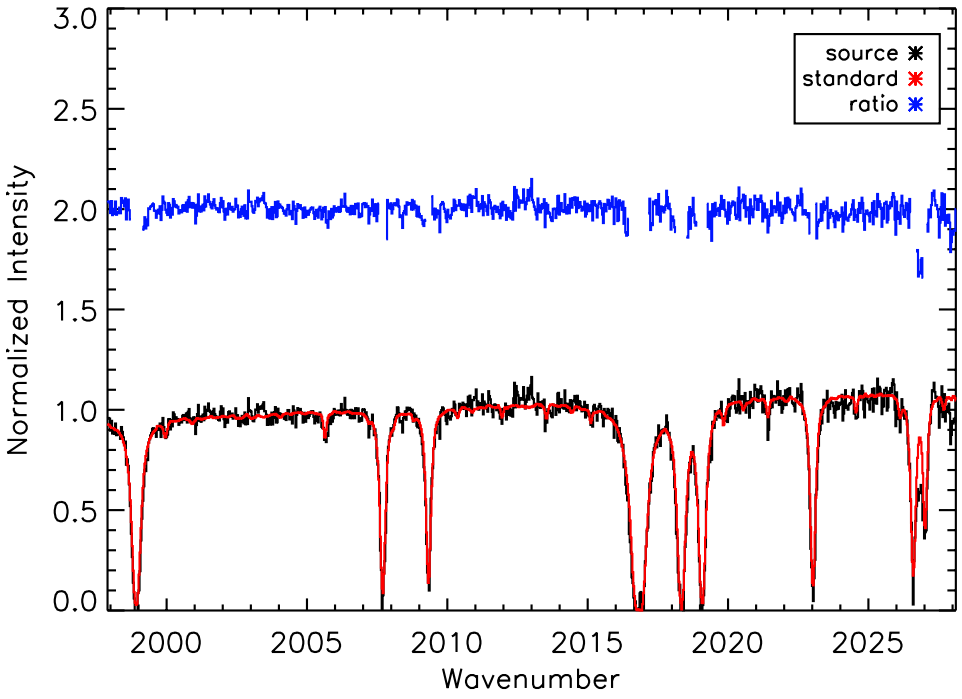

Figure 28: Spectra for RNO order MW(2) 15, data from 2009.

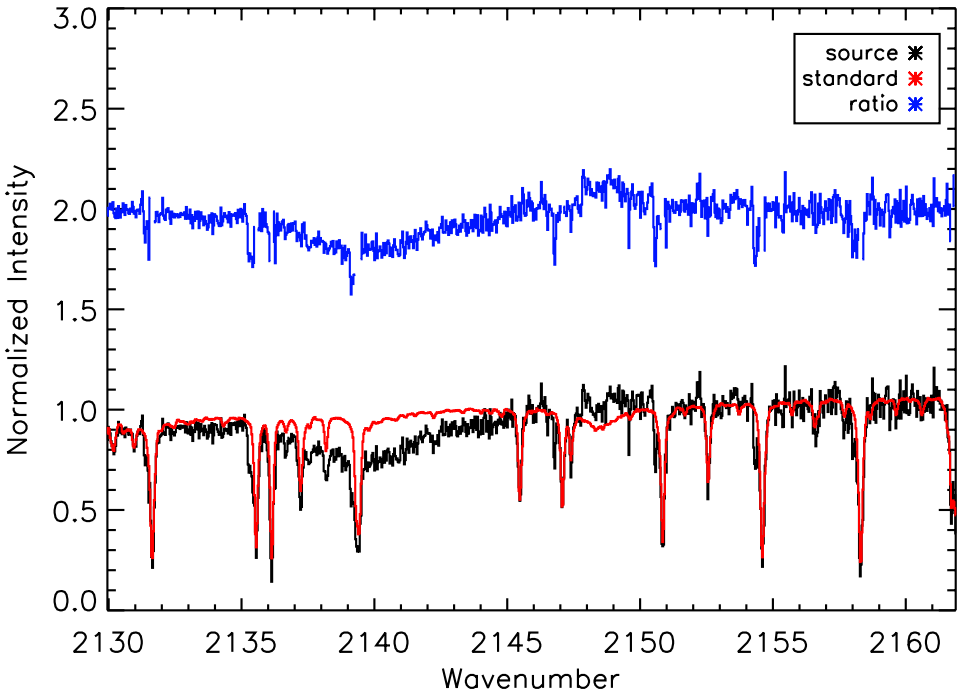

Figure 29: Spectra for RNO order MW(2) 16, data from 2009.

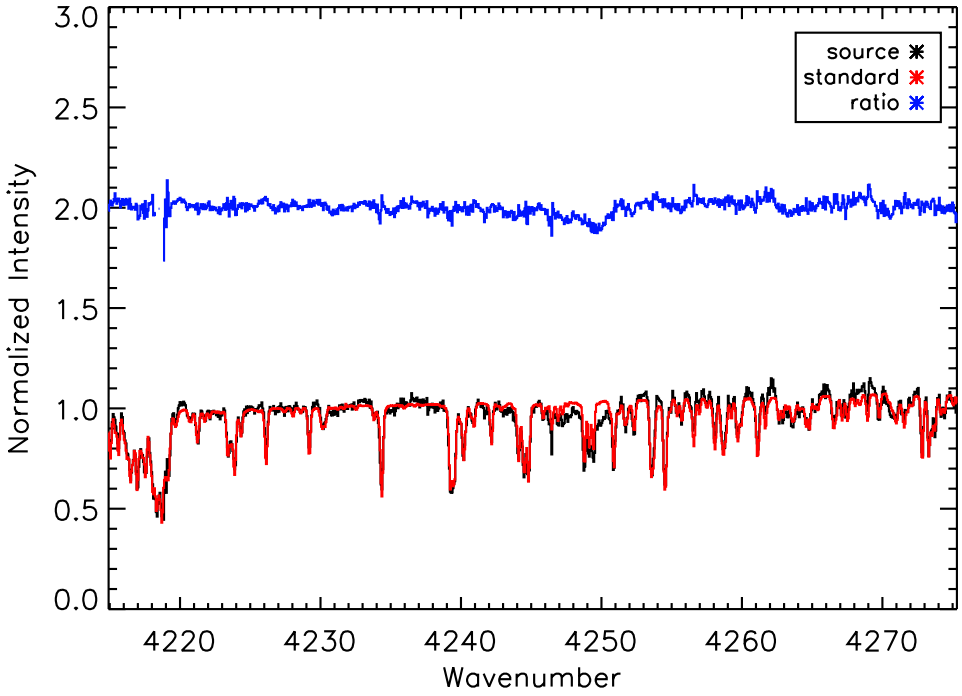

Figure 30: Spectra for RNO order K 32, data from 2009.

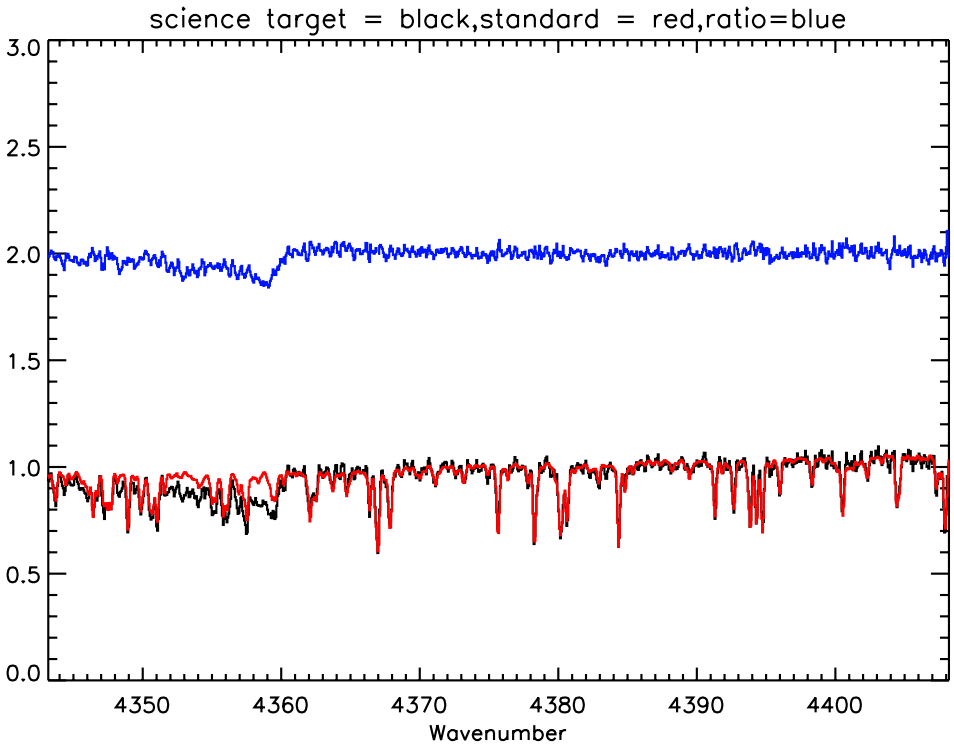

Figure 31: Spectra for RNO order K 33, data from 2009.

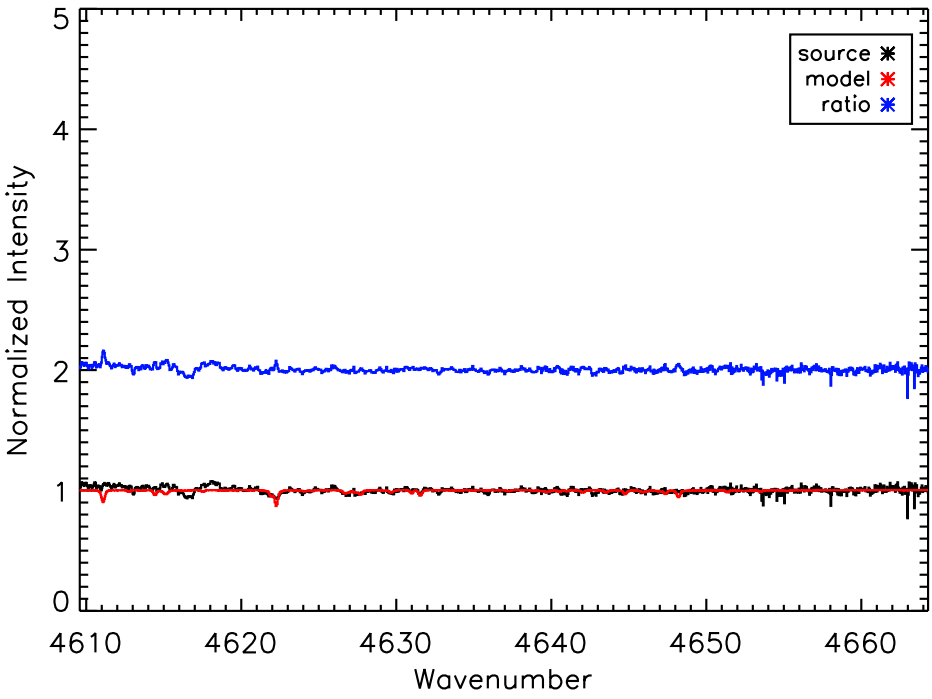

Figure 32: Spectra for RNO order K 35, data from 2009.

Appendix F Reduced Spectra for V1057

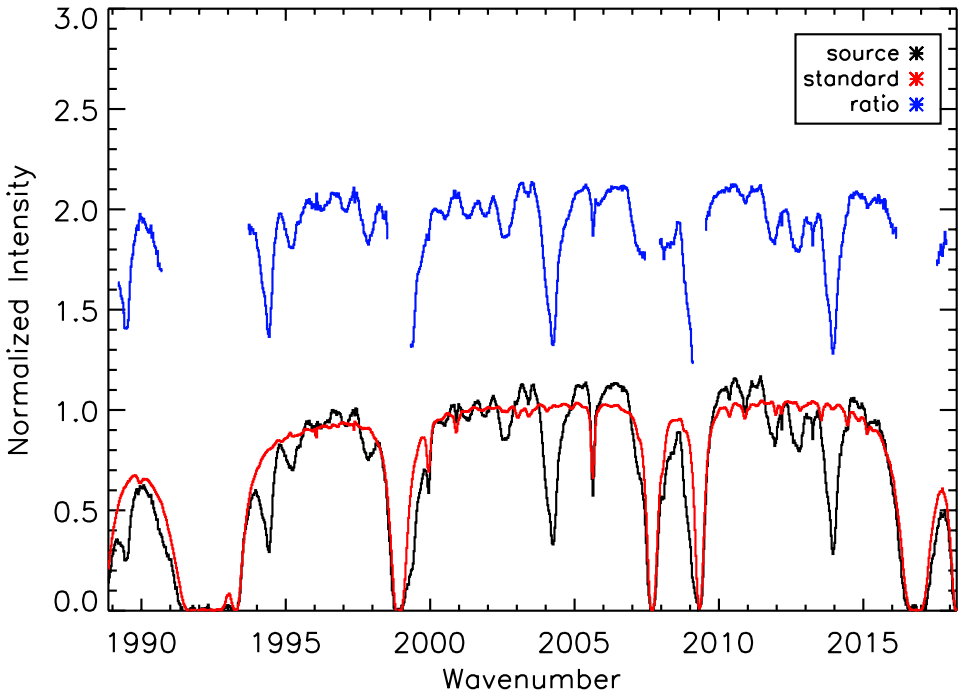

Figure 33: Spectra for V1057 order MW 15, data from 2007.

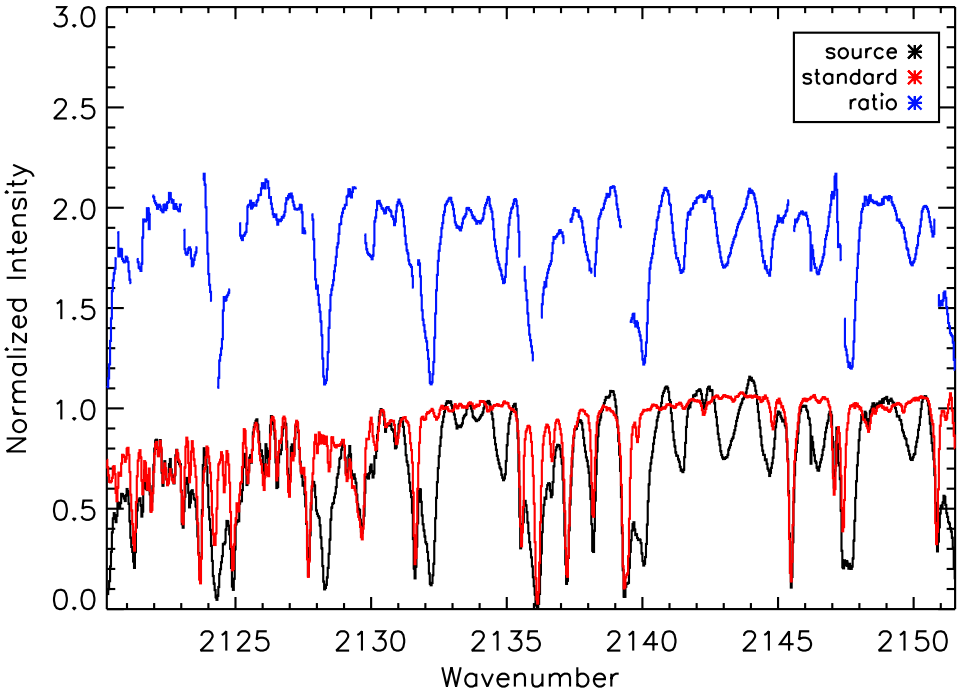

Figure 34: Spectra for V1057 order MW 16, data from 2007.

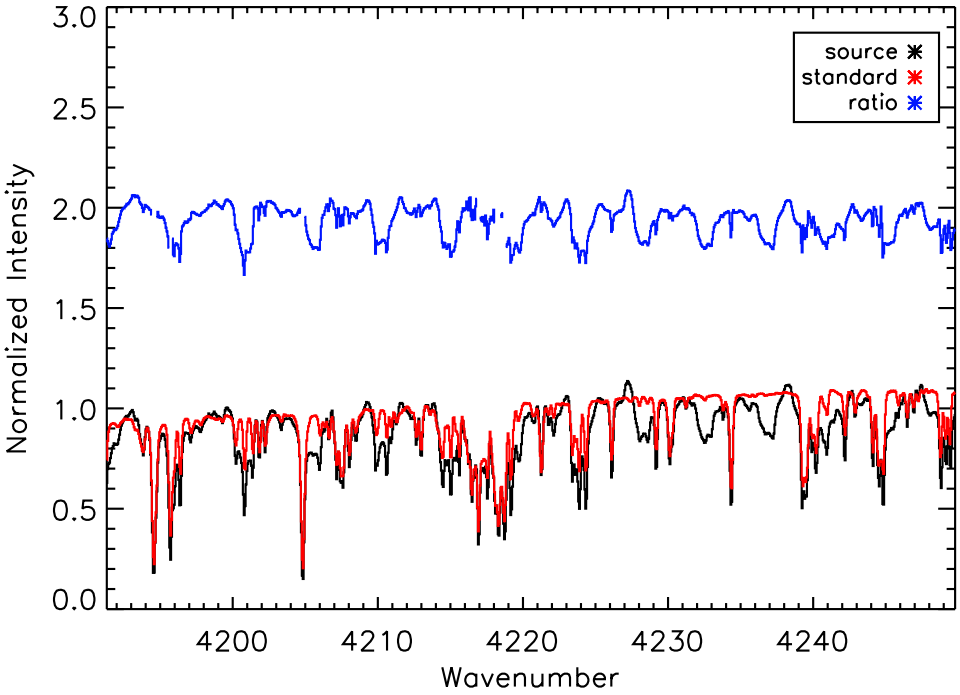

Figure 35: Spectra for V1057 order K 32, data from 2007.

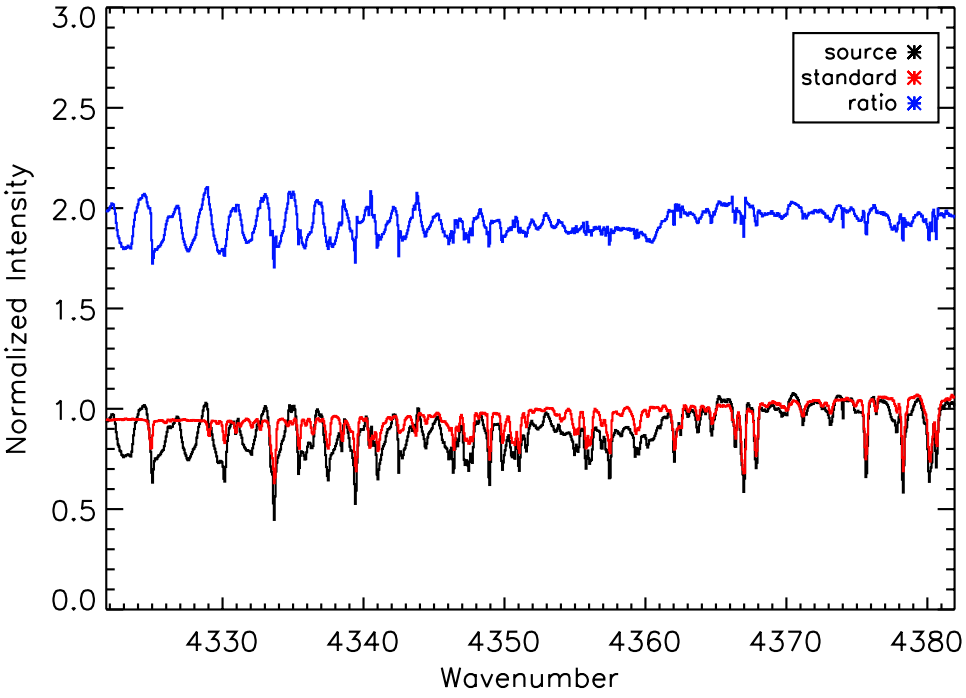

Figure 36: Spectra for V1057 order K 33, data from 2007.

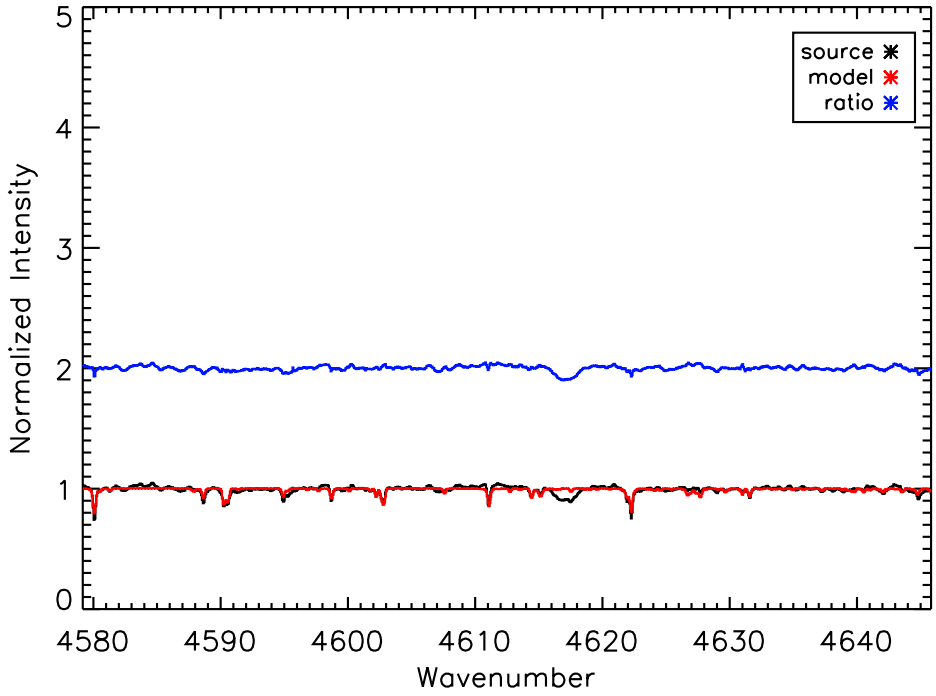

Figure 37: Spectra for V1057 order K 35, data from 2007.

Appendix G Reduced Spectra for V1118

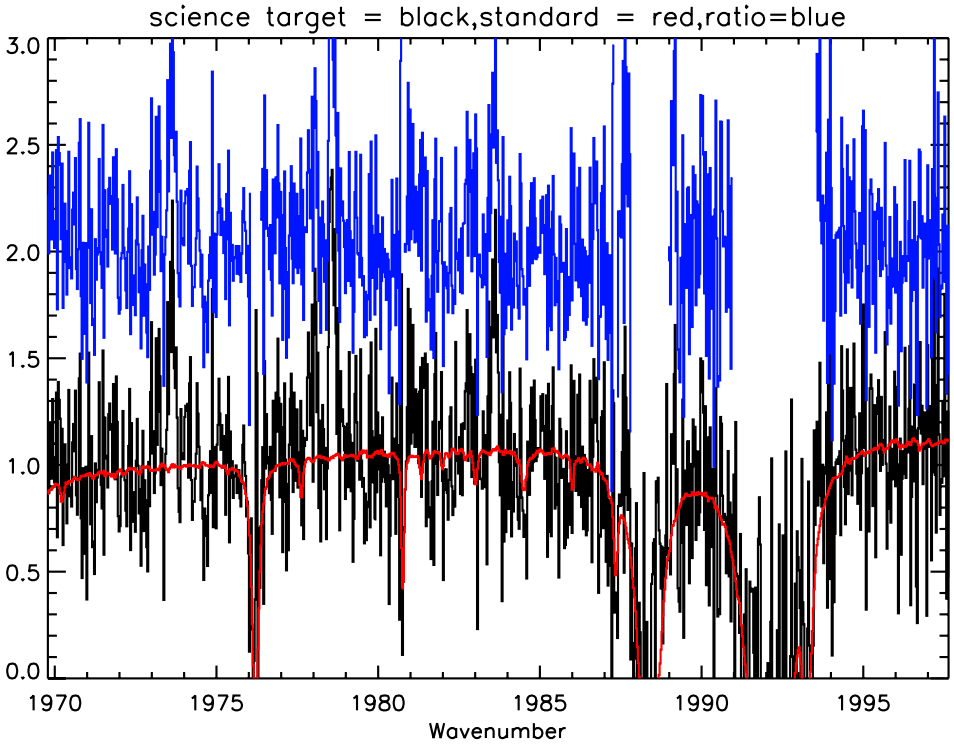

Figure 38: Spectra for V1118 order MW 15, data from 2009.

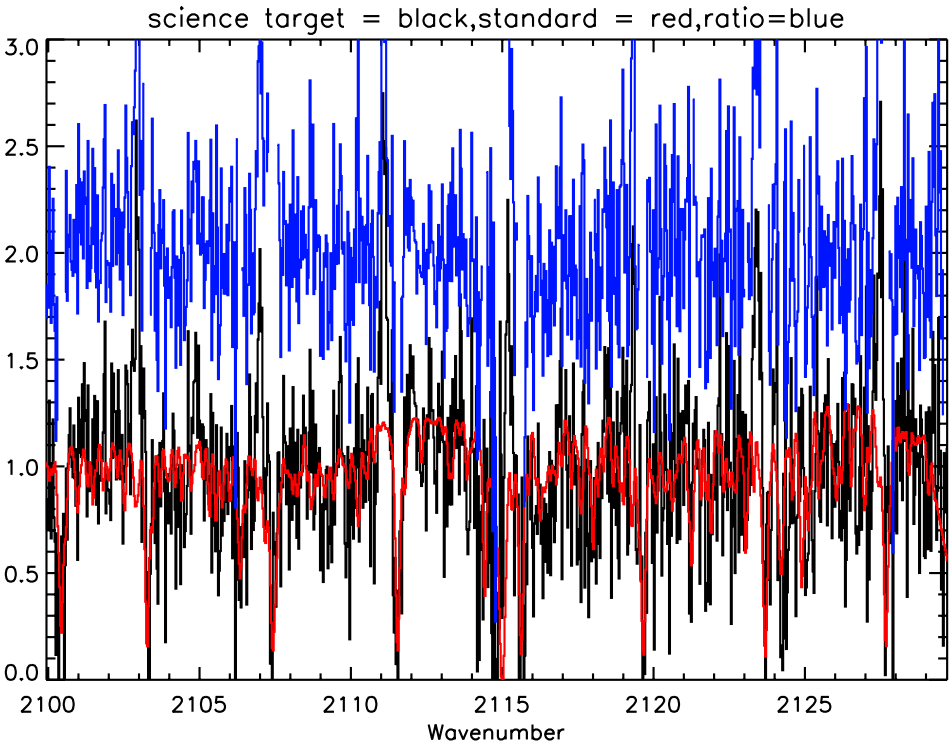

Figure 39: Spectra for V1118 order MW 16, data from 2009.

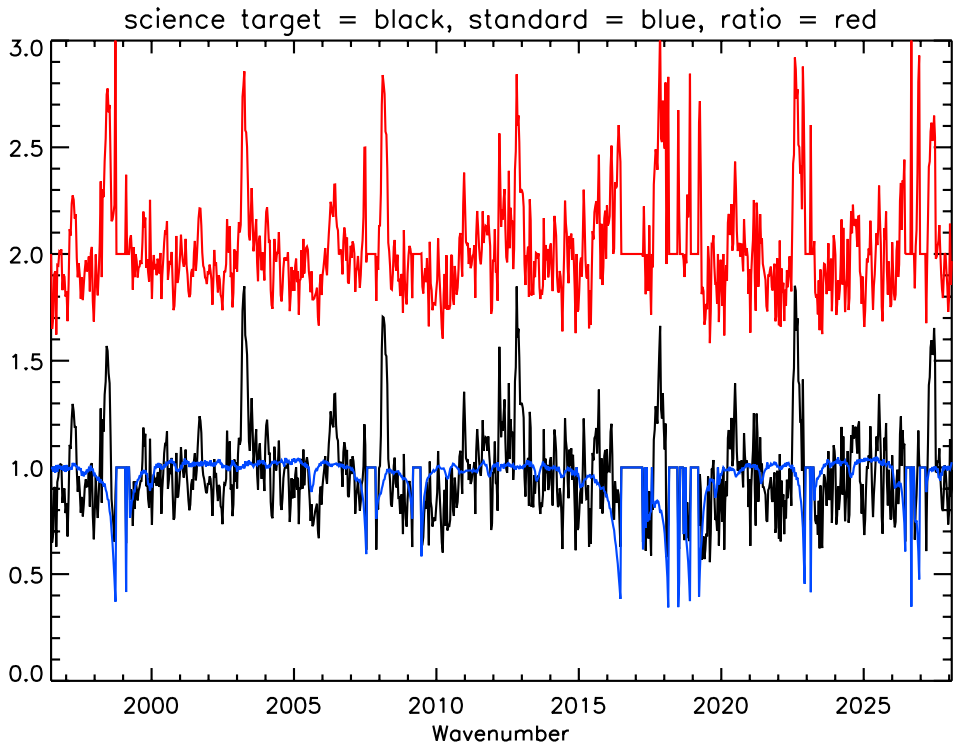

Figure 40: Spectra for V1118 order MW(2) 15, data from 2009.

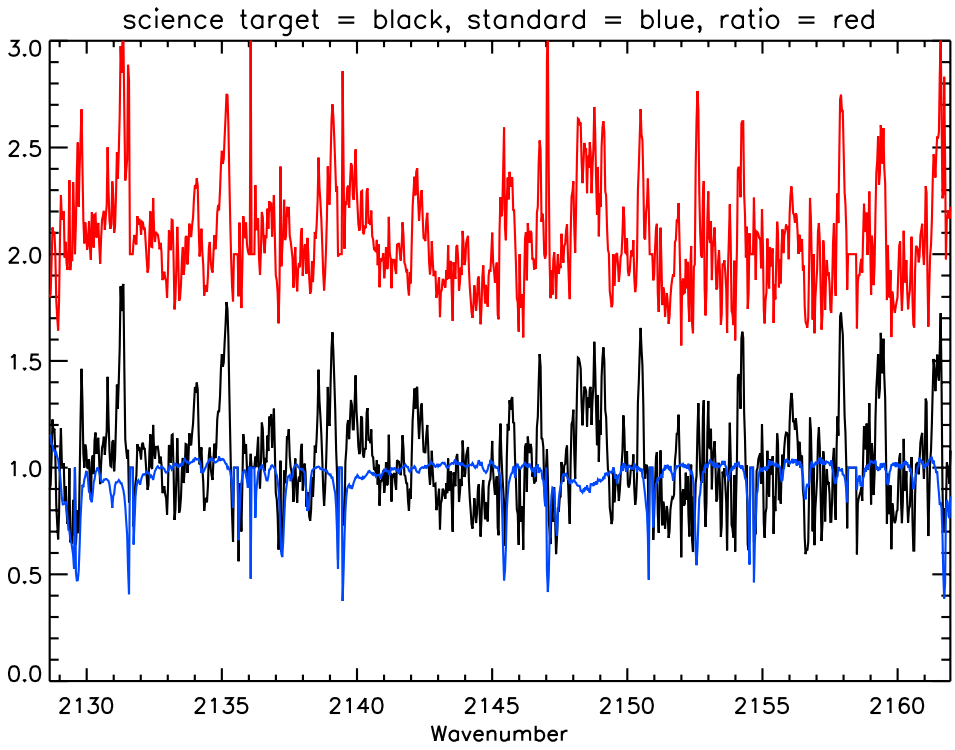

Figure 41: Spectra for V1118 order MW(2) 16, data from 2009.

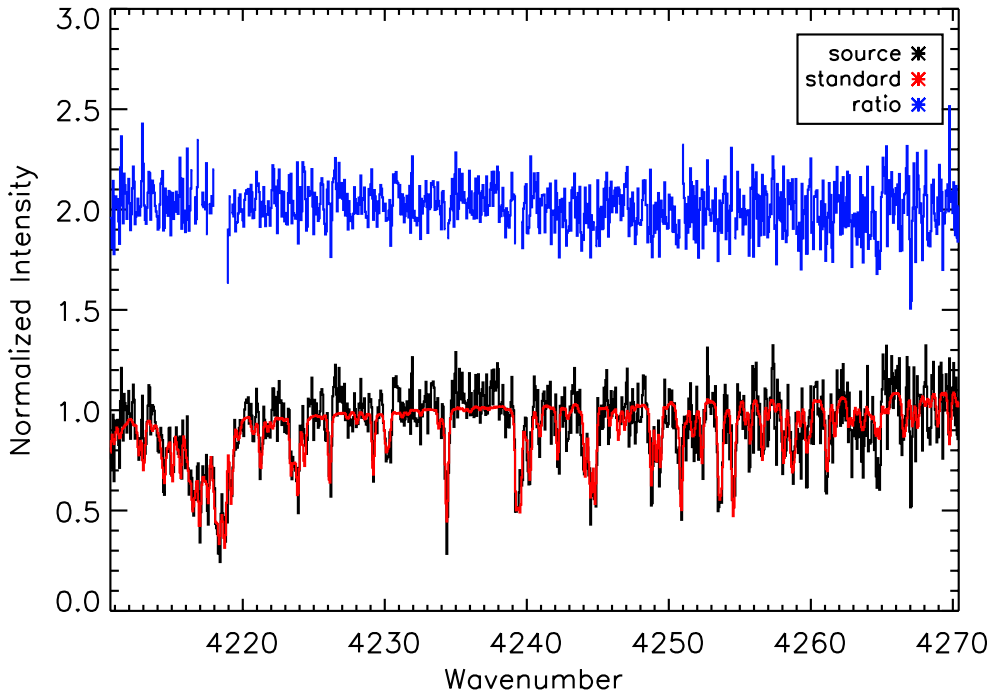

Figure 42: Spectra for V1118 order K 32, data from 2009.

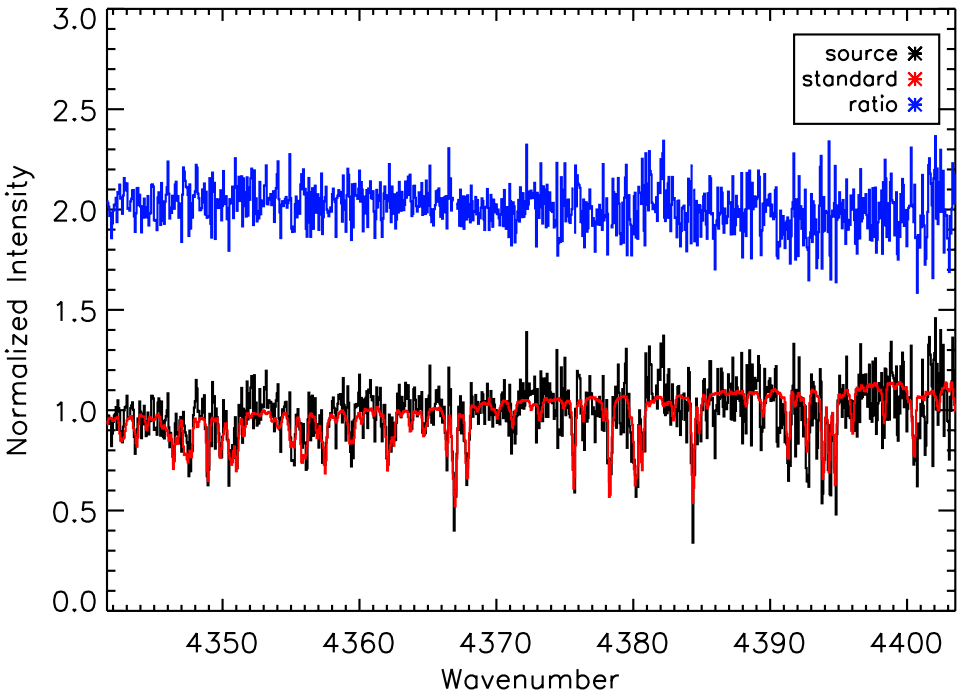

Figure 43: Spectra for V1118 order K 33, data from 2009.

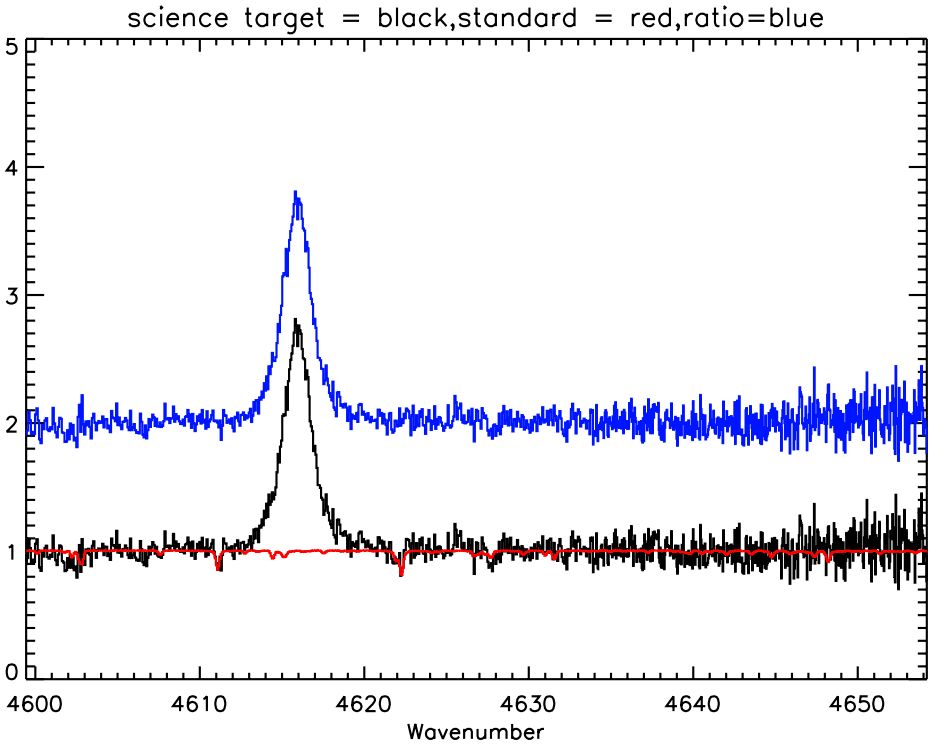

Figure 44: Spectra for V1118 order K 35, data from 2009.

Appendix H Reduced Spectra for V1331

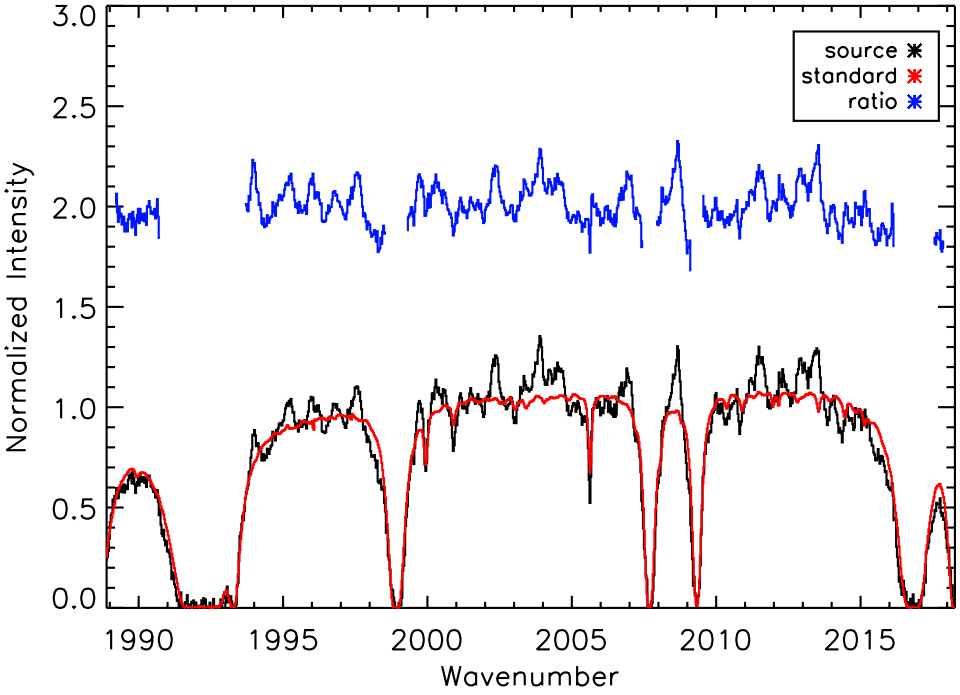

Figure 45: Spectra for V1331 order MW 15, data from 2007.

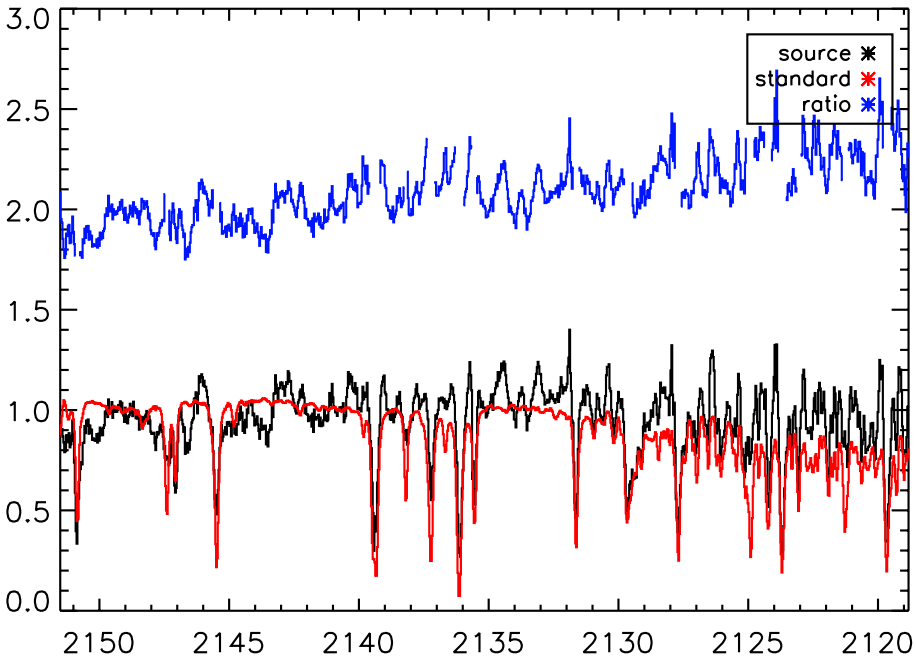

Figure 46: Spectra for V1331 order MW 16, data from 2007.

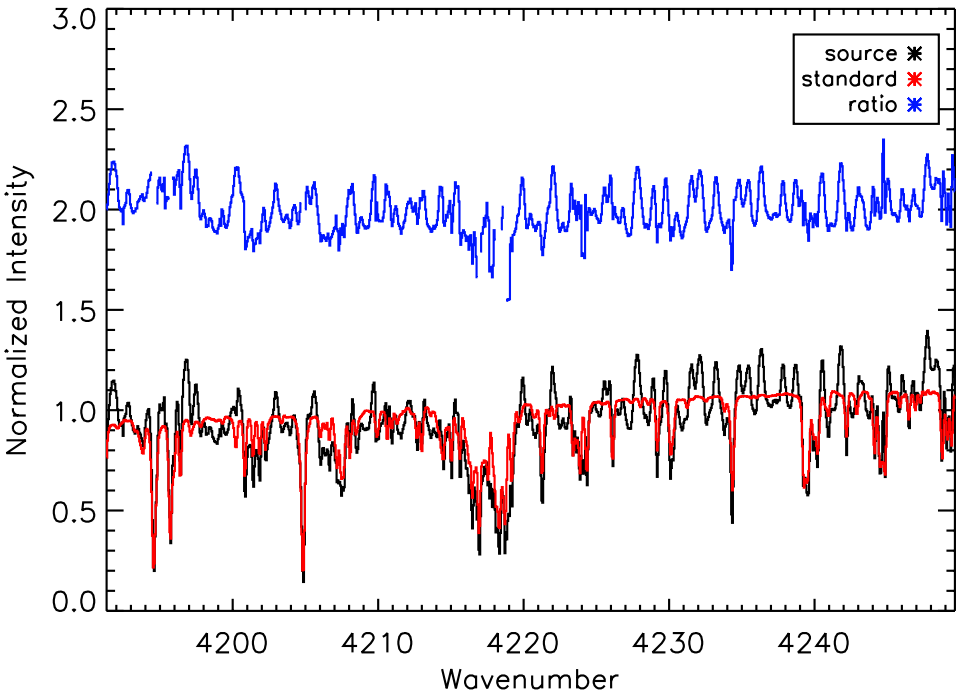

Figure 47: Spectra for V1331 order K 32, data from 2007.

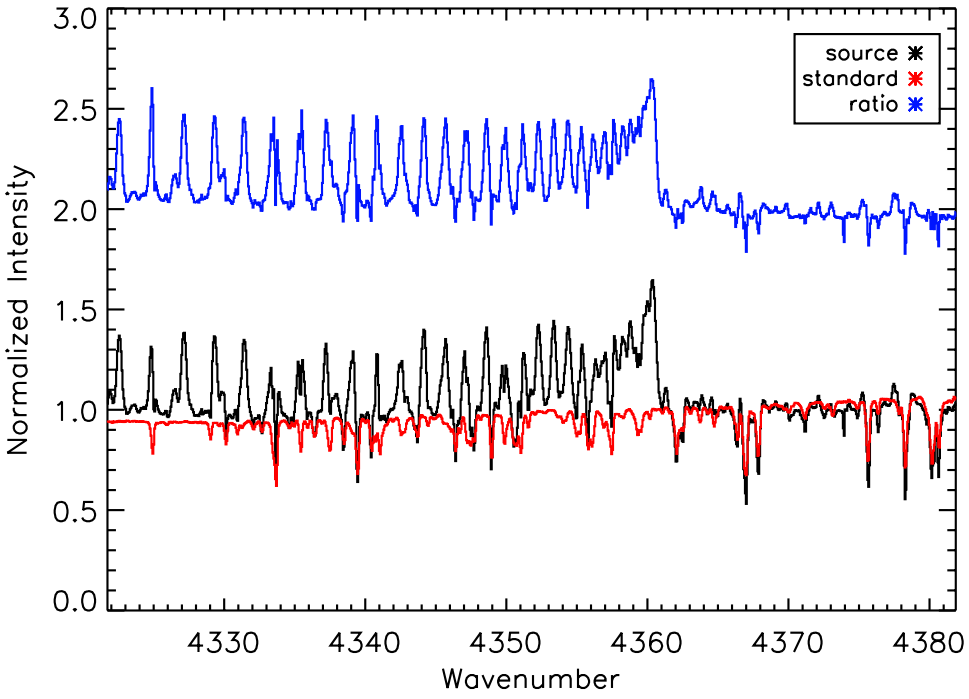

Figure 48: Spectra for V1331 order K 33, data from 2007.

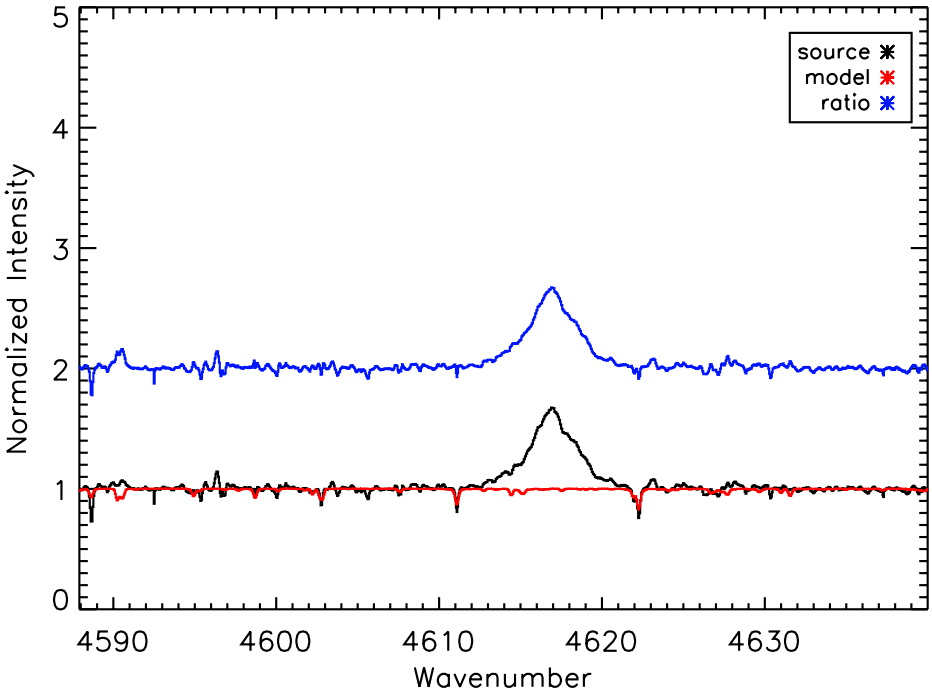

Figure 49: Spectra for V1331 order K 35, data from 2007.

Appendix I Reduced Spectra for V1515

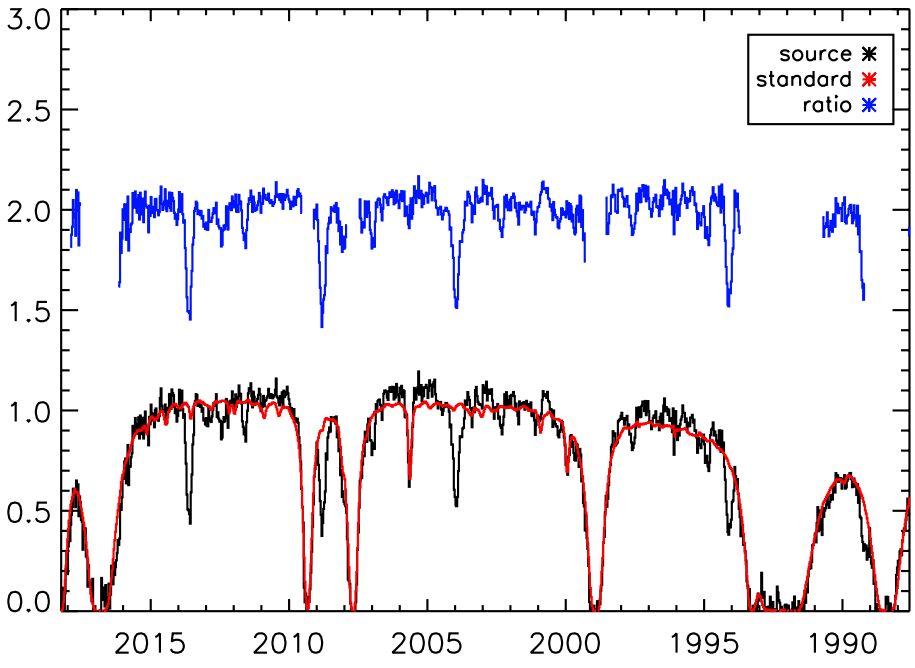

Figure 50: Spectra for V1515 order MW 15, data from 2007.

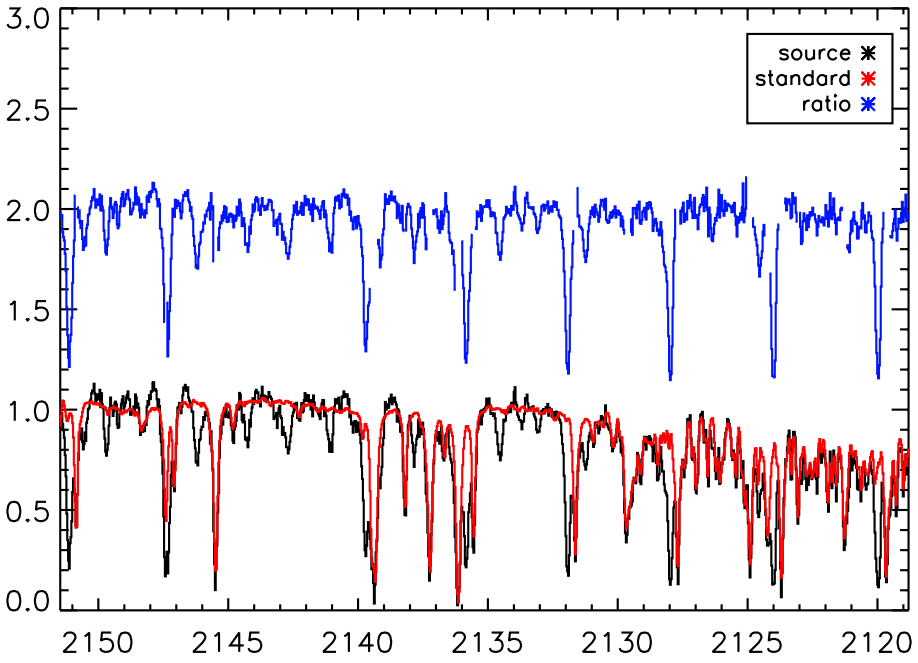

Figure 51: Spectra for V1515 order MW 16, data from 2007.

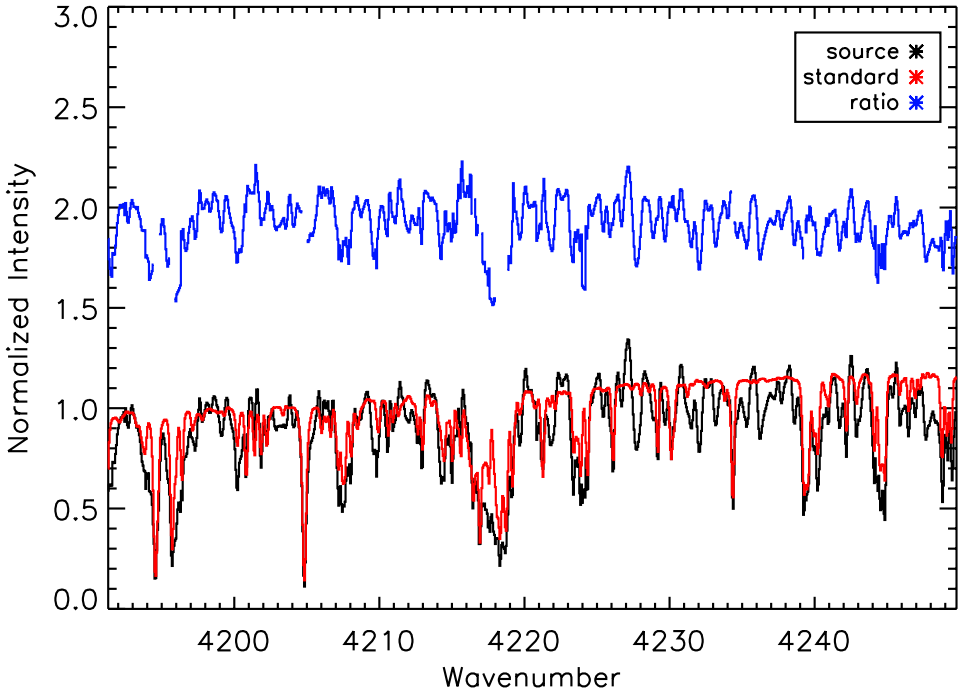

Figure 52: Spectra for V1515 order K 32, data from 2007.

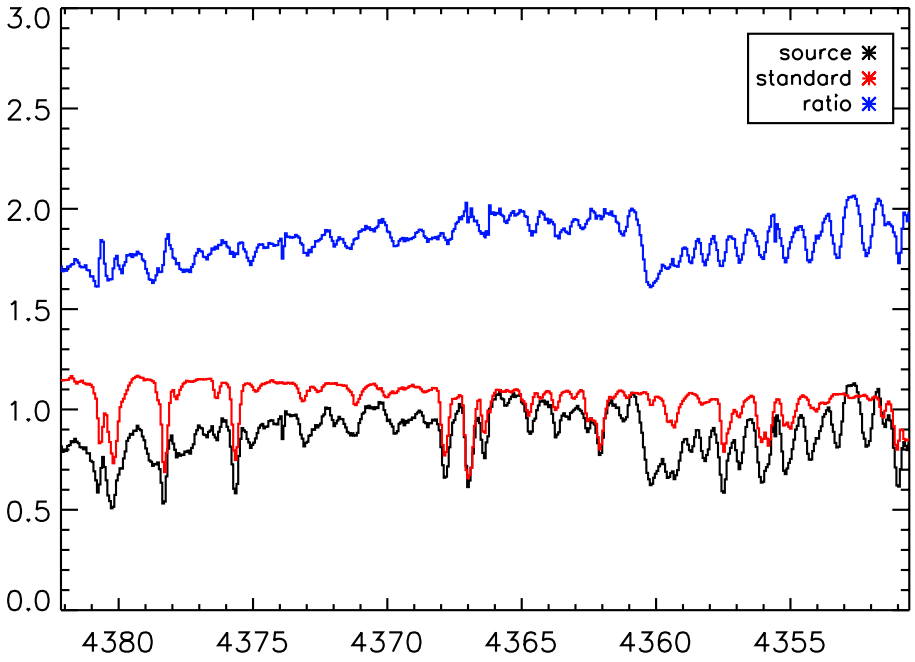

Figure 53: Spectra for V1515 order K 33, data from 2007.

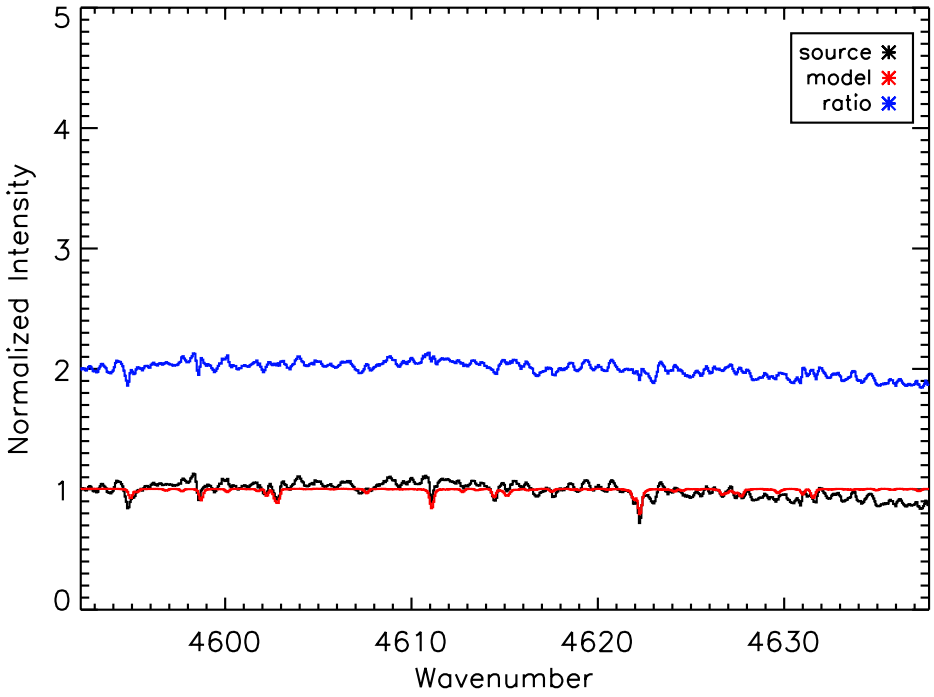

Figure 54: Spectra for V1515 order K 35, data from 2007.

Appendix J Reduced Spectra for V1735

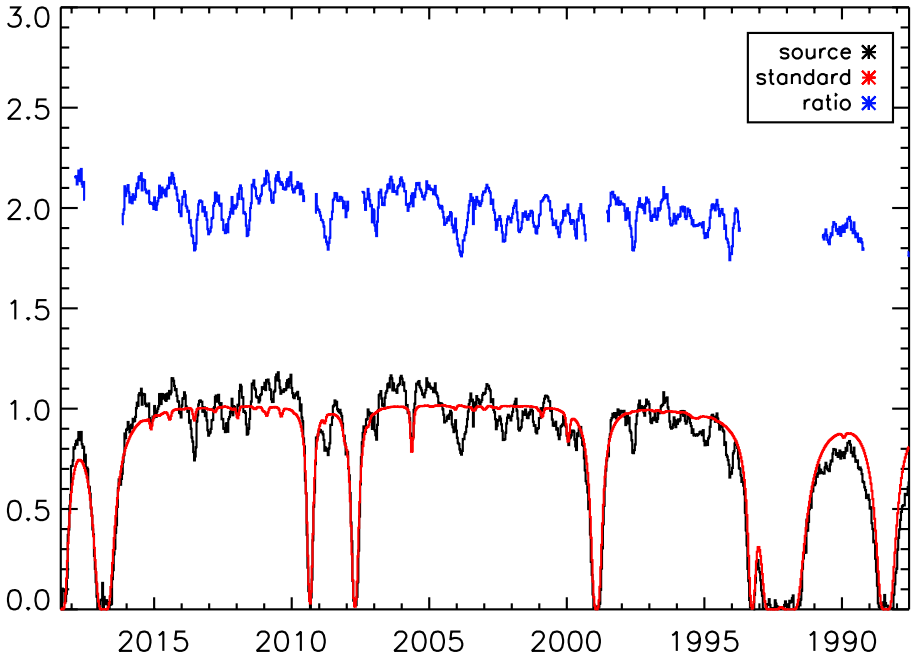

Figure 55: Spectra for V1735 order MW 15, data from 2007.

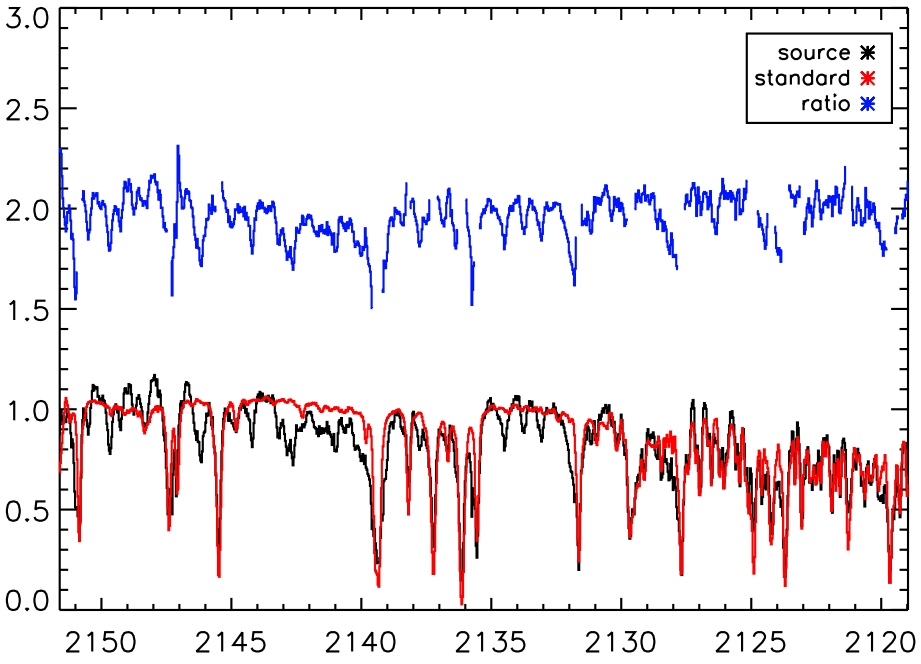

Figure 56: Spectra for V1735 order MW 16, data from 2007.

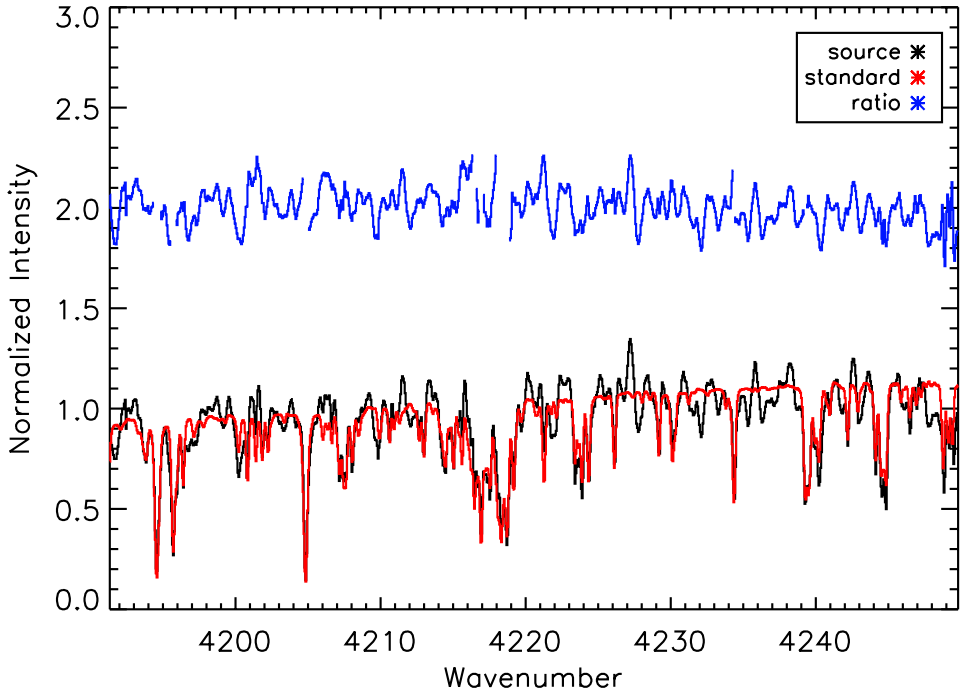

Figure 57: Spectra for V1735 order K 32, data from 2007.

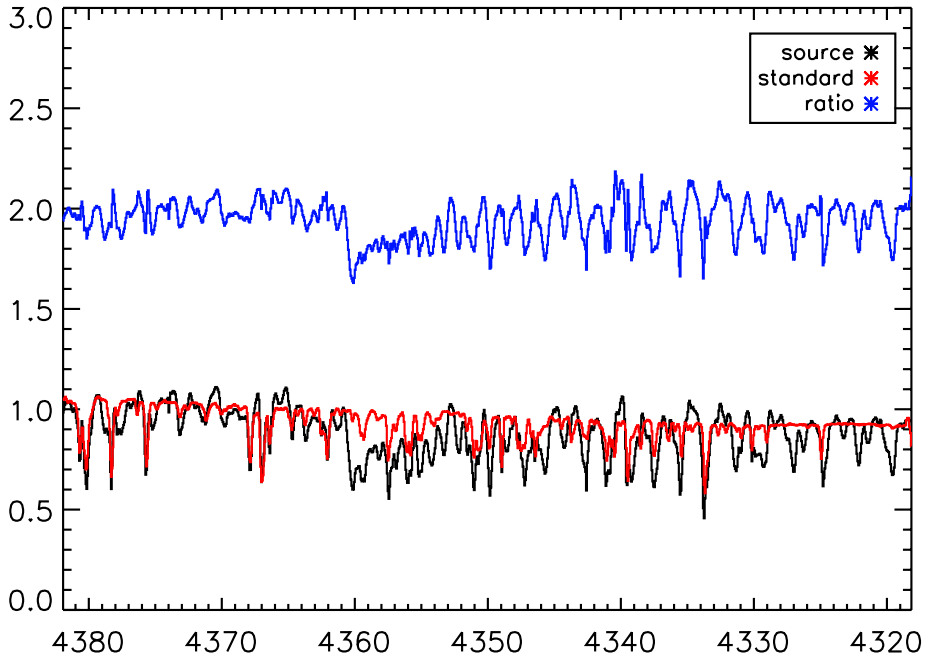

Figure 58: Spectra for V1735 order K 33, data from 2007.

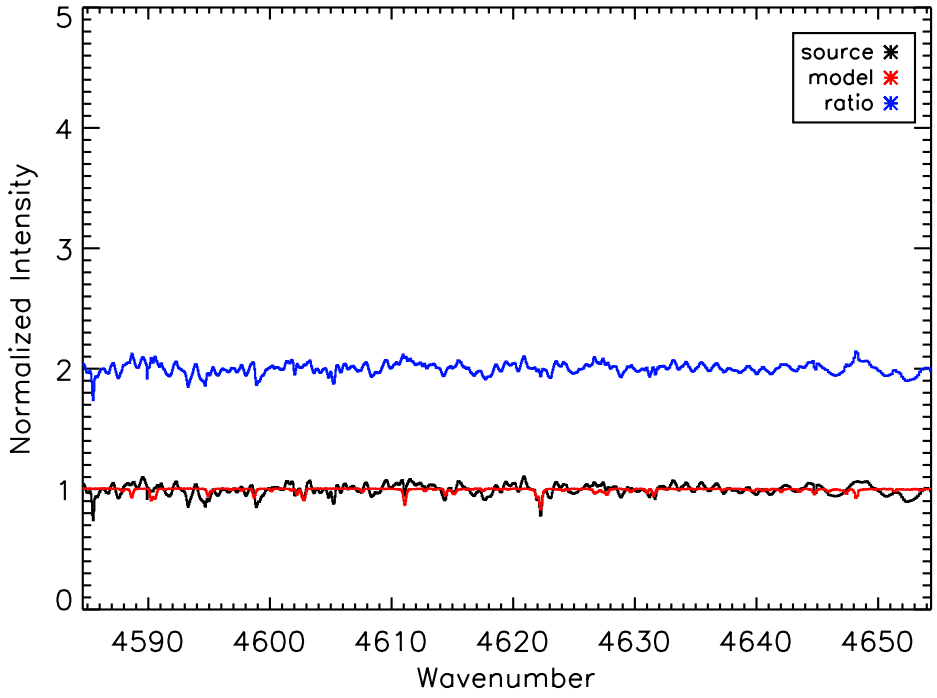

Figure 59: Spectra for V1735 order K 35, data from 2007.

Appendix K Reduced Spectra for XZTau

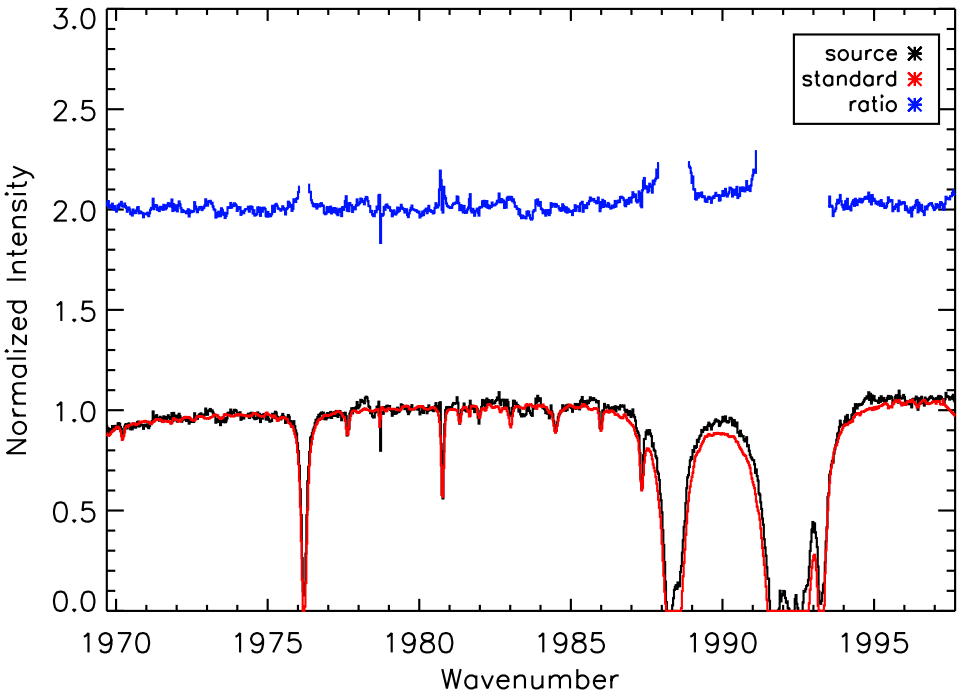

Figure 60: Spectra for XZTau order MW 15, data from 2009.

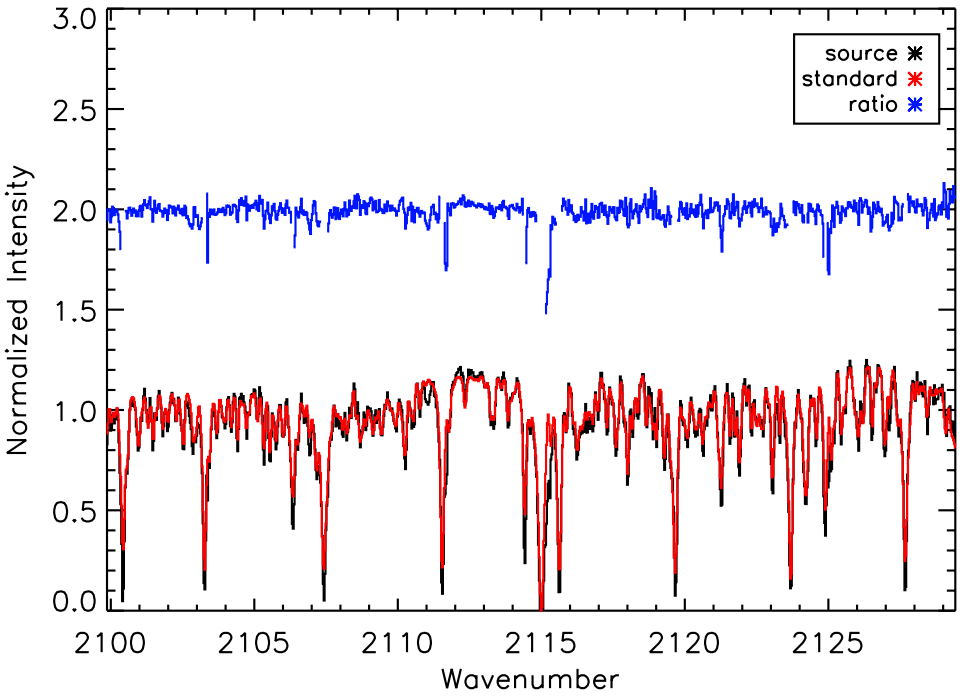

Figure 61: Spectra for XZTau order MW 16, data from 2009.

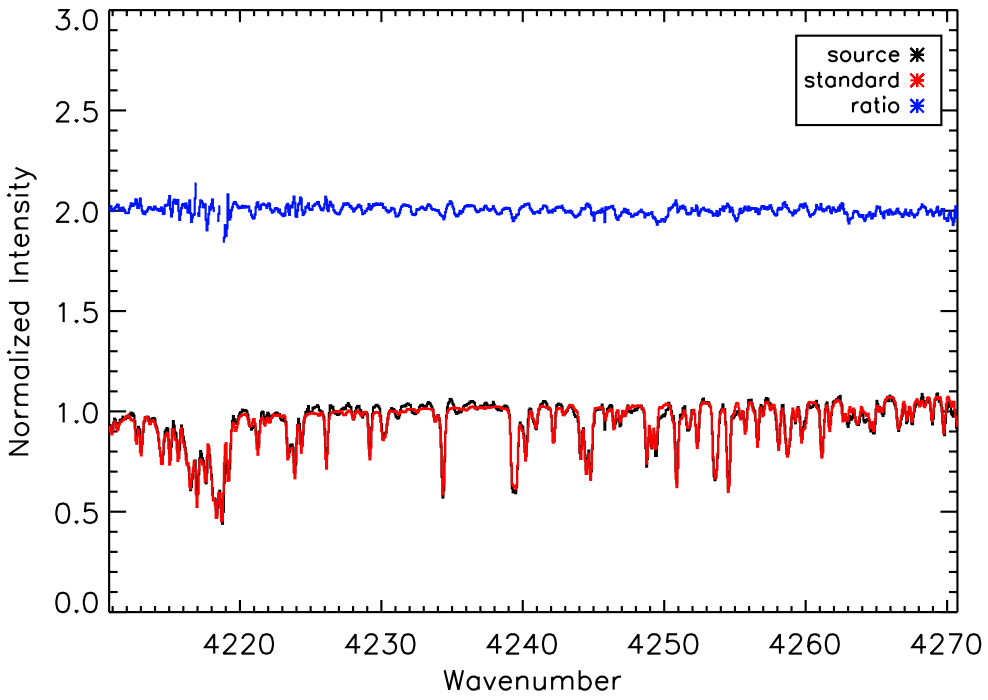

Figure 62: Spectra for XZTau order K 32, data from 2009.

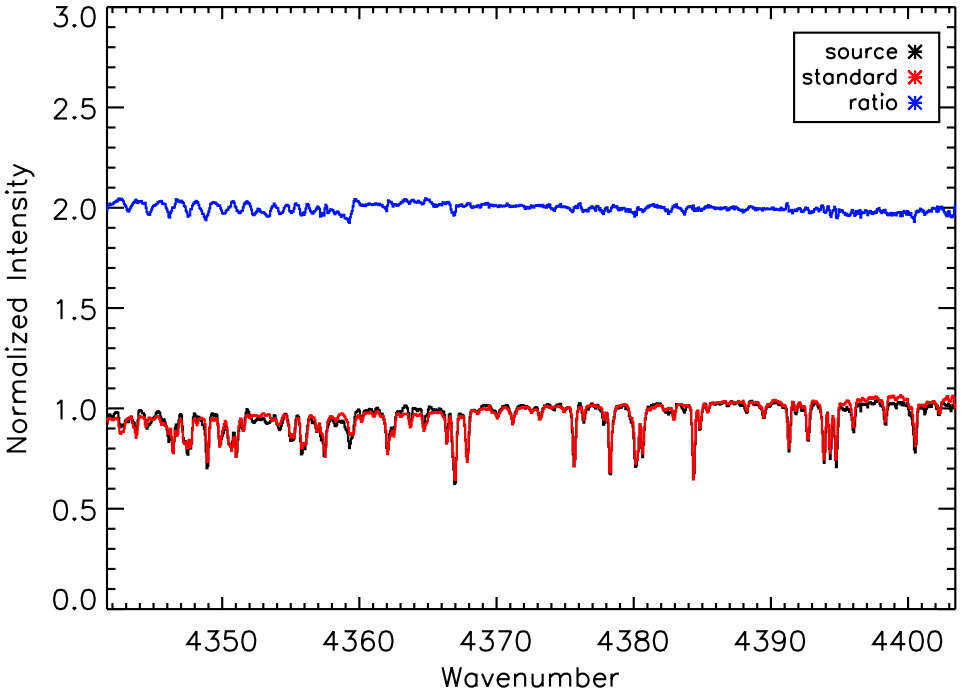

Figure 63: Spectra for XZTau order K 33, data from 2009.

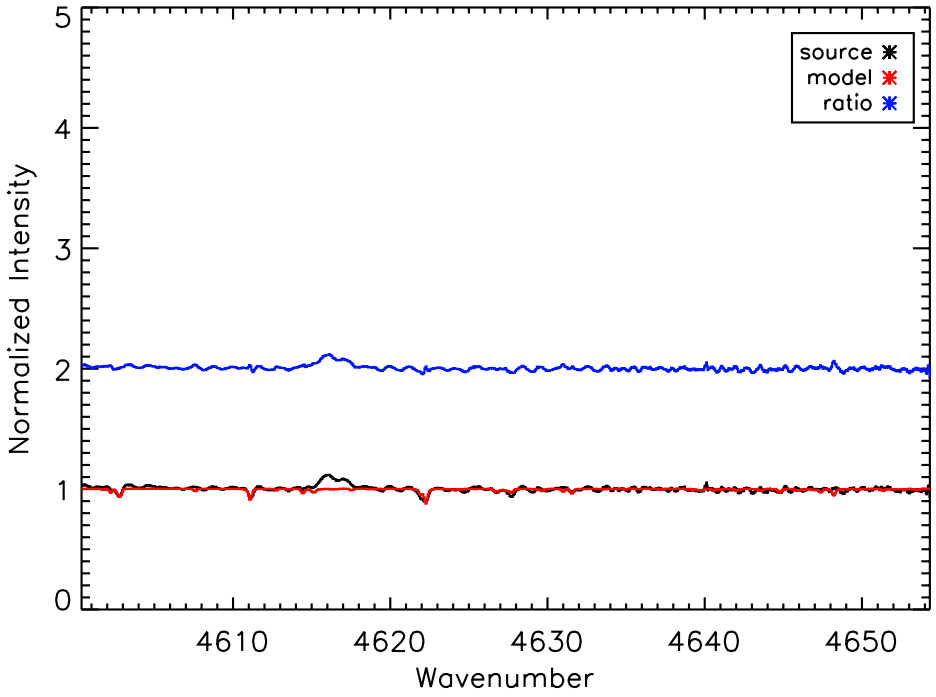

Figure 64: Spectra for XZTau order K 35, data from 2009.

Appendix L Reduced Spectra for ZCMA

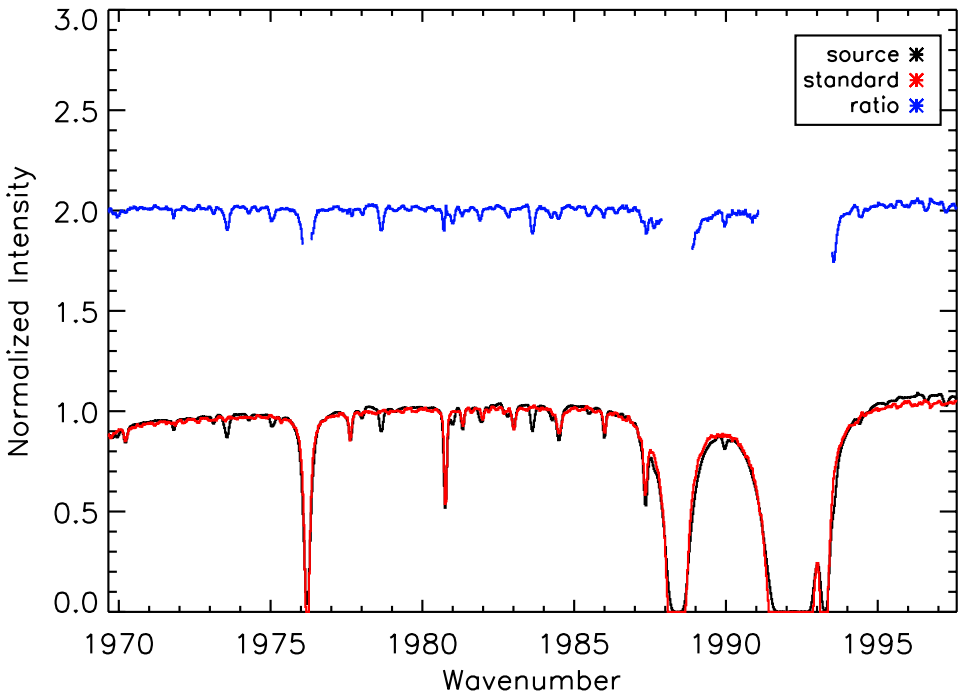

Figure 65: Spectra for ZCMA order MW 15, data from 2009.

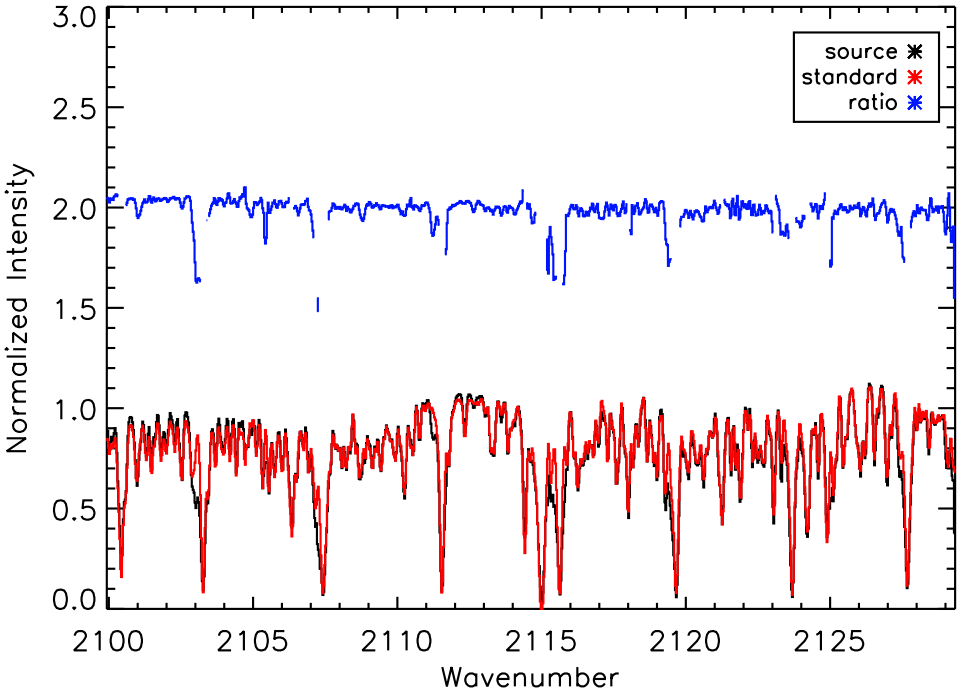

Figure 66: Spectra for ZCMA order MW 16, data from 2009.

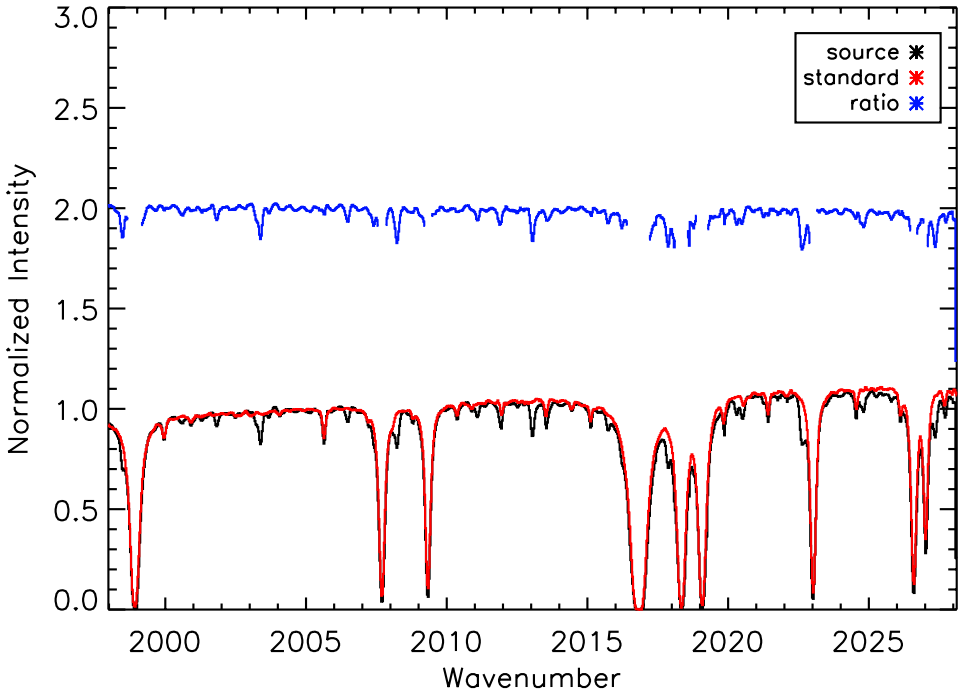

Figure 67: Spectra for ZCMA order MW(2) 15, data from 2009.

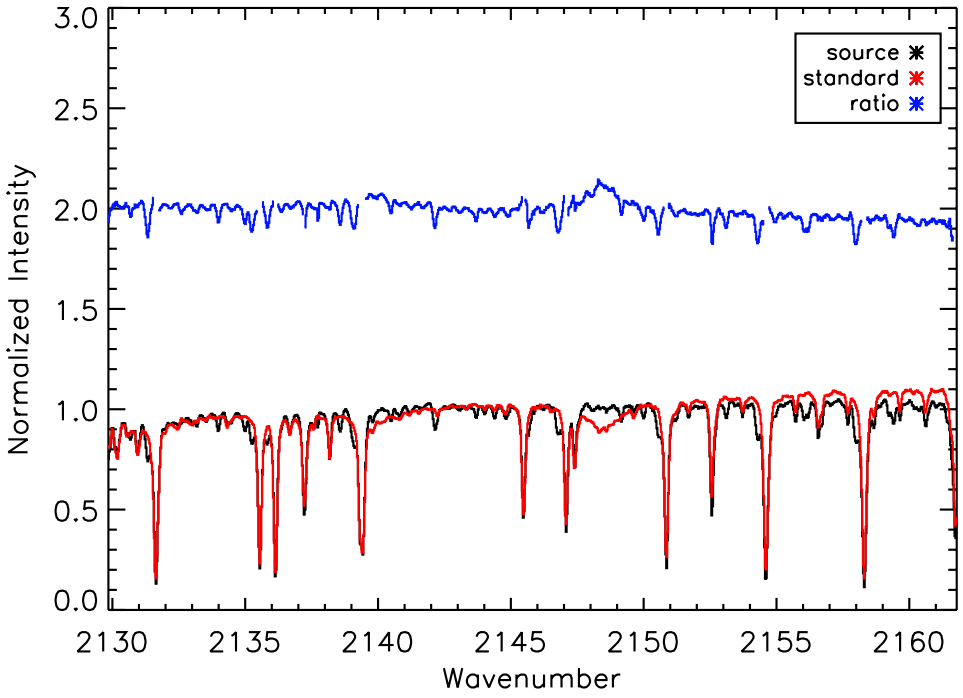

Figure 68: Spectra for ZCMA order MW(2) 16, data from 2009.

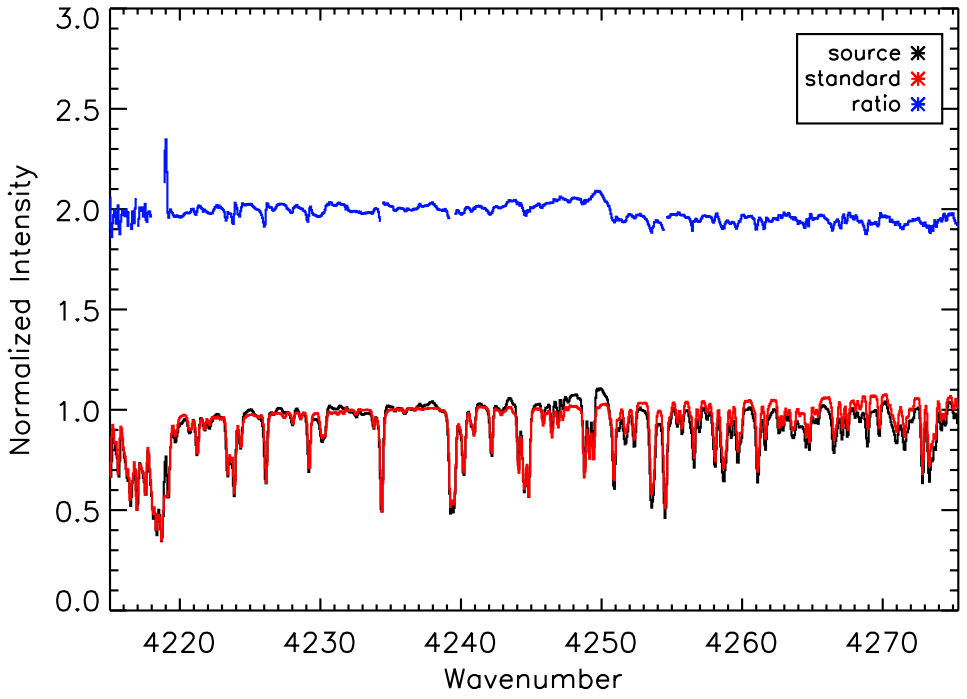

Figure 69: Spectra for ZCMA order K 32, data from 2009.

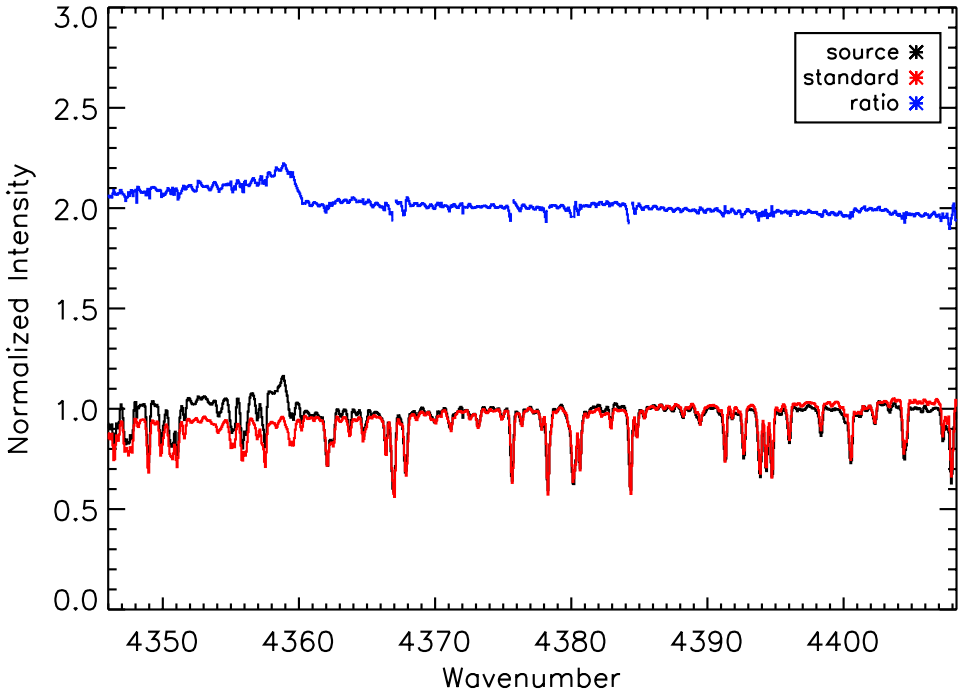

Figure 70: Spectra for ZCMA order K 33, data from 2009.

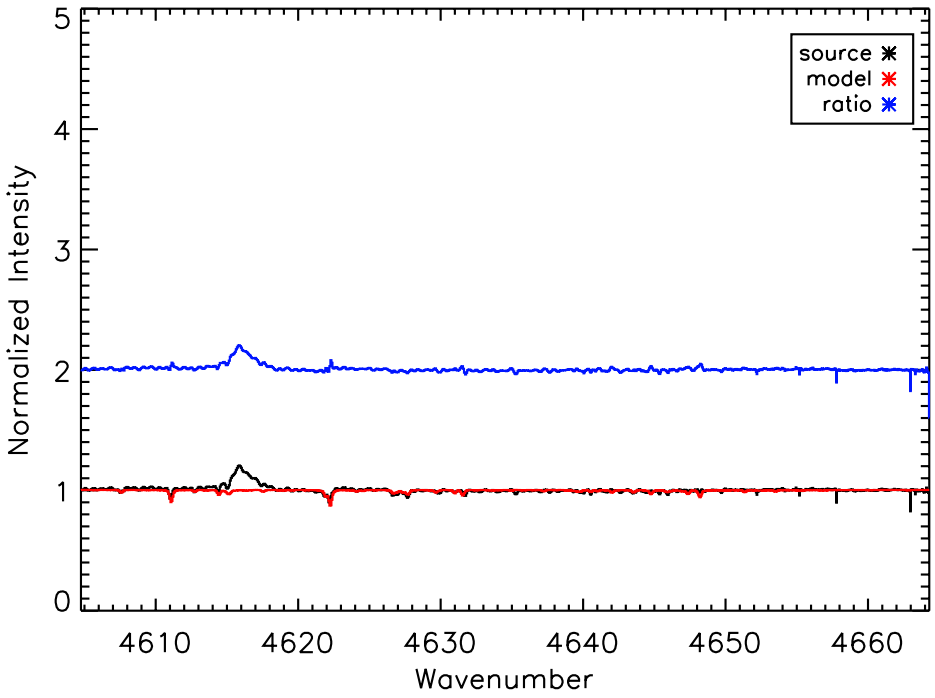

Figure 71: Spectra for ZCMA order K 35, data from 2009.

Appendix M ABBA Nod Pattern Derivation

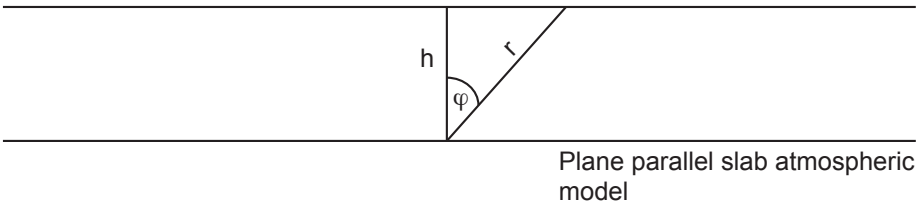

Figure 72: Diagram of plane parallel atmosphere

Because the airmass of the sky is proportional to the secant of the angle from Zenith (see figure), we can compute the spectrum of the ABBA nod pattern using a Taylor expansion of the airmass function near the zenith angle of each nod position. The derivation is given below. Note that the parallel plane geometry gives the approximate answer assuming a constant density (opacity) atmosphere. If we keep this assumption but change to a spherical geometry, we retain the cancellation to second order, however we pick up a multiplicative term, $z(1-\frac{z}{2R_\oplus})$, where z is the atmospheric height above the ground, and $R_\oplus$ is the radius of the earth.

$$r = \frac{h}{cos(\phi)} = hsec(\phi) \tag{2}$$

$$sec(x) = 1 + \frac{x^2}{2} \tag{3}$$

$$A - B - B + A = sec(x) - sec(x + dx) - sec(x + 2dx) + sec(x + 3dx) \tag{4}$$

$$A - B - B + A = 1 + \frac{x^2}{2} - (1 + \frac{(x + dx)^2}{2}) - (1 + \frac{(x + 2dx)^2}{2}) + (1 + \frac{(x + 3dx)^2}{2}) \tag{5}$$

$$A - B - B + A = \frac{x^2}{2} - \frac{(x + dx)^2}{2}) - \frac{(x + 2dx)^2}{2}) + \frac{(x + 3dx)^2}{2} \tag{6}$$

$$A - B - B + A = 2dx^2 \tag{7}$$

Hence, in the limit of a plane-parallel atmosphere, we may cancel the sky emission to second order by using an ABBA nod pattern.

If we take the atmosphere to be thin and as a spherical shell around Earth, we arrive at the geometry shown in the figure.

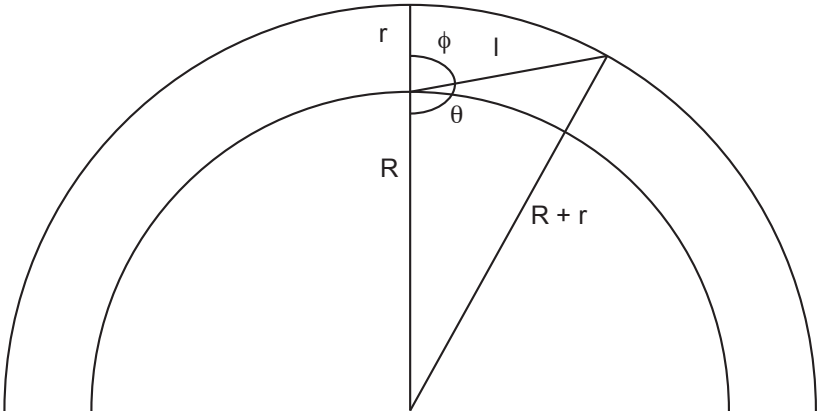

Figure 73: Diagram of spherical shell atmosphere

$$(R+r)^2 = R^2 + l^2 - 2Rlcos(\theta) \tag{8}$$

$$(R+r)^2 = R^2 + l^2 - 2Rlcos(\pi - \phi) \tag{9}$$

$$(R+r)^2 = R^2 + l^2 + 2Rlcos(\phi) \tag{10}$$

$$R^2 + 2Rr + r^2 = R^2 + l^2 + 2Rlcos(\phi) \tag{11}$$

$$2Rr + r^2 = l^2 + 2Rlcos(\phi) \tag{12}$$

$$l^2 + 2Rlcos(\phi) - 2Rr - r^2 = 0 \tag{13}$$

$$l = \frac{-2Rcos(\phi) \pm \sqrt{4R^2cos^2(\phi) + 4(2Rr + r^2)}}{2} \tag{14}$$

$$l = -Rcos(\phi) \pm \sqrt{R^2cos^2(\phi) + (2Rr + r^2)} \tag{15}$$

$$l = -Rcos(\phi) \pm Rcos(\phi)\sqrt{1 + \frac{2r}{Rcos^2(\phi)} + \frac{r^2}{R^2cos^2(\phi)}} \tag{16}$$

assuming that we are only observing at reasonable angles so that we can say $r^2 << R^2cos(\phi)$,

$$l = -Rcos(\phi) \pm Rcos(\phi)(1 + \frac{r}{Rcos^2(\phi)}) \tag{17}$$

becomes

$$l = \frac{r}{cos(\phi)}. \tag{18}$$

Hence, we have retained the original equation assuming reasonable angles for our observations. If we wish to go to $\frac{\pi}{2}$ or beyond (assuming we are on a mountain), we must use equation 15, without making any simplifying assumptions.

Actually, as indicated before, this problem is solvable if we keep the r^2 term under the square root sign.

$$l = -Rcos(\phi) \pm Rcos(\phi)(1 + \frac{r}{Rcos^2(\phi)} + \frac{r^2}{2R^2cos^2(\phi)}) \tag{19}$$

$$l = -Rcos(\phi) \pm (Rcos(\phi) + \frac{r}{cos(\phi)} + \frac{r^2}{2Rcos(\phi)}) \tag{20}$$

$$l = \frac{r}{cos(\phi)}(1 + \frac{r}{2R}) \tag{21}$$

Which is a small correction to the original estimate, again assuming a non-right angle for our zenith estimate.

Appendix N Modeling of Circumstellar Disks and Spectroscopic Components

N.1 Introduction

We present a code to model a CO absorption spectrum from a circumstellar Keplerian disk. This code is still in the development stage, but eventually may be used to determine the velocity structure of the disk, the temperature profile of the disk, the inner and outer radii of the disk, and the inclination angle, within the bounds of degeneracy. Spectra taken at NIR wavelengths can then be compared to this code, and a best fit may be produced to extract the aforementioned information, to the degree that the model provides an accurate interpretation of the physical situation in the disk. We seek to apply this model to a sample of FUor, FUor-like and EXor stars, to constrain the physical parameters that describe the disk. This article will describe the theoretical framework of the calculations done in the code and what possible information may be extracted (as physical parameters of the disk).

We seek to better understand the gas excitation mechanisms in YSOs, especially in the inner AU of the disks. The inner disk region is important to study because this area contains any conceivable habitable zone, and any theory of extra-solar Earth-like planet formation must first require an understanding of the water distribution in that system, which requires a detailed knowledge of the thermodynamic processes that occur in that disk. For a large sample of stars, we seek to understand the water and CO excitation mechanisms, and this code is a first step to understanding the CO spectra. If we can understand what the CO is doing in the disk, it is a stepping stone to understanding what the water is doing in the disk.

When the code is in working order, it is our intention to fit many spectra of FUor, EXor, and FUor-like obects to the model spectra. Running a Monte-Carlo simulation and running a chi-square minimization algorithm on the model and source spectra will ideally constrain the disk parameters. We expect to find degeneracies in the model, and intend on investigating them. Currently, we have approximately ten sources with spectral coverage in the K, L and M bands, all of which are candidates for fitting with this model.

N.2 Discussion

We study a sample of FUor, FUor-like, and EXor stars in an ongoing survey project. To extract physical information from our sample, it is necessary to construct a model which will enable us to fit our data. The model is constructed assuming a Keplerian disk around a central star which has an input mass. This stellar parameter will be free to be varied as the user sees fit. We make the assumption that the disk has an inner and outer radius and that the midplane is a blackbody emitting at a specific temperature at a radial distance, that is, there is a radially dependent temperature profile. We also assume that the disk mass does not affect rotation; we assume a Keplerian disk. The equation for a Keplerian orbit is

$$v(r) = \sqrt{\frac{GM_{\odot}}{r}}. \tag{22}$$

That is, the velocity at a given distance is determined solely by the solar parameters. If we consider all of the zones of the disk, we can derive a velocity field for the disk, with appropriate definitions of the x,y, and z axes. The velocity field is given by

$$\overrightarrow{v(r,\theta)} = \sqrt{\frac{GM_{\odot}}{r}}[sin(\theta)\hat{z} - cos(\theta)\hat{x}]. \tag{23}$$

If we apply a rotation operator to the velocity field's components,

$$R = \begin{pmatrix} cos(i) & sin(i) & 0 \\ -sin(i) & cos(i) & 0 \\ 0 & 0 & 1 \end{pmatrix} \tag{24}$$

we may find a velocity field which is rotated into the appropriate frame for our consideration, specifically one that is inclined with respect to our line of sight. Applying the rotation

$$\overrightarrow{v(r,\theta)}' = R\overrightarrow{v(r,\theta)} \tag{25}$$

we arrive at a rotated field. The velocity doppler shift of any point in the disk is given by

$$v = [1 - \frac{\hat{x}\cdot\overrightarrow{v(r,\theta)}}{c}]v_o. \tag{26}$$

This has a component directed along the line of sight with

$$|\overrightarrow{v(r,\theta)}'|_x = \sqrt{\frac{GM_{\odot}}{r}}cos(\theta)cos(\theta). \tag{27}$$

Using these, we can calculate the Doppler shifted line centers for each of the segments of the disk. We begin our calculations by breaking the disk up into annuli, each consecutive annulus is one velocity resolution element away from the previous. In each annulus we calculate temperature, number density, number of particles in each state, and optical depth. Each of these calculations is given below. All line values and parameters were acquired using the 2008 HITRAN database (Rothman et al., 2009). Temperature and number density are assumed to follow a decaying polynomial; temperature and number density are highest near the star. Populations are calculated using a Boltzmann distribution. This is acceptable because we assume that the levels are collisionally populated. For a more in-depth treatment of the quantum mechanics behind these equations, see Najita et al. (1996, see appendices) and Bernath (2007)

$$T(r) = T_o[R_o/r]^{\alpha} \tag{28}$$

$$S(r) = S_o[R_o/r]^{\beta} \tag{29}$$

$$N_{J',\nu} = N\frac{(2J'+1)e^{-\frac{hcBJ'(J'+1)}{kT(r)}}}{kT(r)/hcB}\,\frac{e^{-3084\nu/T(r)}}{\frac{1}{e^{-3084/T(r)}+1}} \tag{30}$$

where

$$B = B_e - \alpha_e(\nu+\frac{1}{2}) + \gamma_e(\nu+\frac{1}{2})^2 \tag{31}$$

has coefficients given by Mantz et al. (1975). The optical depth is

$$\tau_{J',J'',\nu} = N_{J',\nu}\frac{2J'+1}{2J''+1}\frac{A_{J'\leftarrow J''}}{4\pi\tilde{\nu}^2}\phi(\tilde{\nu}), \tag{32}$$

where

$$\phi(\tilde{\nu}) = \frac{1}{2\pi b}e^{(-\frac{1}{2}(\frac{\nu}{b})^2)}. \tag{33}$$

The optical depth is calculated, and applied to Beer's Law to determine the emergent luminosity from that section of the disk. The luminosity

$$L(\tilde{\nu}) = Area(r,\theta)B(T,\tilde{\nu})e^{-\tau_{\tilde{\nu}}} \tag{34}$$

is a function of temperature, the optical depth, and the area of the sector under consideration. Luminosity is summed over all the appropriate sectors, and calculated for each wavenumber. The synthetic spectra is then convolved with an instrument profile, which is also assumed to be Gaussian. The final convolved spectrum is compared to a spectrum from an FUor, FUor-like, or EXor object.

Future inclusions into this model would be to make the disk dynamic. Currently, the disk assumes steady state. This modification would require use of magnetohydrodynamics (especially near the star). This modification would facilitate a modeling of the FUor accretion event, as well as the ostensibly episodic accretion events of the EXors. More simply, this model could include emission from the disk, as not all parts of the disk will necessarily be absorbing, which would model a disk which transitions from an active disk to a passive disk. Additionally, it would be possible to make the disk non-radially or non-azimuthally symmetric. This would allow us to introduce density variations in the disk and (especially for the unwritten, dynamic model) model these objects' evolutions over time.

N.3 Results

The current version of this code does not produce the desired spectra. The plot below shows a real science spectrum and the model overlaid. The x-axis shows wavenumber, the y-axis shows ratioed luminosity. The calculated spectrum shows CO v(1-0) absorption lines. Clearly, the two do not match. The spectra it is plotted against is from ZCMA, M band, order 15. The star is in black and the model in blue. The model has been scaled to fit the YSO spectrum. Terse statements aside, the two do not agree completely, but the model does seem promising. This test

is the zeroth order check on the code: does it match a simple spectrum? Once this test is passed, the code can be implemented in a Monte-Carlo minimization routine to constrain the chosen disk parameters. The code will also be tested on a variety of other, more complicated spectra once this simple case is correct. Additionally, it would also be prudent to add other lines to this code which are not currently included, such as water lines. The addition of other CO lines is luckily a trivial task.

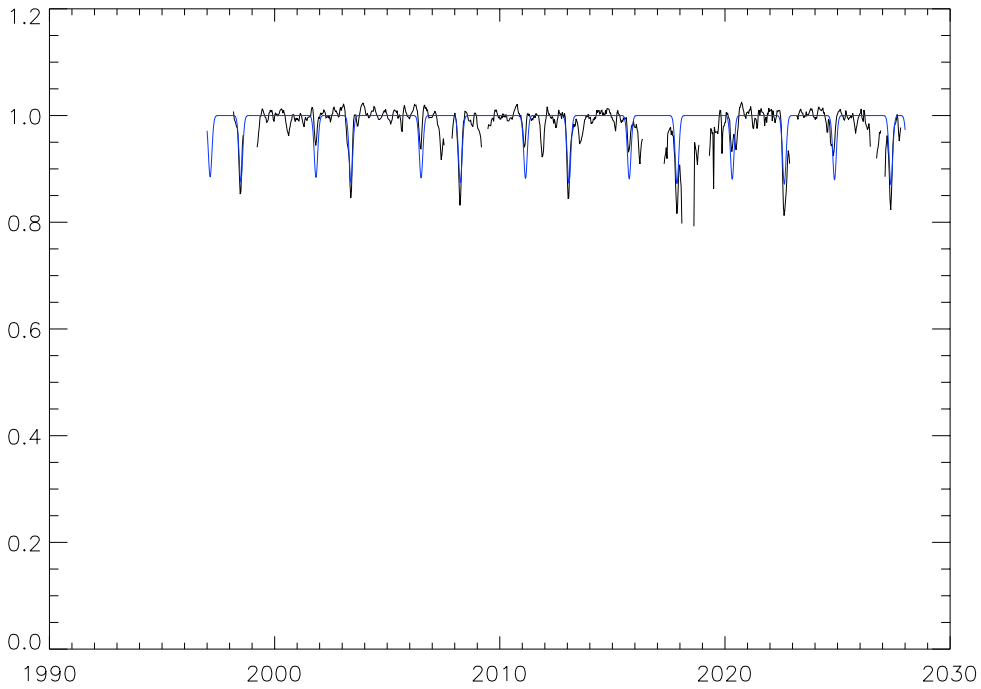

Figure 74: Synthetic and observed CO absorption lines. Spectral data are fit to Z CMa, M band, order 15. and are in black. Synthetic data are in blue. The space between points has been plotted to clarify the spectral structure.

Bibliography

Armitage, P. J., Livio, M., & Pringle, J. E. 2001, MNRAS, 324, 705

Aspin, C., & Reipurth, B. 2003, AJ, 126, 2936

Audard, M., et al. 2010, A&A, 511, A63

Bell, K. R., Lin, D. N. C., Hartmann, L. W., & Kenyon, S. J. 1995, ApJ, 444, 376

Bernath, P. 2005, Oxford University Press

Bertout, C., & Bouvier, J. 1989, European Southern Observatory Conference and Workshop Proceedings, 33, 215

Breger, M. 1969, ApJS, 19, 79

Bonnell, I., & Bastien, P. 1992, ApJ, 401, L31

Brittain, S. D. 2004, Ph.D. Thesis,

Brittain, S. D., Rettig, T. W., Simon, T., Gibb, E. L., & Liskowsky, J. 2010, ApJ, 708, 109

Carr, J. S., Harvey, P. M., & Lester, D. F. 1987, ApJ, 321, L71

Carr, J. S. 1989, ApJ, 345, 522

Chalonge, D., & Divan, L. 1952, Annales d'Astrophysique, 15, 201

Clarke, C. J., & Syer, D. 1996, MNRAS, 278, L23

Cohen, M., & Kuhi, L. V. 1979, ApJS, 41, 743

Cohen, M., Kuhi, L. V., Spinrad, H., & Harlan, E. A. 1981, ApJ, 245, 920

Carrasco-González, C., Rodríguez, L. F., Anglada, G., & Curiel, S. 2009, ApJ, 693, L86

Eggen, O. J. 1956, PASP, 68, 238

Elias, J. H. 1978, ApJ, 223, 859

Elias, J. H. (B) 1978, ApJ, 224, 857

Glassgold, A. E., Najita, J., & Igea, J. 2004, ApJ, 615, 972

Greene, T. P., Aspin, C., & Reipurth, B. 2008, AJ, 135, 1421

Haas, M., Leinert, C., & Zinnecker, H. 1990, A&A, 230, L1

Hartmann, L., & Kenyon, S. J. 1985, ApJ, 299, 462

Hartmann, L., Kenyon, S. J., Hewett, R., Edwards, S., Strom, K. M., Strom, S. E., & Stauffer, J. R. 1989, ApJ, 338, 1001

Herbig, G. H. 1958, ApJ, 128, 259

Herbig, G. H. 1977, ApJ, 217, 693

Herbig, G. H. 2007, AJ, 133, 2679

Herbig, G. H. 2008, AJ, 135, 637

Hoffleit, D. 1939, Harvard College Observatory Bulletin, 911, 41

Kenyon, S. J., Hartmann, L. W., Strom, K. M., & Strom, S. E. 1990, AJ, 99, 869

Krist, J. E., et al. 1999, ApJ, 515, L35

Lorenzetti, D., Larionov, V. M., Giannini, T., Arkharov, A. A., Antoniucci, S., Nisini, B., & Di Paola, A. 2009, ApJ, 693, 1056

Lynden-Bell, D., & Pringle, J. E. 1974, MNRAS, 168, 603

Mantz, A. W., Maillard, J.-P., Roh, W. B., & Narahari Rao, K. 1975, Journal of Molecular Spectroscopy, 57, 155

McLean, I. S., et al. 1998, ProcSPIE, 3354, 566

McMuldroch, S., Sargent, A. I., & Blake, G. A. 1992, BAAS, 24, 1215

McMuldroch, S., Sargent, A. I., & Blake, G. A. 1993, AJ, 106, 2477

Mould, J. R., Hall, D. N. B., Ridgway, S. T., Hintzen, P., & Aaronson, M. 1978, ApJ, 222, L123

Mundt, R., Stocke, J., Strom, S. E., Strom, K. M., & Anderson, E. R. 1985, ApJ, 297, L41

Mundt, R., Buehrke, T., & Ray, T. P. 1988, ApJ, 333, L69

Najita, J., Carr, J. S., Glassgold, A. E., Shu, F. H., & Tokunaga, A. T. 1996, ApJ, 462, 919

Osorio, M., D'Alessio, P., Muzerolle, J., Calvet, N., & Hartmann, L. 2003, ApJ, 586, 1148

Reipurth, B., Guimarães, M. M., Connelley, M. S., & Bally, J. 2007, AJ, 134, 2272

Rothman, L. S., et al. 2009, JQSRT, 110, 533

Shakura, N. I., & Sunyaev, R. A. 1973, X- and Gamma-Ray Astronomy, 55, 155

Shu, F. H. 1977, ApJ, 214, 488

Simon, T. 1975, PASP, 87, 317

Stahler, S. W. 1988, ApJ, 332, 804

Tonry, J., & Davis, M. 1979, AJ, 84, 1511

Welin, G. 1976, A&A, 49, 145

Weintraub, D. A., Sandell, G., & Duncan, W. D. 1991, ApJ, 382, 270